Available online at www.sciencedirect.com
SCIENCE DIRECT®
ELSEVIER
Journal of Magnetism and Magnetic Materials 256 (2003) 449–501
Journal of magnetism and magnetic materials
www.elsevier.com/locate/jmmm

Topical review

Ordered magnetic nanostructures: fabrication and properties

J.I. Martín[a], J. Nogués[b], Kai Liu[c,d], J.L. Vicent[e], Ivan K. Schuller[c,*]

[a] *Depto. Fisica, Facultad de Ciencias, Universidad de Oviedo, 33007 Oviedo, Spain*
[b] *Institució Catalana de Recerca i Estudis Avançats (ICREA) and Department de Fisica, Universitat Autònoma de Barcelona, 08193 Bellaterra, Spain*
[c] *Physics Department, University of California-San Diego, 9500 Gilman Dr. La Jolla, CA 92093-0319, USA*
[d] *Physics Department, University of California-Davis, Davis, CA 95616, USA*
[e] *Depto. Fisica de Materiales, C.C. Fisicas, Universidad Complutense, 28040 Madrid, Spain*

Received 12 November 2001; received in revised form 9 August 2002

Abstract

The fabrication methods and physical properties of ordered magnetic nanostructures with dimensions on the submicron to nanometer scale are reviewed. First, various types of nanofabrication techniques are described, and their capabilities and limitations in achieving magnetic nanostructures are discussed. Specifically, we address electron beam lithography, X-ray lithography, laser interference lithography, scanning probe lithography, step growth methods, nanoimprint, shadow masks, radiation damage, self-assembled structures, and the use of nanotemplates. Then the magnetic properties of these nanostructures are reviewed, including properties of single dots, magnetic interactions in arrays, dynamic effects, magnetic behavior of nanostructured lines and wires, giant magnetoresistance effect, and properties of films with arrays of holes. Finally, the physical properties in hybrid systems, where the magnetic arrays interact with superconducting and semiconducting layers, are summarized.

PACS: 75.75.+a; 81.16.–c; 75.60.–d

Keywords: Magnetic nanostructures; Nanofabrication; Magnetic properties

1. Introduction

Nanostructured materials have attracted intense research interest over recent years, as they provide the critical building blocks for the booming nanoscience and nanotechnology. They typically have structural or chemical restrictions on the nanometer scale along one or more of the dimensions. Due to their intricate nanostructures, extremely small length scale, low dimensionality, and interplay among constituents, they often exhibit new and enhanced properties over their bulk counterparts. Their novel properties can also be tailored through extra degrees of freedom, such as structure and constituent materials, etc. Recent progresses on magnetism and magnetic materials have made magnetic nanostructures a particularly interesting class of materials for both scientific and

*Corresponding author. Tel.: +1-619-5342450; fax: +1-619-5340173.
E-mail address: ischuller@ucsd.edu (I.K. Schuller).

0304-8853/03/$ - see front matter
PII: S0304-8853(02)00898-3

technological explorations. For example, studies on subjects such as interlayer coupling, giant magnetoresistance, colossal magnetoresistance, tunneling magnetoresistance, exchange bias, half-metallic ferromagnets, spin-injection, and current-induced switching have led to the exciting possibility of utilizing electron spin for information processing, or "spintronics" [1–39].

Research on magnetic nanostructures has driven the sample physical size towards ever-smaller dimensions. Fundamentally, novel properties emerge as the sample size becomes comparable to or smaller than certain characteristic length scales, such as spin diffusion length, carrier mean free path, magnetic domain wall width, superconducting coherence length, etc. The effects of confinement, proximity and order govern the interplay between the relevant physical length scales and the sizes of the patterned magnetic materials. For example, ballistic transport appears in material confined to the appropriate length, smaller than the electron mean free path, or magnetization reversal processes can be drastically modified in magnetic structures confined to sizes that preclude the domain wall formation. Also, the proximity of nanoelements could interfere with the physical length scales of long range order phenomena as coherence lengths in superconductivity and spin diffusion lengths in magnetism. Moreover, the order of these magnetic nanostructures, organized in patterned arrays, becomes crucial as the mesoscopic effects produced by the confinement and proximity can be controlled and modified by their geometrical configuration. Technologically, the device miniaturization trend has led to, most visibly, the explosive growth of the magnetic recording density [40–42], and is continuing at an even faster pace. Such demands call for advanced sample growth and patterning techniques to achieve nanometer-scale feature sizes, beyond the limits of conventional photolithography [43–45].

In practice, it is equally challenging to characterize such small nanostructures. It is highly desirable not only to fabricate ultrafine nanostructures, but also to fabricate *arrays* of such nanostructures, more preferably over macroscopic areas. Ordered arrays of magnetic nanostructures are particularly interesting to study, as one can probe both the individual and collective behavior of the elements in a well-defined and reproducible fashion. Technologically, they are also important in such applications as magnetic random access memory (MRAM), patterned recording media, and magnetic switches, etc. [46–49]. Significant amount of work has been done by the scientific community over recent years to address different aspects of ordered magnetic nanostructures, from fabrication to characterization, both theoretically and experimentally.

In this article, we review the recent investigations as well as some open issues in ordered magnetic nanostructures, in terms of the fabrication techniques as well as their physical properties. This subject has been briefly reviewed earlier [50–61], and here we present a more exhaustive description of the state-of-the-art. Note that many techniques discussed here are also common to other types of nanostructures, magnetic or not, ordered or not. The work is organized as follows: Section 2 is dedicated to fabrication techniques, addressing their capabilities and limitations to obtain well-controlled nanostructures. We review electron beam lithography (Section 2.1), X-ray lithography (Section 2.2), laser interference lithography (Section 2.3), and other non-conventional methods (Section 2.4). Section 3 describes the magnetic properties of these nanostructures, including the behavior of individual magnetic dots (Section 3.1), their collective behavior (Section 3.2), dynamic effects (Section 3.3), micromagnetic calculations on nanostructured elements (Section 3.4), properties of line-shaped nanostructures (Sections 3.5 and 3.6) and patterned films (Section 3.7). Finally, Section 4 discusses the interactions of magnetic nanostructures with other systems, such as superconducting films (Section 4.1) and two-dimensional electron gases (2DEG) in semiconductor multilayers (Section 4.2).

2. Fabrication

Central to nanofabrication is lithography, a collective term for several closely related processes, including resist coating, exposure, and development. Although extensive literature exists on the

basic lithography processes [43,62,63], a brief review helps to better illustrate the more advanced techniques.

The work piece, an unpatterned film or a substrate, is first spin-coated with a uniform layer of resist dissolved in certain organic liquid solvent. The resist thickness is typically a few thousand angstroms to a micron, depending on the spinning speed and the resist viscosity. A soft-bake of the resist is necessary to remove the resist solvent and promote adhesion. Selected areas of the resist are then exposed to a radiation source, often through a mask (Fig. 1). Upon sufficient exposure, the polymer chains in the resist are either broken (positive resist), or become cross-linked (negative resist, poorer resolving power). The exposed resist often goes through a post-exposure bake to promote homogeneity, before developed to form a positive or negative image of the mask. As the lithography process transforms a two-dimensional (2D) pattern into a three-dimensional (3D) structure in the resist and eventually the unpatterned film, the depth profiles in both layers are important. By choosing the right developer, temperature and developing time, one can obtain straight, round-off or undercut depth profiles in the resist. In certain applications, multilayer resists may be used to achieve better vertical aspect ratio (height to width), plasma etch resistance, and less substrate reflection [63].

Pattern transfer can be realized in two general processes: from the resist to an unpatterned film by wet or dry etching; or post-deposition onto patterned resist by lift-off and/or electrodeposition (Fig. 1).

For etching, the developed resist is usually hardened by a hard-bake before this process. Wet etching uses chemical or electrochemical processes to dissolve the materials. It is intrinsically isotropic and causes sloped pattern edges. Therefore the resolution is generally limited by the thickness of the film to be patterned. However, anisotropic etching may be achieved in oriented crystalline materials. A useful list of etching recipes for common materials can be found in Ref. [64]. In dry etching, physical processes such as ion milling and sputter etching use ion bombardment to remove the unwanted materials; chemical processes such as plasma etching use active species to react with surface material and form volatile

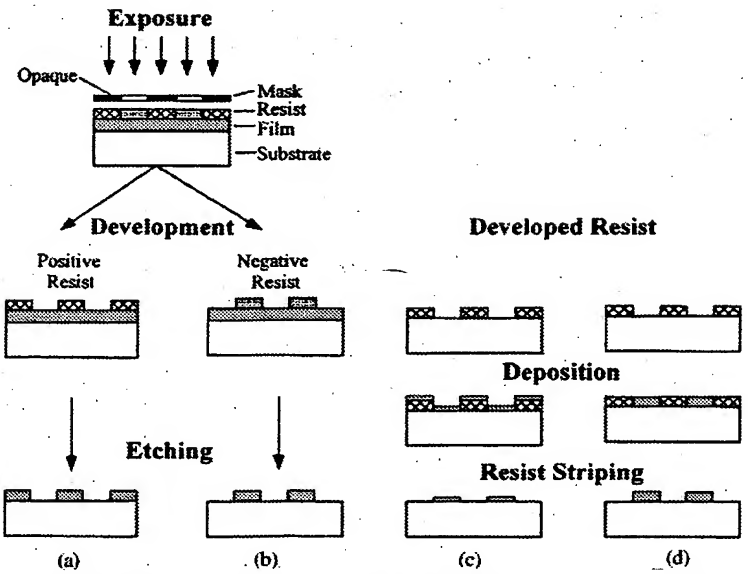

Fig. 1. Schematics of lithography processes for (a) positive and (b) negative resists in conjunction with (a), (b) etching, (c) lift-off, and (d) electrodeposition.

products; a combination of both processes, such as reactive ion etching, takes advantage of both principles. These dry etching processes can produce straight and sharp pattern edges, thus better resolution for a given film thickness [64]. They are more desirable for patterning ultrafine nanostructures. At the end of the process, the remaining resist is striped away.

Alternatively, nanostructures can be fabricated by post-lithography depositions. Lift-off utilizes the height of a developed resist to break apart a subsequently deposited, much thinner, layer of material (Fig. 1). The film deposited on top of the resist is lifted off during resist striping, leaving behind only the portions directly deposited onto the substrate. It is crucial to have a clean break-off of the film at the pattern edges of the resist. Therefore resists developed with undercut edge profiles, as well as directional deposition techniques, are preferred. One method to realize the undercut profile is to slow down the development at the resist surface relative to the bulk by, e.g., immersing the resist in chlorobenzene to harden the surface. Note that the height of the lift-off structures is usually much smaller than the resist thickness (Fig. 1). The idea of lift-off can also be realized in double or multiple layer combination of a resist with other materials [62]. For example, when bilayer resists are used, by either using double exposure or differential development, the bottom resist layer is developed faster than the top, leading to an overhang structure [65]. This allows the in situ fabrication of nanostructures without further post-deposition processing. Metallic bilayer overhang structures have also been fabricated [66,67]. The bilayer is first patterned by e-beam lithography. The opening in the top layer is further shrunk by anodic oxidation of the top layer to form an overhang structure over the bottom layer. The final structure deposited through the top opening can be as small as 15 nm [66].

Electrodeposition, or electroplating, is a general growth technique and is particularly useful for post-lithography depositions. It refers to the deposition of materials from an electrolyte by the passage of an electrical current. Unlike high-vacuum deposition techniques, such as sputtering or evaporation, electrodeposition is an ambient temperature and pressure process. It has the attractive features of cost-effectiveness, simplicity of operation, and the ability to deposit onto substrates with complex geometries. Differing from lift-off, the electrodeposited elements can have heights up to the resist thickness, therefore better vertical aspect ratio (Fig. 1). Over recent years, significant progress has been made in fabricating new materials and novel nanostructures using this technique [68,69]. For example, arrays of high aspect ratio nanowires have been electrodeposited into nanotemplates to form elemental nanowires [70], alloy nanowires [71,72], multilayered wire [73–75], or even tunneling junction nanowires [76].

The lithography resolution limit is ultimately determined by the radiation wavelength. Hence lithography is usually categorized by the radiation source as optical, electron-beam (e-beam), ion beam, and X-ray lithography. In the most common optical (or photo-) lithography, where ultraviolet (UV) light is used, there is an urgent need for the development of shorter wavelength light source (e.g., ArF excimer laser, $\lambda = 193$ nm; F_2, $\lambda = 157$ nm). On the other hand, techniques such as near-field photolithography [77–81] have been able to circumvent the diffraction limit and achieve feature sizes as small as 50 nm [80]. However, these techniques have not been fully utilized in magnetic systems [82]. In the following, other types of lithography and nanopatterning techniques are reviewed.

2.1. Electron beam lithography

The e-beam lithography technique uses an electron beam to expose an electron-sensitive resist [83–85]. Positive resists, such as polymethylmethacrilate (PMMA) dissolved in trichlorobenzene, are used more often than negative resists, although both can produce very efficient results. The exposure is usually done using the e-beam in a scanning electron microscope (SEM), although transmission electron microscopes (TEM) have also been used [86,87]. The e-beam is controlled by a computer through a position generator interface. It allows to write any computer-defined patterns

on the resist, which is subsequently developed to form the desired structure. To obtain different magnetic nanostructures, the e-beam lithography method has been used in combination with various general lithography processes described earlier (lift-off, etching, electrodeposition and mask techniques).

One of the main advantages of this technique is its versatility for the fabrication of well-defined arbitrary element shapes and array configurations. In this way, a variety of magnetic elements have been obtained: simplest cases of dots and lines [83–95]; complex patterns such as rectangles [96], diamonds [97], triangles and pentagons [55], zigzag lines [98], rings [99], dots and lines connected by small constrictions [90,100,101], or dot superlattices [102]; and even unusual shapes such as bars with triangular pointed ends [103,104] or dented edge elements [105] used for the study of magnetization reversal processes. Moreover, this versatility allows the fabrication of small devices, such as non-volatile magnetoresistive magnetic random access memories (MRAM) [46] or "quantum" magnetic disks [106,107].

A large number of magnetic nanostructures have been fabricated by e-beam lithography. The main characteristics of fabrication processes are summarized as follows:

(a) *Combined with lift-off:* This process has been used to produce a variety of polycrystalline magnetic nanostructures such as Co [90,108–110], Fe [102], Ni [90], NiFe [101,110–113], MoNiFe [114,115], CoFe [116], CoPt [117], Fe_3O_4 [118], and NdFeB [119] patterns, as well as amorphous Fe_xSi_{1-x} [120]. More complicated structures such as Co/Pt multilayers with perpendicular anisotropy [93] and Co/Au/Ni structures [97] have also been patterned. High resolution can be achieved in this process, e.g., particles as small as 55 nm [115] or bars with only 15 nm width [121], along with high linear densities of up to 10 Gbits/in^2 [83]. It also allows the production of arrays over relatively large areas (up to $10 \times 10\,mm^2$) [122]. In general, planar elements are more suitable with this method, as their thicknesses are limited to about 50 nm.

(b) *Using mask techniques:* this process is used as a complex variation of the lift-off method, referring to the overhang structures discussed earlier. It allows the fabrication of elements with very high-quality vertical edges. Wires made of Fe, Co, or Co/Cu multilayer have been fabricated with widths smaller than 100 nm [65] and, also, very well defined Co dots with 35 nm of lateral dimension [123].

(c) *Combined with etching processes:* This technique allows the fabrication of nanostructures not only from polycrystalline films, such as Co [85,109,124], NiFe [100,125,126], CoCrPt [127], exchange biased IrMn/CoFe [128] and NiO/Ni [129], or multilayers of Au/Co [89], Co/Pt [91, 130–132] and Co/Cu [133,134], but also from epitaxial films such as Fe(0 0 1) [135–138], Fe(1 1 0) [104], Co(0 0 0 1) [139] or Co(1 0 $\bar{1}$ 0) [140]. This method has patterned elements with only 20 nm in lateral size and vertical aspect ratio (height/width) greater than 1 [141]. Dot array densities as high as 29 Gbits/in^2 have been achieved in magnetic systems [127]. However, in general, the array area is small in comparison with other methods. It must be pointed out that a number of different etching procedures have been designed to obtain nanometric definition in the magnetic structures [142,143].

(d) *Combined with electroplating:* This method allows the fabrication of patterned elements with high vertical aspect ratios (up to 9:1), as thicknesses of up to 700 nm have been achieved [88,144]. For example, Ni columns [145–147] or mushrooms-like pillars with diameters as small as 20 nm [86] have been deposited. This translates to an area density of 65 Gbit/in^2 [144]. On the other hand, the array areas produced so far are not larger than $200 \times 200\,\mu m^2$ for magnetic systems [94]. A SEM image of an array of these Ni elements is shown in Fig. 2.

(e) *Direct writing:* This technique has been designed to pattern nanostructures without using any electron-sensitive resist. It is the electron beam itself that produces the desired pattern [87]. One process to obtain magnetic elements begins with the deposition of a layer of a transition-metal halide on the substrate. Some of these materials (FeF_2 or CoF_2) are sensitive enough to the electron beam to induce a self-developing process resulting in the liberation of the F atoms. Thus,

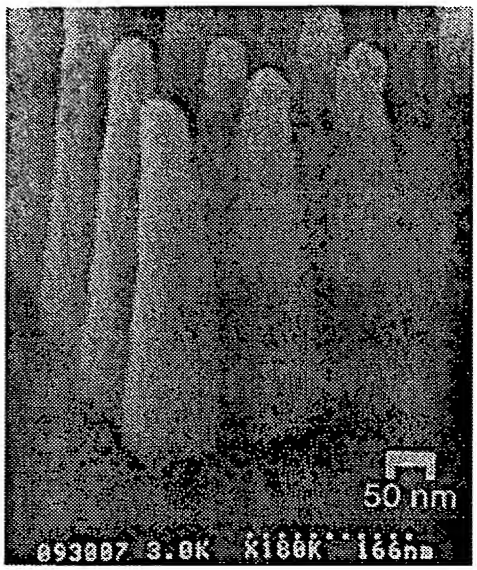

Fig. 2. SEM image of Ni pillar array of average 75 nm diameter, 700 nm height and a 100 nm spacing. The density is 65 Gbits/in^2 and the aspect ratio is 9.3 (courtesy Krauss et al. [144]).

only the metallic atoms remain in the exposed regions. The total areas that have been patterned with this method are very small, of the order of several μm^2, but with high resolution of about 10 nm [87]. A more complex approach to this technique, is to allow a precursor organometallic gas, containing the desired magnetic atom, in the SEM chamber. The electron beam generated by the SEM dissociates the precursor gas into a metal dot at predetermined locations. The size of the elements depends on the voltage, current, pulse duration and the composition and pressure of the precursor gas [148].

As mentioned above, one of the disadvantages of electron beam lithography is the area size patternable in a reasonably short time. This problem is currently being addressed by designing multiple electron beam techniques [149]. Finally, it is worth noting that in several other lithography processes such as X-ray or nanoimprint lithography, e-beam fabricated masks are used.

The main characteristics of magnetic arrays fabricated by e-beam lithography, as well as other techniques, are summarized in Table 1.

2.2. X-ray lithography

The exposure of a resist to X-ray radiation in a parallel replication process is the basis for this technique. In general, a synchrotron radiation facility is used to expose the samples [150]. Similarly to the e-beam lithography method, the sample is covered by a resist layer with high sensitivity in the X-ray wavelength region. Very efficient results can be obtained with either positive or negative commercially available resists [150]. In particular, PMMA resin is also used in this method with excellent resolution [151,152].

Between the radiation source and the sample, at few micrometers above the resist layer, a mask is placed to define the pattern. It is generally agreed that the mask is the most crucial element of this technique. The X-ray masks are usually made of small thickness (around 2 μm) silicon carbide membranes, covered by a metallic pattern with the desired geometry fabricated by e-beam lithography. A high-Z absorber material (such as gold, tungsten or tantalum) is used to prevent X-ray exposure of the sample [150–152]. The advantage is that the mask can be used repeatedly.

After irradiation, the resist is developed and the magnetic pattern is obtained by etching [152–156], lift-off [152,154,155] or electroplating [157]. Arrays of nanostructured magnetic materials prepared include polycrystalline NiFe [155,156,158], epitaxial Co(0 0 0 1) [154,159], Fe(1 1 0) [160–162], Au/Co/Au(1 1 1) sandwiches [152,153,163] or Ni–Cu/Cu(1 0 0) multilayers [157].

The parallel replication process results in excellent verticality of the designed elements, including the possibility to make elements with high vertical aspect ratios [155]. Dot diameters as small as 88 nm have been produced with typical separations of about 100 nm, resulting in magnetic array densities up to 4 Gbits/in^2 [155]. Magnetic arrays with well-defined elements have been prepared over 5×5 mm^2 areas [152,159], which is comparable to other techniques described above. However, the

Table 1
Main characteristics of magnetic arrays fabricated by different nanolithography techniques

Technique	Maximum area	Minimumfeature size	Materials	Thickness/aspect ratio	Density
E-beam and electroplating	$200 \times 200\,\mu m^2$ [94]	20 nm [86,146]	Ni [86,88,94,146]	700 nm/9.3:1 [88]	65 Gbits/in^2 [88]
E-beam and lift-off	$10 \times 10\,mm^2$ [122]	55 nm [115]	Ni [90], Co [90], Fe [102], NiFe [83,122], CoFe [116], MoNiFe [115], CoPt [117], Fe_3O_4 [118], NdFeB [119], Fe_xSi_{1-x} [120]	50 nm/1:2 [83]	10 Gbits/in^2 [83]
E-beam and etching	$750 \times 750\,\mu m^2$ [89]	20 nm [96]	Au/Co [89], NiFe [96,114,126], CoCrPt [127], Co [85], Co/Cu [133], Fe (0 0 1) [135]	50 nm/2:1 [96]	29 Gbits/in^2 [127]
E-beam and direct writing	$1 \times 1\,\mu m^2$ [87]	10 nm [87]	Co[87], Fe[87]	20 nm/2:1 [87]	250 Gbits/in^2 [87]
X-ray	$5 \times 5\,mm^2$ [152]	88 nm [155]	Co [152], NiFe [155]	100 nm/1:1 [155]	4 Gbits/in^2 [155]
Interference lithography and electroplating	$50 \times 50\,mm^2$ [164]	60 nm [167,187]	Co, Ni, Fe, NiCr [164,167,187]	600 nm/4:1 [164]	65 Gbits/in^2 [167,187]
Interference lithography and lift-off	$200 \times 200\,mm^2$ [182]	30 nm [167,178,187]	Co, Ni, Fe, NiCr, MnNiAl, Co/Pt [167,173,176,178,181–187]	120 nm/1.7:1 [183]	65 Gbits/in^2 [167,187]
Interference lithography and etching	$30 \times 30\,mm^2$ [167,187]	40 nm [187]	Co, Ni, Fe, NiCr, CoNi/Pt [166,167,169,170,174,187]	120 nm/3:1 [187]	65 Gbits/in^2 [167,187]
Scanning probe pulses	$0.3 \times 0.3\,\mu m^2$ [188,189]	40 nm [188,189]	Co, Ni, Fe, CoCr [188,189]	55 nm/0.8:1 [188,189]	50 Gbits/in^2 [188,189]
Scanning probe chem. vap. dep.	$0.1 \times 0.1\,mm^2$ [200]	10 nm [200]	Fe [192,194,196–198,200–202]	120 nm/6:1 [196]	100 Gbits/in^2 [201]
Nanoimprint	$30 \times 30\,mm^2$ [253,254]	25 nm [253]	Ni [252–254]	400 nm/6:1 [254]	30 Gbits/in^2 [253]
Step growth V-grooved	$30 \times 30\,mm^2$ [228]	60 nm [228]	Ni, NiFe, Co/Cu, NiFe/Cu [224,225,227–231]	280 nm/1.3:1 [227, 229–231]	16 Gbits/in^2 [227–231]

need for a synchrotron radiation facility makes this technique somewhat disadvantageous.

2.3. Interference or holographic lithography

Similar to electron or X-ray lithographies, interference lithography is based on selectively exposing a resist layer. In this case, the interference of two coherent laser beams is the mechanism to expose the resist [141,164–187]. A laser beam is divided using a beam splitter, and the split beams illuminate the substrate from opposite directions, forming an angle 2θ. This procedure creates an interference pattern of sinusoidal intensity. The periodicity, p, of this standing wave is controlled by the beams incidence angle and the laser wavelength, λ, $p = \lambda/(2\sin\theta)$. This procedure produces a pattern of parallel lines. To produce more complex patterns, successive exposures are necessary. For instance, a second exposure, rotating the sample by 90°, produces a square or rectangular array of dots.

Under normal conditions the periodicity can be tuned between 100 and 2000 nm [167,181]. The size of the elements depends on the exposure time and developing conditions. Magnetic features as small as 30 nm have been fabricated [167,168]. The main advantage of this technique is the possibility to expose simultaneously large areas, e.g., magnetic arrays up to $250 \times 250\,\text{mm}^2$ have been produced [169]. Its main drawback is that the possible structures (elements or arrays) that can be obtained are limited to interference patterns, i.e., highly symmetrical ones only.

Similarly to e-beam and X-ray lithography, this technique can be combined with lift off, electroplating or etching.

2.4. Other techniques

2.4.1. Ordered structures

2.4.1.1. Scanning probe lithography. Basically three different fabrication techniques based on scanning probe microscopes (scanning tunneling microscope, STM, and atomic force microscope, AFM) have been used to produce ordered arrays of *magnetic* nanostructures: AFM or STM voltage pulses [188–191], STM chemical vapor deposition [192–202] and STM local electrodeposition [203,204].

In the voltage pulse technique, an AFM (or STM) tip, made of, or coated with, a magnetic material, is brought to within a few nanometers of the substrate. Subsequently a negative voltage pulse (in the range of 5–30 V) is applied during a few ms between the tip and the sample. This negative voltage pulse induces material transfer from the tip to the substrate, creating the desired magnetic structures. The element size depends on the substrate and tip materials, applied voltage, pulse duration, and tip-substrate separation. Using this technique, elements as small as 10 nm can be produced [188–191]. Moreover, the position of the elements can be controlled at will. However, it has a number of disadvantages, such as poor reproducibility (the tip changes after every pulse), difficulty to produce elements other than dots, very slow throughput, and small patternable area (limited by the microscope's scanning length to about a few μm across).

The STM chemical vapor deposition is analogous to the one described in the e-beam direct writing (Section 2.1). A precursor organometallic gas, containing the desired magnetic atom, is introduced in the STM chamber. When the tip is at the appropriate position, a voltage pulse of a few mV is applied between the tip and the substrate. Similar to the electron beam method, this voltage dissociates the precursor gas into a metal mound. The size of the elements depends on the amplitude and duration of the voltage pulse, the distance between tip and substrate and the composition and pressure of the precursor gas [192–202]. Comparing to the previous technique, STM chemical vapor deposition is much more reproducible and allows producing virtually any type of elements. However, it has the disadvantages of slow throughput and small patternable area, with the additional undesirable organic contamination of the fabricated elements.

Finally, if a substrate is immersed in an electrochemical cell and the STM tip is approached to the substrate, the tip can be used as a *local* counter-electrode, allowing for selective nanometer electrodeposition [203,204]. This technique has the advantage of being reproducible and

avoiding organic contamination, however it has the disadvantage of having to work inside an electrochemical cell. Moreover, the typical disadvantages of the other scanning probe techniques, i.e., slow throughput and small patternable area, are still present.

2.4.1.2. Step growth methods. The main characteristics of the step growth techniques are to modify the substrate such that when the magnetic material is deposited it creates the desired nanostructures. The basic design is to create a series of steps on the substrate, either by optical, electron, X-ray or interference lithography and etching [205–221], or by laser focused atomic deposition [222,223]. Subsequently the magnetic material is grown on the substrate, thus isolated patterns of magnetic material are produced on the valleys and plateaus of the substrate steps. This technique is limited by the advantages and/or disadvantages of the method utilized to create the steps on the substrate. In particular, the simple and low-cost standard optical lithography has only been used to obtain magnetic elements down to the 500 nm range, although state of the art optical lithography can reach the 100–200 nm range. Another problem with this technique is that magnetic material is deposited on both the ridges and grooves of the substrate, hence there are two different contributions to the magnetic signal. Two methods have been used to circumvent this problem: (i) deposit the magnetic layer at grazing angle to the substrate, thus the material is only deposited on their side walls [220]; (ii) use lithography to define parallel lines on a substrate and thereafter create periodically V-shaped substrates by selective etching. The deposition of the magnetic materials is then carried out at an angle to the substrate normal, thus the peaks of the V-shaped substrate shadow to some extent the incoming atom flux. Hence, depending on the deposition angle, elements of different size can be fabricated. This technique is designed mainly for long lines [224–232], thus the range of possible structures is very limited.

There are several other variations of the step growth. However, these variations, contrary to the ones just described, have the disadvantage that they are only locally ordered.

(i) One variation is based on growth on miscut substrates. Certain miscut substrates tend to have a very homogeneous step height and width (e.g. Cu, W, Pt or Si), thus suitable to grow lines of magnetic materials [233–240]. However, the thickness of the lines is limited to the step thickness, which in turn can be controlled to some extent by such mechanisms as step bunching [238–240]. Moreover, by low-angle deposition on strained induced SiGe structures, arrays of magnetic dots have also been produced [241].

(ii) A second variation of this method is to produce an ordered array of steps by annealing NaCl crystals in vacuum, which tends to facet the surface of the crystal [242–245]. One advantage is that by changing the crystallographic direction of the crystal, arrays of dots can also be produced [244,245].

(iii) Another variation, *atomic saw* method, is to create steps on the substrate after the deposition of magnetic materials. This method is based on the dislocation slipping induced in some materials when subjected to a plastic deformation. This dislocation slipping creates a series of lattice shifts that transforms to shifted homogeneous parallel stripes [246–250]. In certain cases, arrays of squares can also be obtained [247–250]. The main drawback with this technique is the limited types of structures possible and the minimum size achievable so far (slightly below 1 μm).

2.4.1.3. Nanoimprint. Most of the techniques available to obtain large areas of arrays of nanostructures are usually costly, complex and slow. The nanoimprint technique may have potential to overcome some of these disadvantages. Nanoimprint, uses a mold to physically deform a resist, followed by ion etching [88,251–256]. However, first a master mold of the pattern to be reproduced has to be manufactured of a hard material by conventional electron, X-ray or interference lithography. This master mold can be

reused or copied and this rather simple technique can have a large and fast throughput. Magnetic structures as small as 25 nm with periods of 150 nm have been fabricated using this technique [256].

There are some interesting variations of this technique. For example, in microplow-row lithography, the mold is not just pressed into the resist, but it is dragged to form arrays of lines on the resist [257]. Dragging the mold in different directions can create more complex patterns.

A second example consists of using the mold as a "rubber-stamp". An "ink" (a chemical solution with the desired properties) is applied to the mold, which is subsequently applied on the substrate. This creates a chemical layer on the areas of contact, which can be used as a mask [258,259].

2.4.1.4. Shadow masks. In standard lithography (Sections 2.1, 2.2 or 2.3), templates of the desired patterns are produced using photon or electron sensitive resists deposited on the substrate or the film. Such resist may affect the properties of the substrate or the film. To avoid this, a very thin (e.g. 1 μm) shadow mask with nanometric holes (playing the role of the resist) is placed very close to the substrate. Subsequently, depositing magnetic materials through the holes creates the desired nanostructures on the substrate. Features in the 400 nm range have been fabricated using this technique [260,261]. However, this technique has severe technical difficulties. For example, like any shadow mask technique, the resolution achievable is limited by the mask thickness.

2.4.1.5. Focused ion beam milling. In ion beam milling, a beam of ions (usually ionized inert gases, although other ions such as Ga^+ are often used) is accelerated and collides with the atoms on a surface under processing. If the beam is sufficiently energetic, these collisions cause the ejection or sputtering of the atoms from the surface through momentum transfer, resulting in the removal or milling of the material [262]. The ion beam can be easily focused down to a narrow size, using electromagnetic lenses, as small as few nanometers. Once focused, it can also be scanned across a surface with great precision. Hence, focused ion beams can be controlled to mill any computer-defined pattern on a film directly without the need of resists or masks.

This technique has been utilized successfully to produce rather dense ($\sim$130 Gbit/in^2) arrays of dots from CrCoPt-based recording media films [263,264]. Other structures such as arrays of lines or "antidots" have also been fabricated [265–267].

The main advantage of this technique is the direct-writing capability. However, like e-beam lithography, it is a slow process and needs highly specialized equipment.

2.4.1.6. Radiation damage. Other methods to produce arrays of magnetic nanostructures are based on radiation damage. Most of these processes cannot be strictly considered as producing isolated particles, because they actually only change locally the properties of a material. Here we give some examples of such processes:

(i) Fe migration by laser irradiation: Thin films of Fe–C, Co–C or Fe–Cr were irradiated by an interfering laser standing wave (see Section 2.3). The power of the standing wave is enough to locally heat up the film, which in turn produces a migration of the Fe atoms. This procedure creates Fe-rich lines or dots (ferromagnetic) embedded in a Fe-poor matrix (paramagnetic) [268,269].

(ii) High-energy heavy ion irradiation: Ion irradiation occurs usually at random positions of the sample. However, if a mask is formed on the surface or a focused ion beam is utilized, localized irradiation can be carried out. Following this procedure, Co/Pt multilayers and ordered FePt films were irradiated. Due to the irradiation, the unprotected areas become intermixed Co–Pt or disordered FePt, becoming paramagnetic or at least magnetically softer. Hence, an array of ferromagnetic elements embedded in a paramagnetic (or soft) matrix is obtained [91,130,131,270–277].

(iii) Some of the techniques described as direct writing in Section 2.1, could also be considered as a radiation damage technique [87].

2.4.2. Pseudo-ordered structures

2.4.2.1. Self-assembled nanostructures. There are a wide variety of natural processes which tend to form ordered arrays of nanostructures. However, although most of these processes are ordered locally, they usually do not have true long-range order. Here we mention a few of these processes that have been used in conjunction with magnetic materials, without trying to be exhaustive.

(a) *Heterogeneous nucleation of magnetic atoms on metallic surfaces*: Some simple cases are Co and Ni on Au(1 1 1), Fe and Co on Cu(1 1 1), Co on N_2-adsorbed Cu(1 0 0) and Cu(1 1 0), or Fe–Ag on Mo(1 1 0). For example, Co atoms tend to nucleate at specific sites of the reconstructed Au(1 1 1) surface, hence, forming arrays of Co dots [278–282]; and similarly with Ni atoms [283]. Fe tends to grow at the step edges of the Cu(1 1 1) surface or to form ordered arrays of dislocations to relieve the stress caused by the mismatch, thus forming arrays of Fe lines or dots [284–286]; Co lines can also be obtained with this process [287]. Moreover, N_2 molecules tend to form lines and islands on Cu(1 0 0). If Co is grown on N_2-adsorbed Cu(1 0 0) or Cu(1 1 0), the underlying island or line morphology of the N_2 can be maintained [288,289]. A similar process allows the fabrication of Fe nanowires on stepped Si(1 1 1) using CaF_2 growth as a mask [290]. Also, very regular monoatomic Co nanowires can also grow at the steps of the Pt(9 9 7) surface [291]. Finally, Fe and Ag are immiscible, and when grown on Mo(1 1 0), they tend to arrange in alternating few nanometer wide stripes [292].

(b) *Seeded growth*: Several approaches have been reported. For example, a substrate with an array of nanostructures (not necessarily magnetic) is dipped in an electroplating bath containing the magnetic ions. The existing array acts as a seed for the growing magnetic atoms, which after some time cover the seed particles, therefore forming an array of magnetic particles [293]. A second approach is to use arrays of nanostructures as substrates to deposit magnetic materials at glancing incidence while rotating the substrate. The magnetic material grows then selectively on the seed nanostructure, hence forming arrays of nanostructures [294,295].

(i) *Reverse Micelles*: In this case, the magnetic particles are grown and coated in microemulsions (reverse micelles). These micelles are then deposited onto a substrate and under certain conditions they tend to form an ordered array on the substrate [296–301].

(ii) *Metallic reduction in a magnetic field*: The reduction of salts containing magnetic ions with acids tends to form magnetic nanoparticles. If this process is carried out in the presence of a magnetic field, the particles tend to spontaneously align in long chains [302,303] or arrays [304] of particles.

2.4.2.2. Nanotemplates. There are a variety of techniques available to fabricate nanotemplates other than standard e-beam lithography. These templates differ in material, pattern, feature size, overall template size, periodicity, etc, and can all be used to fabricate other nanostructures.

(a) *Copolymer nanolithography*: This technique utilizes diblock copolymers, which consists of two chemically different polymer chains joined by a covalent bond [305–310]. If the blocks are immiscible, the diblock copolymers spontaneously self-assemble into microdomains. The microdomain morphologies that are useful for nanolithography are lamellae or ordered arrays of cylinders or spheres, whose sizes and separations are of molecular dimensions, of the order of 10 nm. A monolayer of such copolymer ($\sim$30 nm thick) can be spin-coated onto a selected working surface, typically an oxide or a nitride. Using a chemical process such as UV irradiation, one type of the polymer chains can be selectively broken or hardened, leading to the formation of a template of either a porous network or arrays of dots. This template can then be used for pattern transfer, either by direct replication into the sample through etching or used as a growth matrix [307]. The template pore/dot size and the periodicity can be tuned by the size of the polymers used. This technique has been used to fabricate an exchange-biased bilayer structure of nanoporous Fe-network on top of a uniform FeF_2 [309]. Thicker templates (beyond a monolayer) can also be achieved by using an electric field to align the polymers during the copolymer phase separation stage that forms the microdomains. These

templates have been used to electrodeposit arrays of Co nanowires with high vertical aspect ratios (36:1) and high packing density ($2 \times 10^{11}/cm^2$) [310]. The main advantage of this technique is that nanoscale features can be achieved over a macroscopic area ($\sim 10\,cm^2$ or more [305]) cost-effectively.

(b) *Spheres lithography*: In this technique, the substrate is first coated with a chemical solution containing nanometer scale polymer (e.g., latex, polysterene) spheres. Upon drying, a hexagonal close packed (HCP) monolayer or bilayer of spheres is formed. A layer of material is then deposited into the interstitial areas, forming an array of nanodots (e.g., Co) [311–314], which eventually coalesce into a nanoporous template [315,316]. The pore size and pore density are determined by the polymer sphere size. Furthermore, the spheres may be etched into smaller sizes after forming the HCP arrays, therefore altering the pore separations in the template [315]. This technique is capable of obtaining large patterned areas in a quick, simple and cost-effective way. Although large defect-free areas have been obtained using this technique, it is not long-range order by nature. Moreover, the range of types of patterns and pattern conditions is rather limited.

(c) *Alumina membranes*: Porous aluminum oxide membranes have been fabricated by anodic oxidation of aluminum [317,318]. The oxidized film consists of packed columnar arrays of hexagonal cells, each with a cylindrical nanopore in the center. By controlling the electrolyte species, temperature, anodizing voltage and time, one can adjust the pore size, density, and height [318,319]. Beyond the anodization process, the pore size and depth can be further adjusted by etching the oxide in an appropriate acid. The resultant oxide layer has arrays of parallel cylindrical pores, perpendicular to the layer, separated from the unoxidized aluminum metal by a very thin layer of aluminum oxide. This thin oxide layer potentially can be used for single electron tunneling [320]. The porous membrane itself, up to tens of microns thick, can be etched away from the aluminum metal. Typically, high-density pores (1–500 nm in diameter, 10^9–10^{12} pores/cm^2) can be achieved over a macroscopic area ($> 10\,cm^2$) with small pore size variations. The pore separation is comparable to the pore size. These porous alumina membranes have been used as growth matrix for arrays of nanowires of Ni [321–324], Fe [325,326], Co [327,328], NiFe [329] and CoNiCu/Cu multilayers [330], arrays of Fe nanodots [331], or replicating molds [332,333] to fabricate Fe, NiFe or Ni networks [334–337].

(d) *Nanochannel glass template*: Glass templates with regular array of pores have been fabricated using the Taylor process [338]. An acid-etchable glass rod (core) is first inserted into a matching inert glass tube (matrix glass). They are subsequently drawn into a finer filament at high temperature under vacuum. The filament is then stacked in a desirable fashion, refused and redrawn, until reaching the final filament size. The etchable glass cores are then removed, leaving the porous inert matrix glass network that can be cut into thin templates. By controlling the stacking geometry, one can obtain regular array of pores with different symmetries. Templates with pore size as small as 10 nm and packing density of 3×10^9 pores/cm^2 have been achieved [339]. Like the copolymer and alumina templates, the pore separation is comparable to the pore size. These glass templates have been used for replicating the network structure [339], growth matrix for Ni and Co nanowires [340], or as shadow mask for fabricating nanopillars [341].

(e) *Nuclear-track etched membranes*: Porous membranes of polycarbonate or mica have been fabricated by nuclear track etch method [70,342]. When decay fragments from a radioactive source pass through a dielectric material, they leave behind damaged tracks that are chemically more active than undamaged areas. The damaged tracks are then preferentially etched in certain etchants to create pores through the thickness of the dielectric membrane (microns). The pore sizes are controlled by the etching process, variable from several nanometers to microns. However, unlike other templates aforementioned, the pore separation, and therefore pore density, is independent of the pore size. The pore density is determined only by the irradiation process, variable over a wide range from 1 to $10^9/cm^2$. The arrangement of the pores over the membrane is random. Polycarbonate

Table 2
Main parameters of different nanotemplates

Nanotemplate type	Copolymer	Alumina	Glass	Track-etched membrane	
				Polycarbonate	Mica
Pore size (nm)	10	$1–10^2$	>10	$1–10^3$	$1–10^3$
Pore density (cm^2)	10^{11}	$10^9–10^{12}$	10^{10}	$1–10^9$	$1–10^9$
Pore arrangement	Pseudo-order	Pseudo-order	Ordered	Random	Random
Thickness (nm)	30–500	$10^2–10^3$	10^3	10^3	10^3
Temperature tolerance	<150°C	<450°C	<600°C	<150°C	<1000°C

membranes have circular pores, and are commercially available. But they have the undesirable floppiness and a limited tolerance to high temperature. Mica membranes have diamond-shaped pores [343]. They are rigid but fragile. These track-etched membranes have been used as growth matrix for nanowires to study localization [70], perpendicular magnetic anisotropy [344], magnetoresistance [71–75,345–348], magnetization reversal [349,350], tunneling [76], finite size effects [351,352], coupling [353], etc.

A comparison of the characteristics of these nanotemplates are given in Table 2.

3. Magnetic properties

The magnetic properties of nanoparticles are rather difficult to study due to the small signals. In practice, most researchers resort to standard *averaging* techniques to study the magnetic properties of large arrays of "identical" nanoparticles, e.g., vibrating sample magnetometry (VSM) [122,141,160,164–173,354], alternating gradient magnetometry (AGM) [118,136,153,155,162,166,174–178,355–367], superconducting quantum interference device (SQUID) [83,92,93,109,116,118,119,123,160–162,167–169,172,179–181,258,259,357,368–377], magneto-optical Kerr effect (MOKE) [55,102,104,114,115,128,139,152,154,156,163,169,170,182,183,378–394], Brillouin light scattering (BLS) [156,158,385,386,393–395], ferromagnetic resonance (FMR) [119,396,397], neutron diffraction [398], scanning Hall microscopy [399], scanning magnetoresistance (MR) microscopy [94,400–402], or torque magnetometry [83,169,170,358,403]. However, there are also certain advanced *local* techniques for measuring single nanoparticles, such as magnetic force microscopy (MFM) [404,405], micro-SQUID (μ-SQUID) [406,407], Hall bars [408–414], focused-MOKE [114], Lorentz microscopy [415,416], electron holography [417–419], spin polarized STM [420], ballistic electron magnetic microscopy [34], magnetostriction AFM [269,421], magnetic transmission X-ray microscopy [422], or certain transport measurements [423–428]. Some of these local techniques (MFM [56,86,93,94,102,104,106,107,109,110,116,121,123,124,127,128,132,136,137,139–141,144–147,153,155,159,169–173,177,178,180,181,184–186,188,189,192–195,219,258,259,263,264,357–364,366,367,372–376,386–390,403–405,429–445], electron holography [97,419,446,447], Lorentz microcopy [103,108,111,113,117,448–450], Hall magnetometry [192–199,451], μ-SQUID [200–202], magnetostriction AFM [269,421] or transport measurements [33,35,134,445,452]) have also been utilized to characterize arrays.

In studying arrays of nanoparticles, there are additional parameters that complicate the interpretation of the results. Several examples are given below.

(i) The reduced size of the elements implies that polycrystalline systems contain only a finite number of grains. Thus no true averaging of the grain properties is possible [453]. Therefore, variations in grain size or orientation among the elements can lead to a spread in the magnetic properties of the array [55,93,102,124,132,139,140,162,168,178,184,186,218,359,362,364,365,369,375,376,383,387,389,390,412,432,438,454,455].

(ii) Although nominally identical, the elements may still have small differences, either due to the lithography process (usually limited by the polymer chain length) or different grain structures, resulting in different edge roughness or other kinds of random defects [55,93,102,124,132,139,140,162,168,178,184, 186,218,359,362,364,365,369,375,376,383,387, 389,390,412,432,438,454,455]. These defects are of fundamental importance for the magnetization reversal, especially if they are of the order of or larger than the exchange length of the magnetic material [105,383,456,457]. An example of a distribution of coercivity (H_C) in nominally identical dots can be seen in Fig. 3. Note that in the figure, different dots switch at different applied fields, hence the hysteresis loop deduced from the MFM measurements exhibits broad transitions [359].

(iii) The interactions among the elements can also play an important role. For example, the field H_d created by a dipole, with moment m and length ℓ, at distance r is [458]

$$H_d \sim \frac{2mr}{[r^2-(\ell/2)^2]^2} \underset{r\gg\ell}{\rightarrow} \frac{2m}{r^3} \quad (1)$$

for a point along the line of the dipole, or

$$H_d \sim \frac{m}{[r^2-(\ell/2)^2]^{3/2}} \underset{r\gg\ell}{\rightarrow} \frac{m}{r^3} \quad (2)$$

for a point in the direction perpendicular to the dipole. Thus, for example, the field created by a Fe square dot of $100\times100\,nm^2$ and 20 nm thickness, if treated as a dipole of length $\ell = 100$ nm, at distance $r > 1\,\mu m$ can be negligible ($H < 5$ Oe). However, as the distance approaches the $r < 100$ nm regime, the field becomes increasingly larger ($H > 150$ Oe).

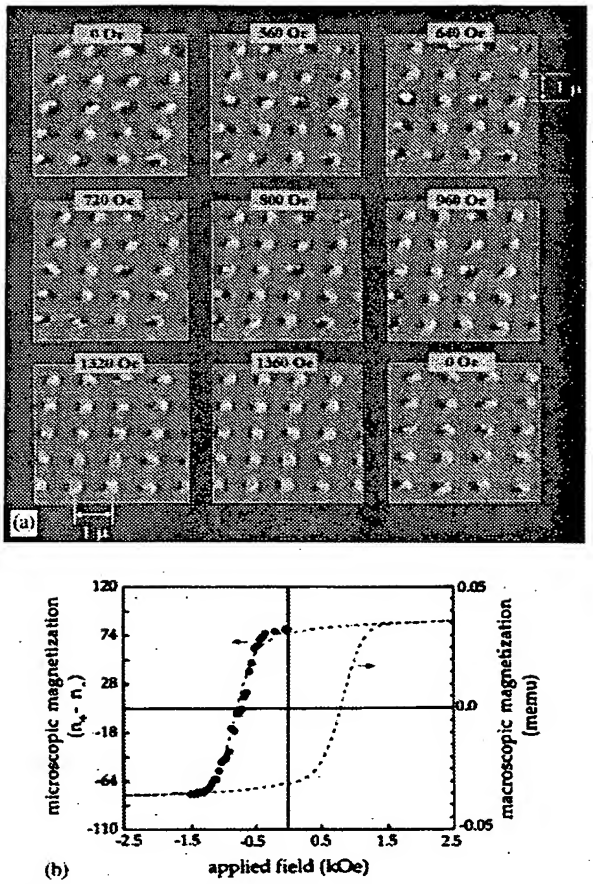

Fig. 3. (a) Microscopic magnetic evolution of $0.2\times0.4\times0.02\,\mu m^3$ Co islands with magnetic field. (b) Microscopic and macroscopic magnetization curves of these islands. The microscopic curve was derived from a set of 80 switching particles from MFM images and the macroscopic curve was obtained on a $5\times5\,mm^2$ sample using an alternating gradient magnetometer. $n_{+/-}$ denotes number of particles polarized parallel or antiparallel with applied field (courtesy Gomez et al. [359]).

In this section, we review the magnetic properties of nanostructured elements. First, we discuss the properties of single dots (based mainly on results from arrays), followed by a more detailed account of the role of interparticle interactions on their magnetic properties and the studies about their dynamic effects. Then, different aspects of the magnetic behavior of lines and wires are described: magnetization reversal processes, magnetic interactions, domain wall resistance and giant magnetoresistance. Finally, the magnetic properties of continuous films with arrays of holes or "antidots" are summarized.

3.1. Single dots

The magnetic properties of single dots depend on the balance of the exchange energy (which

favors spins alignment), the magnetic anisotropy (which favors alignment of spins along a particular direction), and the demagnetizing field (created by the magnetization of the particles, which has be to minimal).

Typical magnetic anisotropies include magnetocrystalline, shape, surface, interface, and other induced anisotropies. Crystalline anisotropy depends on both the type of material and its crystal structure. For example, bulk Fe has cubic crystal anisotropy, while HCP-Co has uniaxial anisotropy. The microstructure also plays an important role, e.g., the anisotropy of a polycrystalline film is given by the average of the different constituent grains [458]. Shape anisotropy is of special importance in nanostructured elements and will be discussed later. Other anisotropies such as induced anisotropy (e.g., due to stress created by substrate–film mismatch [215,216,227–231], or growth in the presence of magnetic fields), and surface [391] or interface [97,169,172,181–183,218,377] anisotropy (due to the change in coordination number of the surface/interface atoms) may also play an important role and, therefore, strongly modify the magnetic anisotropy relative to the bulk material. Note that the effect of surface oxidation [116,168], or the presence of exchange coupling with antiferromagnetic (AF) layers, can be of great importance [128,168].

The demagnetizing field inside a magnetized body is proportional to its magnetization, by a factor determined by the shape of the body [458]. Therefore geometrical details of a magnetic element, such as the in-plane aspect ratio (square vs. rectangular or circular vs. elliptical) [56,83,97,116,175,180,219,357,364,373,388,404–407, 416,430,434,440,441,445,450,453,459,460], shape (rectangular, elliptical, triangular, pentagonal, pointed ends, etc.) [55,97,103,104,108,117,128, 136,380,382,387,390,448,449,461] or thickness (pancake-like vs. columnar) [169,175,180,184,185,371] are all important in determining the demagnetizing field. It is noteworthy that only ellipsoids have uniform demagnetizing fields [458,462]. Hence, basically all dot samples (even those with circular or elliptical in-plane shape) have inhomogeneous demagnetizing fields, as observed in micromagnetic studies [463–475] or demagnetizing field calculations [476] (see Section 3.4 for more details). Fortunately, many of them can be approximated by prolate or oblate spheroids where simple expressions of uniform demagnetizing field can be obtained.

It is well known that, in ferromagnetic materials, magnetic domains can be formed to decrease the demagnetizing fields and thus the magnetostatic energy. The formation of these domains depends on the balance of the exchange and magnetostatic energies, i.e. the gain in magnetostatic energy, due to the reduced demagnetizing field, has to be larger than the energy cost of domain wall formation [458]. However, the formation of domains in magnetic nanoparticles has mainly two critical length scales.

The first one is directly related to the balance of energies in each nanoparticle, and corresponds to the size at which the presence of a domain wall in the material is energetically favorable. It differs for different nanostructured materials since the energy to create a domain wall is proportional to the square root of the anisotropy of the material but the magnetostatic energy is mainly related to the shape and the magnetic moment. This size is usually denoted as *critical single domain radius*, R_{SD} [477]. For example, for spherical single crystal nanoparticles the R_{SD} can range from $R_{SD}(Fe) = 6\,nm$ or $R_{SD}(Co) = 34\,nm$ to $R_{SD}(SmCo_5) = 764\,nm$, for Fe, Co and SmCo5, respectively. However, these critical radii can be considerably reduced for polycrystalline nanoparticles due to the reduced net anisotropy.

The second critical length scale for nanoparticles is the *domain wall thickness* δ, that is, the width of the transition between the uniformly magnetized states of two domains. The domain wall thickness is determined by the counterbalance between the exchange energy (which tends to increase it) and the anisotropy energy (which tends to diminish it) [458], e.g. $\delta(Fe) = 40\,nm$, $\delta(Co) = 14\,nm$ or $\delta(SmCo_5) = 4\,nm$, for Fe, Co or $SmCo_5$, respectively. For nanostructures, it is evident that if the size of the nanostructure is of the order of the domain wall thickness, δ, it can not accommodate a domain wall. Hence, nanostructures with sizes smaller than δ will remain single domain.

However, as previously mentioned "single domain" does not necessarily indicate a state where the nanostructures have uniform magnetization, but rather a state where no domain walls are present. Actually, micromagnetic calculations (discussed in Section 3.4) show that there are many different possible stable "single domain" magnetic structures depending on the shape, size or material of the nanostructures, such the so called "flower state" (with macroscopic net magnetization) or the "vortex state" (with zero net magnetization). However, the different possible magnetization states have the characteristic that the magnetization must be uniform within the *exchange length*, l_{ex}. The exchange length, $l_{ex} = (A/\mu_0 M_S^2)^{1/2}$, is the distance where atomic exchange interactions dominate the magnetostatic fields (A being the exchange constant, μ_0 the vacuum permeability, and M_S the saturation magnetization of the material), and is rather similar for most magnetic materials [477], (e.g. $l_{ex}(Fe) = 1.5\,nm$, $l_{ex}(Co) = 2\,nm$ or $l_{ex}(SmCo_5) = 4.9\,nm$, for Fe, Co or $SmCo_5$, respectively). Thus, a nanostructure with a size of the order of l_{ex} should have a uniform magnetization state, i.e. a "true" single domain state.

To put the two length scales into perspective, although the single domain critical size could be exactly calculated from energy considerations, knowing the anisotropy, shape, etc., the domain wall size is often comparable to, thus a good measure of, the critical size. The exception to this is when the anisotropy is very strong, where the domain wall width may be a fraction of the single domain critical size from rigorous energy minima calculations [458]. It is important to point out that the above considerations are only first order estimates to get an intuitive view of the processes involved in domain formation in nanostructures. For example, concepts developed for bulk ferromagnets (e.g. Bloch walls) are applied to nanostructures and effects mainly relevant in nanostructures (e.g. surface anisotropy) have been neglected. One clear example of the effects of oversimplification is permalloy nanostructures. Bulk permalloy has a domain wall thickness of about $\delta(\text{Permalloy}) \geqslant 500\,nm$. However, permalloy nanostructures of dimensions considerably smaller than δ(Permalloy) have been found to be able to maintain several magnetic domains [108,155,405].

Note also that for the remaining of the text we refer to "single domain state" to all magnetization configurations with no domain walls and a non-zero net magnetization, even those that are not completely uniform (e.g. flower state).

The main effects on the magnetization state of single dots are sketched in Fig. 4. One of the basic properties of magnetic nanodots is the reduced number of magnetic domains at remanence (i.e., at zero applied field after saturation). At constant temperature, if the size of the dot is sufficiently small, it becomes "single domain" [55,56,88,93,94,106,107,109,115–117,121,123,124,127,132,139,141,144,146,147,155,169–173,177,180–185,192–195,218,219,251–255,357,359–363,373–377,380,387,388,390,401,402,404,405,429–434,436–440,442,443,445,446,448,450]. The critical size for a single domain element depends on the material, its microstructure, and the particle shape, as discussed and also evidenced by the "phase diagrams" of various systems [115,155,367,

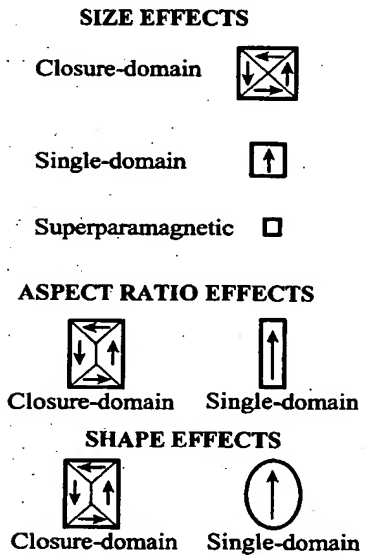

Fig. 4. Schematic illustration of some of the typical effects that changes in size, aspect ratio and shape can produce on the magnetic configuration at $H = 0$ (for the same magnetic material at constant temperature).

404–407,478,479]. However, there are several general features about these domain states:

(i) The remanent state is essentially metastable, thus depends on the magnetic history of the sample. For example, it may have a different magnetic domain configuration than the virgin state [123,140,169,178,377,389,404, 405,429,480,481]. Moreover, the magnetic domains at remanence can depend on the magnitude and direction of the last applied field [122,153,175,178,354,367,389], as can be seen in Fig. 5.

(ii) If the shape of the dots is not an ellipsoid, the demagnetizing field is non-uniform, i.e., not all the spins are parallel to one another. This effect is minimal for circular or ellipsoidal dots, but maximal for square or rectangular dots. As a consequence, elliptical dots should reach single domain states at remanence for much larger elements and smaller length-to-width ratios (or lateral aspect ratio) than rectangular dots of the same material and lateral aspect ratio. However, there are no systematic studies of this issue. Due to the sensitivity of the magnetic properties of dots on the fabrication process (which affects the microstructure or edge roughness) and other parameters (e.g., thickness), it is virtually impossible to draw any conclusion from the existing results on similar systems.

(iii) For large dots, domains are formed so as to minimize the external magnetic flux and thus the demagnetizing field (closure domain [102,103,108,109,116,123,136,183,186,375,386, 389,404,405,421,441,446–449] or vortex states [55,83,97,102,110,113,115,155,174–178,363, 364,369,373,374,389,419,444–446]). Dots with sharp corners produce large magnetic flux at corners (much larger than ellipses), thus it is energetically favorable to form domains to reduce the demagnetizing field. Consequently, in principle, it should be harder to keep a single domain state in square or rectangular dot than in circular or elliptical ones. However, other factors, such as crystalline anisotropy, also play an important role.

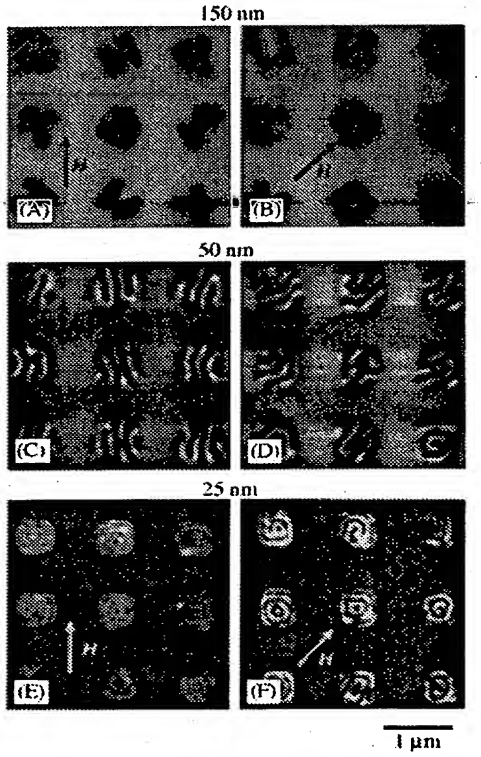

Fig. 5. MFM images in zero applied field after parallel demagnetization along the side of the dot for (a) 150 nm thick, (c) 50 nm thick, and (e) 25 nm thick Co dot arrays and after parallel demagnetization along the diagonal of the dot for (b) 150 nm thick, (d) 50 nm thick, and (f) 25 nm thick Co dot arrays (courtesy Hehn et al. [153]).

Many other properties of magnetic dots stem from their domain structures. On the one hand, single domain dots tend to have larger coercivities than corresponding continuous films [55,83,132,138,141,152,160,163,169,175,176,182,183, 218,354,379,380], due to the change in reversal mechanism (e.g., from domain nucleation to coherent rotation) and/or the increase in demagnetizing field. On the other hand, systems with closure domain structure or vortex states will have reduced remnant magnetization [136,175, 176,358,375,380,381]. In other words, the magnetization process, and thus the hysteresis loop, may be radically different between dots of different sizes and continuous films of the same material.

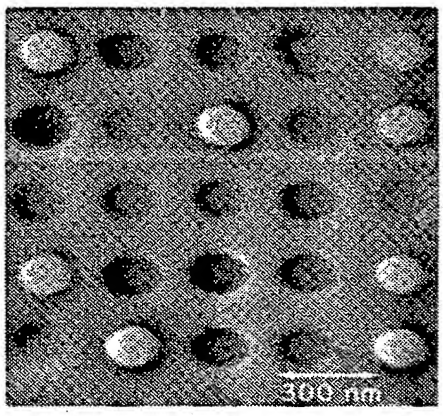

Fig. 6. MFM image of an array of Co dots which are 70 nm in diameter and 100 nm tall. The symmetry of the images shows that the moments are out-of-plane (courtesy Fernandez et al. [183]).

Another important property of the dots is the presence of new anisotropies absent in continuous films. There are essentially four such anisotropies: (i) the most important is related to the shape of the dots (shape anisotropy). Strictly speaking shape anisotropy is not a new anisotropy, since it is also present in bulk and thin film ferromagnets. However, shape anisotropy reaches a more critical role in nanostructures, since it is one of the most important aspects determining the magnetic state of the nanostructures, especially for polycrystalline systems and systems with small magnetic anisotropy. In these cases, the shape anisotropy becomes much larger than the intrinsic anisotropies and can therefore dominate the magnetic behavior of the system. For example, polycrystalline rectangular or elliptical dots tend to have the easy axis along the long axis of the elements [458], or columnar dots along their length (Fig. 6); (ii) surface anisotropy which becomes pronounced in dots where the surface-to-volume ratio is high. The reduction in coordination numbers of the surface atoms can introduce frustration and spin disorder [482–484]. Even antiferromagnetic nanodots could develop net magnetizations at very small sizes [485,486] (iii) The configurational anisotropy is related to the small deviations of the spins from the parallel state at the corners of non-ellipsoidal dots, due to the non-homogeneous demagnetizing field [55,378,380,382]; (iv) as will be discussed later, the interactions between dots can also induce new anisotropies in the system [156,381,394].

A more subtle effect is the quantization of the spin wave spectrum as observed by Brillouin light scattering (BLS), where only certain spin wave modes can exist due to small size of the dots [158,386,395]. Similar effects have been observed by ferromagnetic resonance (FMR), where multiple resonance appear for nanostructured dots [396,397], as can be observed in Fig. 7. These effects are probably related to quantization of spin waves by the lateral size of the dots.

Finally, for dots of small volume V, the anisotropy energy, $K_u V$, becomes comparable to or smaller than the thermal energy, $k_B T$, and they become "superparamagnetic" [168,179,180,381, 487,488]. The thermal fluctuations are sufficient to overcome the energy barriers that separate the different spin states within the time frame of the measurement, thus the dots are no longer ferromagnetic (FM) [458]. However, they become again ferromagnetic for sufficiently low temperatures [168,180]. This effect should be easier to observe in the smallest possible dots made with materials with low-crystalline anisotropy (e.g., permalloy-$Fe_{20}Ni_{80}$) and shapes with small shape anisotropy (e.g., disks) [180,382].

3.2. Interaction in arrays of dots

Due to the $1/r^3$ dependence of the dipole–dipole interaction, the effects of the interactions between dots depend strongly not only on the distance between the centers of the dots but also the distance between edges of the dots. Moreover, the effects of interaction, e.g. changes in the coercivity, will be more significant in systems with a small crystalline and shape anisotropy, i.e., with small saturation and coercive fields. In other words, it is easier to observe an effect of a 20 Oe interaction field in a system with a coercivity of 100 Oe than one of 3000 Oe. Another important factor influencing the interaction among dots is the magnetization state of the dots. Usually the dots are assumed to be single domains, so they can be approximated by dipoles. However, often the dots are in

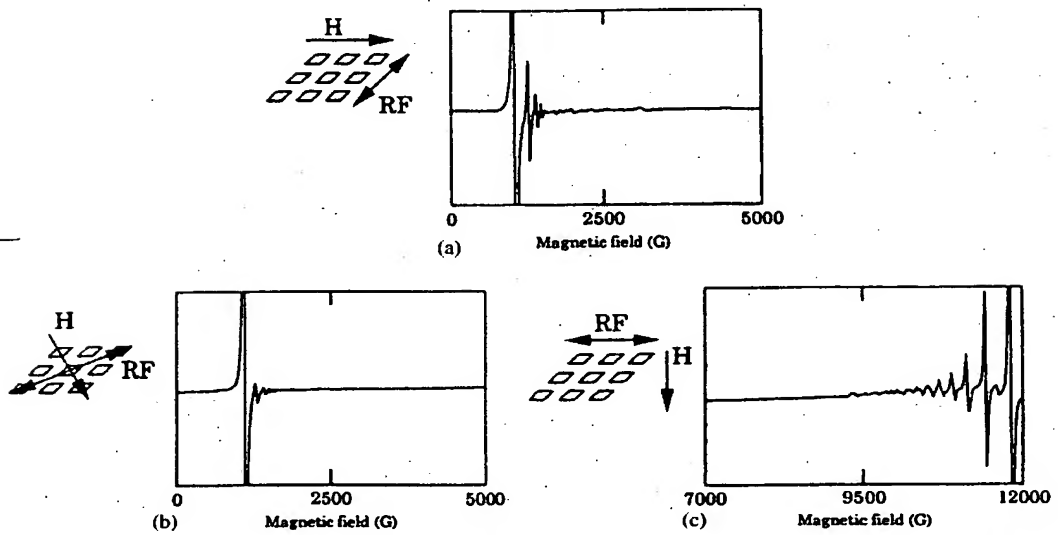

Fig. 7. Microwave absorption of 60 nm thick $Ni_{80}Fe_{20}$ square dot array with a width and a spacing of 1 μm (courtesy Maeda et al. [397]).

magnetization states with reduced or no external flux at remanence (e.g., closure domains or vortex state). Such systems should have negligible interactions at fields close to $H = 0$ due to the $m \sim 0$ state and the corresponding lack of stray fields. Nevertheless, interactions could become significant as the external field is increased, resulting in non-zero dipolar moments; and they are often important for large applied fields when the dots become saturated. It is noteworthy that, due to the relation between the dipolar field (H_d) and the magnetic moment (Eqs. (1) and (2)), the interaction field between two single domain dots depends on their thickness; e.g. if the thickness is reduced by one half, H_d will also be reduced to half. Similarly, if the material of the dots changes, the interaction field will also change; e.g. the interaction field between two single domain Fe dots is about 3.5 times larger than if the same dots were made of Ni, since $M_S(Fe)/M_S(Ni) \approx 3.5$ [489]. The direction of the moment, e.g., in-plane or out-of-plane, also plays an important role due to the different kinds of dipolar fields. Finally, another factor strongly affecting the interaction is the number and distribution of nearest neighbors, e.g. one dot has four nearest neighbors in a square lattice, but six in a hexagonal lattice.

Hence, due to a combination of the above factors, although some researchers claim negligible effects of interactions in arrays of dots [116,152,163,168,172,175,217,260,261,359,384,391], others describe drastic changes [55,83,88,103,111, 117,121,122,127,131,137,147,155,156,158,167,170, 173,180,218,271–274,278–280,354,360,361,370,375, 376,381,384,393–395,397,421,430,434,444,448,449, 451]. In this section, we describe some of the observed effects of dipolar interaction.

To give an intuitive picture, to first order, of the effect of the dipolar interaction, we first examine two dipoles with moments parallel to each other but perpendicular to their separation (Fig. 8(a)–(b)). The dipolar field (H_d, Eq. (1)) created by one on the other is opposite to the magnetization direction and thus tends to reverse it. Assume that the dipoles have slightly different switching fields, H_{SW1} and H_{SW2} ($H_{SW1} \cong H_{SW2} \cong H_{SW}$). Note that the switching fields for dipoles are equivalent to the coercive fields for realistic magnetic entities. When an external reversal field (H_{Appl}) is applied against the dipole moment direction, one of the

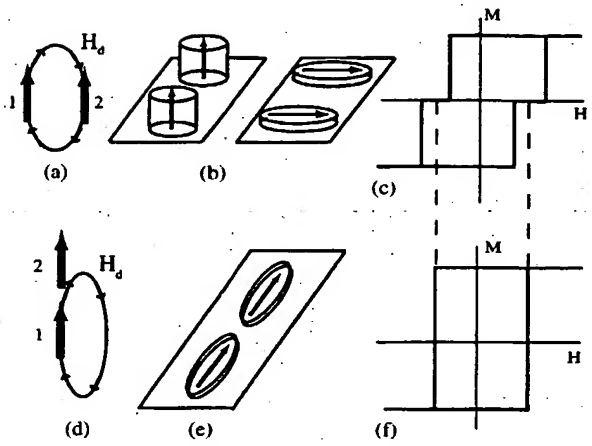

Fig. 8. Sketch of the effect of dipolar interaction between two magnetic moments. (a), (b) and (c) represent respectively the dipolar field, examples of magnetic dots configuration and hysteresis loop for the case where the moments are parallel to each other but perpendicular to their separation. (d), (e) and (f) represent the case where the magnetic moments are not only parallel to each other but also parallel to the separation distance.

dipoles will switch sooner at $|H_{SW1}| - |H_d|$, where H_d is the dipolar field created by the second dipole. Once switched, this dipole's dipolar field now helps to stabilize the unswitched dipole. So the second dipole reverses at $|H_{SW2}| + |H_d|$. This means that the hysteresis loop, instead of having a single jump of magnetization at H_{SW} (as for a single dipole), will have two jumps, at $|H_{SW1}| - |H_d|$ and $|H_{SW2}| + |H_d|$ (Fig. 8(c)). The switching field of the interacting dipoles is still essentially H_{SW}. Nevertheless the switching width (ΔH_{SW}) changes from zero for an isolated dipole to $2|H_d|$. Had both dots been *truly* identical ($H_{SW1} = H_{SW2}$), they would feel exactly the same net field at all times and would consequently switch simultaneously. Therefore, the observed switching field should be smaller than that for a single dipole. It is noteworthy that this simple picture depends notably on the relative orientation of the spins [490–499]. For example, two collinear dipoles (i.e., head-to-tail dipoles, see Fig. 8(d)–(e)) would have a switching field *larger* than the individual dipoles, since in this case the dipolar field is in the direction of the dipole's moment (see Fig. 8(d)), hence opposite to the applied field before switching. Consequently, in this case H_d tends to stabilize the unswitched dipoles. Moreover, ideally in this case the switching width ΔH_{SW} should be zero (Fig. 8(f)). Even if there was some difference between the switching fields in the individual dipoles, this non-zero ΔH_{SW} will be reduced due to the dipolar field.

In arrays this simple intuitive picture becomes more complex. Depending on the configuration of the dipoles, the dipolar field amplitude and direction could be different for different dots. For example, in a hexagonal array of dipoles with magnetization aligned out-of-plane, the dipolar field felt by the central dipole due to its nearest neighbors would be 6 times of that from each. However, the dipolar field of the *same* array when they are magnetized in-plane would be completely different and even more complex. For example, when a dipole in such an in-plane array is switched, the dipolar field not only changes its amplitude (as in the case of out-of-plane moments) but also its direction. Another related consequence of the array geometry is that the switching field of one dipole will depend on the number of switched neighbors [88,103,117,451]. Also notice that the dipolar interactions depend on the size of a finite array [385,500] and that in many cases it may not be enough to only consider the effects of nearest neighbors [501].

It must also be considered that nanostructured magnetic dots have a finite size, consequently the dipolar field created by a dot may be quite different from the one created by a dipole, especially at short distances. Moreover, the dipolar field felt by a dot may depend on the position, i.e., larger at one edge than at the center [414]. Hence, in most cases magnetic dots cannot be strictly considered as dipoles. This effect is best seen in large dots where the domain structure of the dots depends on the distance between dots, i.e. due to the non-uniform dipolar field felt by the dot [137,502–505]. Although in many cases the dipole approximation can give a valuable intuitive picture, it is important to stress that, the simple dipolar approach, i.e. assuming that the nanostructures behave like dipoles, is only valid if the size of the nanostructure is much smaller than the distance between nanostructures. To carry out

a more accurate estimate of the effects of the dipolar fields in arrays of nanostructures, the magnetostatic self-energy, due to the demagnetizing field, needs to be evaluated, $W_{ms} \propto \int M(r) H_{Dem}(r)\, dv$, where $M(r)$ is the spatial distribution of the magnetization and $H_{Dem}(r)$ is the local demagnetizing field at each point [462,506,507]. The stable magnetic configuration can subsequently be found by minimizing W_{ms}. Nevertheless, one has to take into account that $M(r)$ and consequently $H_{Dem}(r)$ depend on the position. For example, if we assume an array of uniformly magnetized disks, the magnetization, $M(r)$, can be defined as $M(r) = M_S$ at the disks and $M(r) = 0$ between the disks [507]. However, if more realistic magnetization states are used for the nanostructures the evaluation of the self-energy integral becomes increasingly complex.

It is noteworthy that we have only considered dipolar effects. However, in certain cases, higher order terms (e.g. quadropolar) may become relevant, especially when $m \sim 0$ [508–510]. Moreover, exchange effects are in theory possible if the dot separation is small enough to allow tunneling (on the order of 1 nm) [511,512]. Although no ordered arrays have attained these small separations, some pseudo-ordered arrays are approaching this limit [298–301,513].

3.2.1. Direct observation

Electron holography has been used to probe the fringing fields of magnetic nanostructures. This technique relies on the interference of a reference electron beam and another probing beam that goes through the sample, both of which were split from one original beam. The phase shift observed in the interference pattern is proportional to the flux emanating from the element. However, since the fringing fields exist in 3D, electron holography renders a 2D *projection* of the 3D field. In specimens with complex geometries, fringing fields in excess of 1500 Oe have been observed at distances 15 nm away from the elements [514]. Measurements on arrays of Co dots have shown that the fringing fields strongly depend on the magnetization state of the dots. Dots with small net moments (Fig. 9), e.g. closure domains or vortex states, have negligible stray fields, while single domain dots have much larger stray fields [97,419,446,447,514].

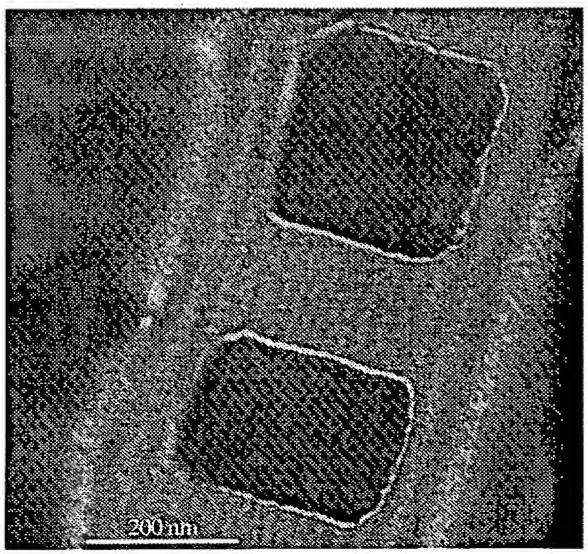

Fig. 9. Representative off-axis electron hologram showing two patterned Co nanostructures from linear chain of elements (courtesy Dunin-Borkowski et al. [419]).

3.2.2. Changes in coercivity

One of the reported effects of dot interaction is the change in coercivity, which corresponds to the switching field discussed under the dipole context (Section 3.2). Contradictory results have been reported in different materials (e.g., Co, Ni, $Ni_{80}Fe_{20}$) [55,83,88,103,111,121,147,155,218,360, 361,370,376,381,384,430,434,446,448,449,451], or for differently shaped elements or arrays of the same material (e.g., $Ni_{80}Fe_{20}$) [55,83,103,111,155, 218,360,361,370,381,448,449]. Coercivity enhancement, reduction or insensitivity to dot separation can be found in the literature. For example, an increase of H_C of 800 Oe has been reported for pairs of rectangular Co dots when the center-to-center distance between dots has been decreased from 1 μm to 150 nm (with a corresponding 50 nm gap between dot edges) [88]; while rectangular arrays of rectangular $Ni_{80}Fe_{20}$ dots exhibit a decrease of 100 Oe in H_C when reducing the center-to-center distance from about 1 μm to 200 nm (50 nm gap) [360,361] (see Fig. 10); or no

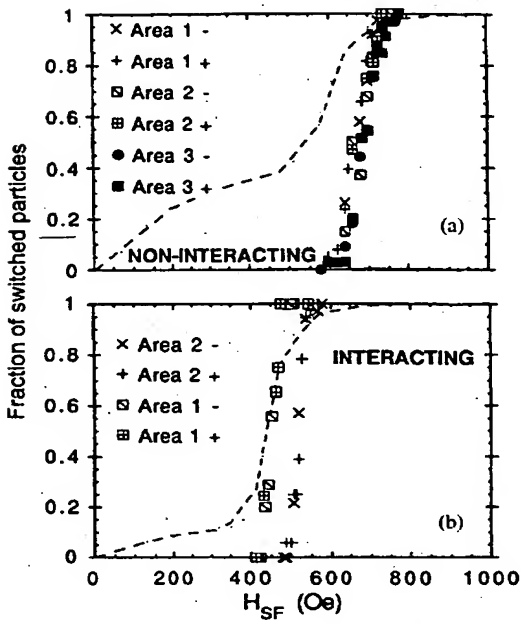

Fig. 10. Fraction of switched particles reversed from their original saturation direction as a function of switching field (H_{SF}) in (a) non-interacting array and (b) a weakly interacting array. Approximately 100 particles were observed in three different regions of array (a), and 90 particles in two different areas of array (b). "+" in the legend indicates data taken starting from saturation in positive field direction, and "−" indicates initial negative field saturation. The dashed curves display AGM measurements of the fractional change in the remanent magnetization from its saturated value, for the same arrays (courtesy Gibson et al. [360]).

change in the collective coercivity has been observed in a linear array of rectangular $Ni_{80}Fe_{20}$ dots when reducing spacing from 2 μm to 250 nm (50 nm gap) [103]. Hence, these discrepancies are probably due to a number of factors, such as the type of array, magnetization state of the dots, switching mechanisms, and the fact that the nanodots are *not* simple dipoles. We have to stress that the field resulting from the dipolar interaction depends on the magnetization state of each dot, which in turn depends on the effective field of the neighboring elements. Consequently, the dipolar fields will change during the magnetization process. An example of the complex behavior due to interaction can be found in Fig. 11, where the switching mechanism appears to change (from rotation to vortex creation) as the dots are brought closer together with the resulting reduction in coercivity.

3.2.3. Switching width

Most studies seem to agree that, as discussed for the case of two parallel dipoles, dipolar interaction tends to change the switching width ΔH_{SW} as compared to isolated dots. However, similar to the results on H_C, reports of increase [88,103,111, 117,448,449,451,515] or decrease [121,360,361,376, 384,430,434] of ΔH_{SW} can be found in the literature. An example of increase of ΔH_{SW} with decreasing dot distance can be seen in Fig. 12. Again these discrepancies can be attributed to the different types of arrays (linear, square, hexagonal) and the reversal mechanisms for the dots (coherent rotation, domain formation, vortex formation). Unfortunately, generalization of the behavior would be rather complex with the limited number of studies in completely different systems.

Note that a consequence of the intuitive interacting dipole model described earlier is that the loop will become more sheared while maintaining the coercivity [455,516,517]. This shearing is indeed observed experimentally for some interacting systems [155,167,171,173].

3.2.4. Induced anisotropies

In principle the dipolar interaction fields in symmetric arrays (e.g., square or hexagonal) should be isotropic, hence there should be no angular dependence of the interaction field. However, Brillouin light scattering measurements of a square array of permalloy dots exhibited an anisotropic in-plane coupling. The authors attributed this anisotropy to the dipolar interaction between unsaturated parts of the dots due to domain formation [156,393,394], although quadrupolar effects could result in similar induced anisotropies [509]. Others claimed the anisotropies to be related to slight shape anisotropies of the individual dots [385]. These results stress the importance of the magnetization state of the dots. Moreover, if the lattice itself has low symmetry (e.g., rectangular), anisotropies should

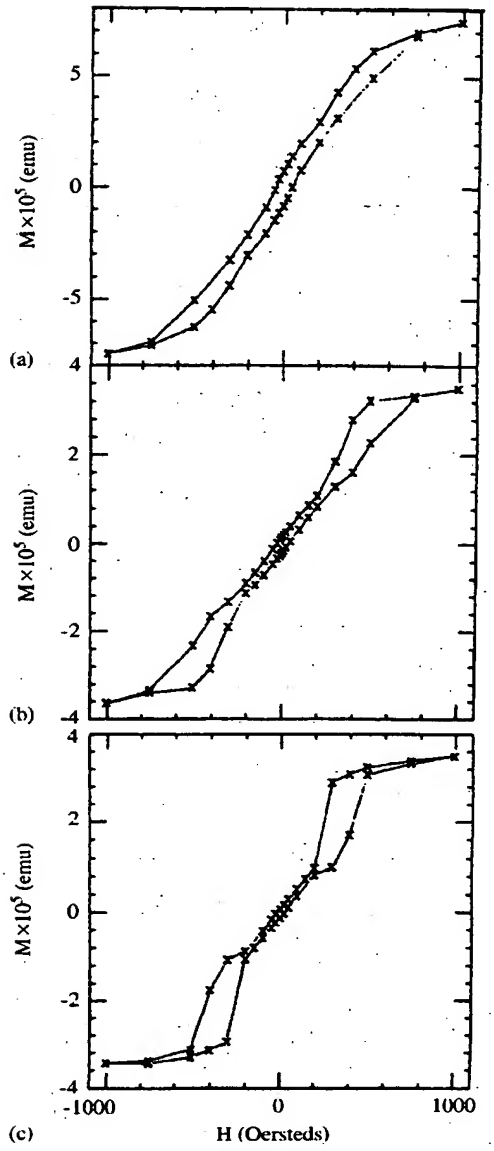

Fig. 11. Hysteresis loops for different arrays of rectangular ($a \times b$) permalloy particles. In this series the particle size was held constant at $0.21 \times 0.41\,\mu m^2$ and the center-to-center interparticle spacings were varied as follows: (a) 1.7 μm along a direction and 2.2 μm along b direction, (b) 0.8 μm along a and 1.0 μm along b, (c) 0.5 μm along a and 0.6 μm along b. Note that although the coercivity (taken as usual where $M = 0$) does decrease with decreasing particle spacing, the other changes in the loop indicate a complicated magnetic behavior (courtesy Smyth et al. [83]).

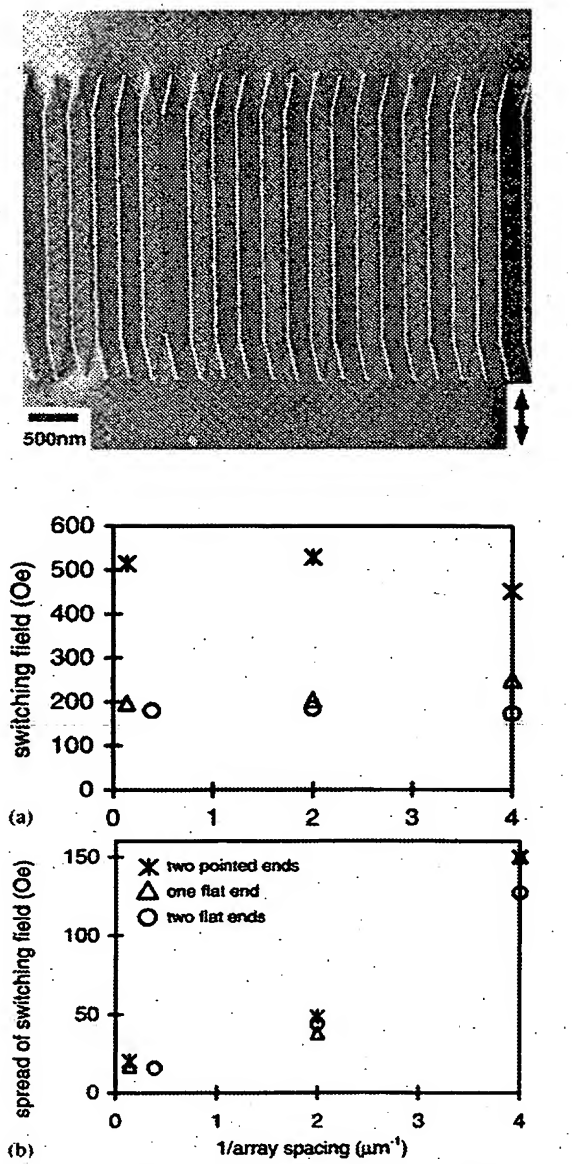

Fig. 12. Top panel shows a Foucault image of NiFe elements with two pointed ends in an array with 250 nm center-to-center spacing. Component of induction mapped in direction of arrow. The bottom panel presents the effect of element spacing for NiFe elements 200 nm wide and 26 nm thick on (a) the switching field, and (b) the standard deviation of switching field measurements (courtesy Kirk et al. [103]).

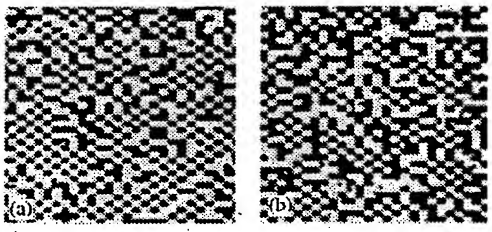

Fig. 13. Demagnetized states for arrays of rectangular (1.35 μm × 1 μm) Pt/Co/Pt dots separated by weakly magnetic lines of width (a) 60 nm and (b) 100 nm. The image is over a $34.6 \times 34.6\,\mu m^2$ area and obtained by Faraday rotation magneto-optical microscopy (courtesy Aign et al. [271]).

be expected. This has been demonstrated in rectangular arrays of permalloy dots, where the effects of the interaction along the short and long axes are completely different [55,381], as discussed in the next section.

3.2.5. Collective behavior

The minimum energy state for two parallel dipoles is different if they are collinear (e.g., two out-of-plane dots, Fig. 8(b)) or coaxial (e.g., two in-plane elliptical dots along the ellipse main axis, Fig. 8(e)), while the first is *antiferromagnetic* the second is *ferromagnetic*. The minimum energy states due to the dipolar field for different kinds of spin lattices have been studied theoretically. Similarly to the two-dipole case, the minimum energy state depends on the exact spin arrangement and the size of the system [500,518–522].

It has been frequently reported that the switching of dot arrays with in-plane magnetization takes place along rows [111,122,376,384,451,523]. This could be a consequence of the fact that the minimum energy state for head-to-tail dipoles in a row is a FM state [508]. However, for parallel rows in a square lattice, the minimum energy state is with antiparallel rows (i.e., essentially an "AF" state). Moreover, as can be seen in Fig. 13, studies of the magnetization state of arrays of out-of-plane dots after ac-demagnetization (i.e., low-energy state) exhibits a checkerboard state (with spins up and down) [127,173,180,218,263,264,271]. This is in agreement with theoretical studies of a square lattice of spins that predict an AF minimum energy state [498,499,501,506,507,524,525].

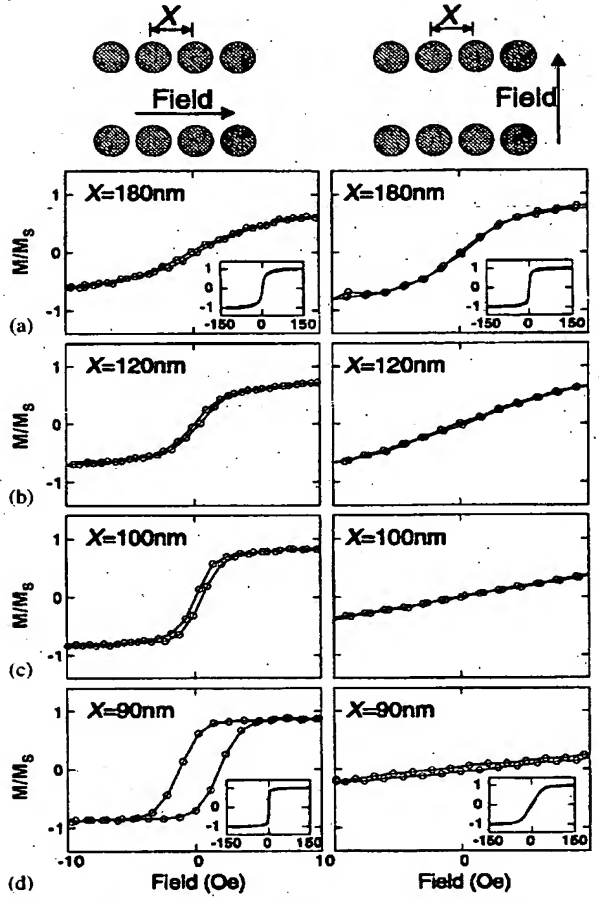

Fig. 14. Hysteresis loops measured in arrays of circular supermalloy $Ni_{80}Fe_{14}Mo_5$ particles for different lattice spacings and applied field directions. All loops were measured within the field range ±150 Oe: the large panels show high-magnification views around zero field; insets show the full measured loop. The vertical axis of all loops is magnetization normalized by the saturation value. Panels (a) and (b) show the lattice to be magnetically disordered. Panel (d) shows the lattice to be magnetically ordered. Panel (c) is near the transition point between ordered and disordered lattices (courtesy Cowburn et al. [381]).

However, the ground state may be more complex if the dots present no anisotropy axis (e.g. polycrystalline disks) or random anisotropy axes [525–527].

Moreover, the competition between different effects may produce some unusual phenomena in the magnetic properties of arrays of magnetic dots.

For example, switching from in-plane to out-of-plane behavior have been observed in certain systems when decreasing interdot distance (i.e., increasing the dipolar coupling) [164,171,173,506] or increasing temperature (i.e., reduction of the crystal anisotropy) [354,403,524].

However, a more striking demonstration of these collective effects is shown in Fig. 14 for permalloy dots in a rectangular lattice. The dots are sufficiently small to be superparamagnetic at room temperature for large separations. If the field is applied along the short axis of the rectangular lattice, as the dot separation is reduced the dots interact due to the increased dipolar field. Thus, the originally random (superparamagnetic) moments, align along the row of dots, evidenced by an increase of remanence and coercivity. This effect is the strongest for the smallest distances achieved (20 nm gap between the edges of the dots). At this distance, the row of dots becomes fully FM with essentially 100% remanence [55,381]. This is in agreement with the minimum energy state of a row of dipoles, which should have a FM arrangement as the low-energy state. Interestingly, if the field is applied along the long axis of the rectangular lattice, the system becomes increasingly less magnetic, although the individual rows are ferromagnetically aligned. This implies that the moments of the dots in each row, as a whole, align antiferromagnetically to the magnetization of the dots in the next row, as expected from the low-energy state of such a dipole arrangement (similar to two dipoles with out-of-plane moments).

It would be interesting to study the temperature dependence of these effects, since if there was a phase transition one would expect a temperature-dependent critical dot separation for aligning the moments.

Finally, note that the properties described in this subsection are possibly related to the "superferromagnetism" effects studied in pseudo-ordered and disordered systems [241,284,394,513,528]. Moreover, the spin-glass like states ("superspin-glass states") observed in disordered systems with frustrated dipolar interactions [528] could also be relevant for systems with random anisotropy axes.

More complex magnetic systems, such as hard magnetic dots embedded in a soft magnetic matrix [91,130,131,268,270–277,529], fine particles [530], or magnetic dots deposited on ferromagnetic [195] or antiferromagnetic layers [331], are not being discussed in detail in this review. Such systems are often strongly affected by the specific exchange and dipolar coupling between both magnetic phases, making the analysis of their properties increasingly complicated.

3.3. Dynamic effects

The dynamic effects in magnetic nanostructures are becoming increasingly important at extremely small physical length scales and time scales [531]. Issues such as magnetization reversal mechanisms, thermal stability, and ultrafast switching are both fundamentally interesting and practically important, for example, in ultrahigh density and high data rate magnetic recording and magnetic memory applications. Over recent years, advancements in nanolithography and magnetic characterization (imaging, μ-SQUID, etc) have enabled the study of individual magnetic entities [88,349,368,406,532–535], whose properties are often masked in a collection of entities with certain size and shape distributions. In the following, we will first discuss the dynamic effects in individual magnetic entities, then the collective behavior.

In typical magnetization reversal studies on individual magnetic entities, a reversal magnetic field is applied opposite to the magnetization direction, and the reversal is characterized by MFM [88,533], Lorentz-TEM [534], μ-SQUID [349,536], Kerr microscopy [368], or scanning electron microscopy with polarization analysis (SEMPA) [260]. Although most of these techniques do not have ultrafast time resolution, the short time scale is indirectly extrapolated from the measurements. However, the exact reversal mechanism is still difficult to understand. Even in the simplest case of single-domain particles, there are deviations from the Néel–Brown model of thermally assisted magnetization reversal over a single potential barrier [198,533,537,538]. Magnetization reversal can assume curling and buckling modes, or in general a complex path in the configurational space [533]. Such deviations have been attributed to defects, ends, and other imperfections in real samples, and

have been shown to vanish in well-prepared single-domain particles [536]. Under such collinear field-magnetization configuration, the reversal speed is limited to the nanosecond level [533,536,537,539].

Alternatively, the reversal can be achieved by precession of the magnetization, induced by a pulsed reversal field applied perpendicular to the magnetization [540–546]. For micro and nanomagnets, the reversal details are measured by Kerr microscopy [540,542,543], spin-dependent tunneling and magnetotransport measurements [544,547–549], or time-resolved X-ray magnetic circular dichroism [550], which provide direct as well as indirect characterizations at the extremely short time scale. In particular, picosecond time-resolved Kerr microscopy provides powerful insights into the spatiotemporal evolution of the magnetization reversal processes [540,542,543]. Much shorter reversal time scale due to the precessional reversal mode, in the picosecond range, has been observed [540,542–544]. It has also been shown that the demagnetization field may be used to assist the reversal via the precession motion [545]. Thus a moderate field-strength of a few kOe, well within the typical magnetic recording write-head field range, is sufficient to induce such ultrafast reversal via precession. Although the precessional mode is clearly associated with the symmetry of the underlying equilibrium spin configuration [542], much details still awaits further understanding.

For arrays of magnetic entities, the collective behavior is also important. The shift of the spin wave frequency observed by BLS is the most clear dynamic effect of interdot interactions [395], in agreement with theoretical predictions [551,552]. Furthermore, small changes in the FMR resonance spectrum have also been reported [397]. Although as mentioned above it is not easy to distinguish anisotropies arising from interactions, with those arising from the individual dots [385].

3.4. Micromagnetic calculations in nanostructured elements

As mentioned in the different sections, some of the magnetic properties of arrays of nanostructured dots have been studied theoretically, both by micromagnetic calculations and analytical modeling [168,218,455,490–492,498,499,502–507,509, 516,517,523,524,526,527,551–556]. The models are often tailored to specific cases, and consequently they are difficult to generalize. However, the main models and some representative results deserve to be considered.

The ability of micromagnetics to obtain a theoretical approach to understand the magnetic behavior of magnetic materials [557–565] has been used to address the magnetization reversal in patterned dots or elements with submicrometric dimensions, with particular emphasis on the effects of the shape, size, or material of the elements. In these studies, each magnetic element is usually divided into a Cartesian array of parallelepiped cells, and a magnetization vector at the center of each cell (M_i) is defined (with $|M_i| = M_S$). In order to consider $|M_i| = M_S$ within each cell, the size of each individual cell is usually taken to be the order of the exchange length, l_{ex}. The equilibrium distribution of magnetization for a given value of the applied magnetic field is then found by numerically integrating the coupled Landau–Lifschitz–Gilbert equations [557] of each discrete cell (denoted by i), that govern the magnetization dynamics:

$$\mathrm{d}\boldsymbol{M}_i/\mathrm{dt} = -\gamma \boldsymbol{M}_i \times [\boldsymbol{H}_{\mathrm{eff}}]^i - (\alpha\gamma/M_S)\boldsymbol{M}_i \times (\boldsymbol{M}_i[\boldsymbol{H}_{\mathrm{eff}}]^i), \quad (3)$$

where γ is the electron gyromagnetic ratio, α is a damping constant, and $\boldsymbol{H}_{\mathrm{eff}}$ is the effective magnetic field. The latter is defined as $\boldsymbol{H}_{\mathrm{eff}} \equiv -\mu_0^{-1}\,\partial E/\partial \boldsymbol{M}$, where E is the average energy density. $\boldsymbol{H}_{\mathrm{eff}}$ includes all relevant sources of magnetic field, such as exchange, crystalline anisotropy, demagnetization, and Zeeman energy terms, which are evaluated within each particular case.

Some of the submicron elements that have been studied are parallelepiped planar squares or prisms [471–473,505,566–569], and rectangular bars with pointed ends of NiFe [505]; circular [478], elliptical [454], and rectangular [570,571] planar dots of Co; rectangular [104,572] and diamond-shaped [572] Fe(1 1 0) elements; circular Fe(1 0 0) dots [137]; Ni truncated pyramids [168]; spin valve elements with different end shapes [97,571,573,574]; and

elongated tape media elements [499,575]. Other shapes have also been considered, like spheres and prolate ellipsoids [464], octagons [502], or complex geometries [502,576]. In these systems, different magnetic properties have been investigated, such as domain configuration or the presence of vortex and flower states as a function of field [104,137,168,456,464,471–473,478, 566–568,570,571], magnetization reversal by curling modes [577], the influence of the particular material parameters [578], edge and shape effects [97,454,456,470,472,474,505,572–576], or the behavior of magnetoresistance [568]. Several of these studies present a direct comparison with experimental results, allowing a better interpretation of the different observed magnetic behaviors. Some examples are the existence of a single domain configuration with small boundary deviations from uniformity in 1 μm-sized Fe(1 0 0) dots [137]; the presence and size of stripe and flux closure domains at remanence in Fe(1 1 0) rectangles of 0.5 μm in width, for longitudinal and transverse applied magnetic fields [104,572], as well as the dependence of the hysteresis loops on the element shape for both field configurations in diamonds and rectangles of the same material [572]; the incoherent magnetization reversal in Ni truncated pyramids, governed by the microstructural columnar grains [168]; a reversible vortex growth in a wide field range in Co polycrystalline dots [478]; and the antiferromagnetic coupling between magnetic layers and the shape dependence of the coercive field in Co/Au/Ni elements [97].

Micromagnetic simulation studies have also been applied to small arrays of magnetic particles with interactions through magnetostatic fields. Several of the investigated systems consist of arrays of rectangular-like permalloy elements with different shapes at the ends [498,503,504,523], cubic particles arranged in different configurations [490,491], Ni cylindrical nanowires [579], networks of Co spherical nanoparticles [526,527], and Co/Pt multilayers deposited on silicon substrates with arrays of dots [218]. Some of the main new findings of these calculations, taking into account dots interactions, are the presence of plateaus in the hysteresis loops [498,523], the existence of antiferromagnetically aligned states [218,498,527], a significant decrease in the number of domains in the central elements of the array at the remanence [503], and changes in the switching fields [218,490,491,504,523,527,579].

Other theoretical models and approaches, different than the micromagnetic ones, have also addressed important issues concerning arrays of submicron structures. Some of them are based in mean-field theories [580], analyzing or predicting properties of magnetostatically coupled single-domain element arrays. Among them, the following can be found: studies about the geometry effects on the coupling energy, the corresponding configurational ground states and induced anisotropies in the arrays [507,509,553]; the analysis of the magnetization and magnetic susceptibility of the interacting system [554]; the study of the dependence of magnetization processes on temperature, field direction and array size [524]; the simulation of the hysteresis loops characteristics [455]; the analysis of the high-frequency dynamic response [551]; a model about the existence of reorientational transitions from in-plane to out-of plane magnetization states in the arrays as the sizes are modified [506]; and the deduction of the easy-axis distribution and interaction strength at remanence in the system [581].

Finally, it is worth mentioning other models that investigate the effects of magnetocrystalline anisotropy in polycrystalline islands [432], the shape and size effects on the demagnetizing factor tensor of the elements [462], the relaxation processes [162], the magnetization switching of spherical particles by Monte Carlo simulations [582], the shape and edge effects on the magnetostatic mode spectrum [396], the oscillating size dependence of the magnetic moment in very small dots [511], and the presence of quantization effects in the spin-wave frequencies due to small dot size [583].

3.5. Nanostructured lines and wires

Contrary to single dots, the magnetic properties of single lines are rather simple to measure with conventional magneto-transport measurements. For arrays of magnetic lines, a variety of measurement techniques have been used, such

as magneto-transport [100,112,122,126,135,219, 220,224–231,350,584–594], magnetization (VSM [215,216,586–588,595], SQUID [227–231,589], MOKE [100,120,126,135,241–245,257,590–594, 596–598], AGM [599], Magneto-Optical Torque [600]), domain imaging (MFM [220,260,261,585, 594], scanning electron microscope with spin analysis [222,223], and dynamic magnetic measurements (FMR [122,397,595] or BLS [89,601–606]).

3.5.1. Magnetization reversal in single lines

In nanostructured lines, three main effects have been studied: (i) the width of the lines [122,126,591–593,602,605,607–609], (ii) the composition (polycrystalline single phase [89,95,98, 100,101,112,122,126,224–226,397,584,585,589,591–597,599,601,602,605–623], amorphous [120], single crystal single phase [135,590,600,624,625], multilayers [122,133,224–226,586–588,607,626–634], or FM/AF bilayers [129,586,587,635,636]) and (iii) the "shape" of the lines (e.g., constrictions, zigzag or modified ends) [98,100,101,585,587,589,609, 10,614–623,626,631,635].

(i) The basic effects of reducing the width can be sorted into four main classes

(a) *Increase in* H_C for longitudinal fields (applied parallel to the lines) [95,120,122,126,135,224–226,257,586,587,590,592,593,595–597,599,605,617, 627] (see Fig. 15). This increase is due to the existence of a small magnetic ripple structure in the line (related to the width of the line). When a reversal field is applied, the magnetic poles created by the ripple structure cause the magnetization to buckle. This buckling structure gives rise to domains with magnetization perpendicular to the line, which block the reversal domain propagation along the length of the line. Hence there is an increase in coercivity [637].

(b) *Increase in saturation fields* for fields applied perpendicular to the lines [95,112,122,126,135, 257,586,587,590,592,593,595,596,599,605,613,631] (see Fig. 15). This increase is simply related to the shape anisotropy. The saturation field of a line can be estimated by $H_S \approx 3/2\ H_{Demag} = 3/2\ (t/w)\ M_S$ (in SI units), where H_{Demag} is the demagnetizing field of the wire, and t and w are the thickness and the width [638]. Therefore, for a fixed thickness,

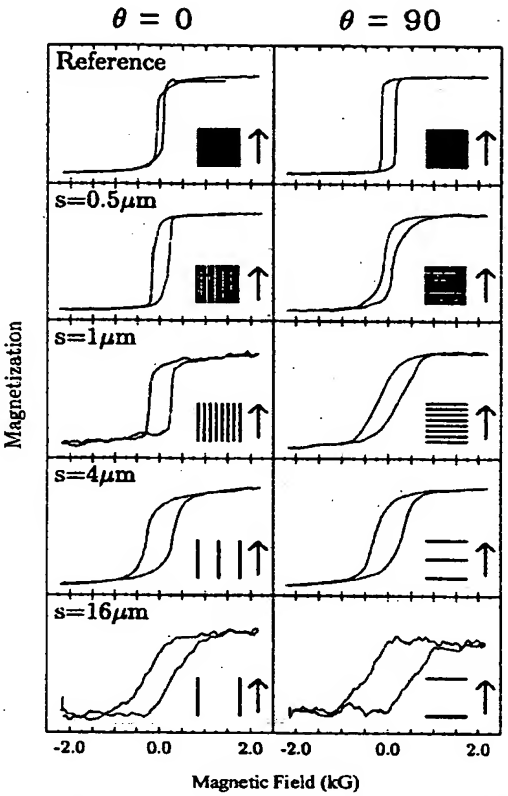

Fig. 15. The magnetization, as inferred from the magnetooptical Kerr effect (MOKE) measurements on a range of Fe(0 0 1) gratings with wire width fixed at 0.5 μm and variable separations s, for the field applied in-plane magnetic field parallel ($\theta = 0°$) and perpendicular ($\theta = 90°$) to the wires. The reference sample is an unpatterned Fe mesa of the same dimensions as the grating structures. The inserts show the measurement direction schematically, with the arrow indicating the direction of the applied magnetic field (courtesy Shearwood et al. [135]).

the saturating field will increase when reducing the line width as $1/w$ [126].

(c) *Change in domain structure* [101,220,260, 261,460,594,608,621,624]: as films, usually multidomained, are patterned into lines, the number of domains that can nucleate is drastically reduced. A first stage is to obtain closure domains for moderately wide lines. Finally, the lines become single-domained when the width is sufficiently narrow.

(d) *Change of reversal mechanisms* for in-plane perpendicular fields [112,122,126,135,586,587,590,

592,593,595,596,599,605]: in a continuous polycrystalline film, the reversal mechanism is usually dominated by domain nucleation and motion, hence some irreversibility (i.e., coercivity) is expected. As the width of the lines is increasingly reduced, when the field is applied perpendicular to the line, the domains can no longer nucleate. Consequently the reversal has to be dominated by magnetization rotation, thus reducing the irreversibility. This effect is analogous to the one observed when measuring a thin film with the field in-plane or out-of-plane.

Other unusual effects of the line width reduction include: the quantization of the spin wave modes [122,397,595,601], similar to nanostructured dots, although lines with large crystal anisotropy may not exhibit this quantization [603,604]; localization or surface effects, which result in the reduction of T_C or the presence of multiple T_C [352,639,640]; the increase in domain wall size [608]; or strong magnetoelastic effects in embedded wires [641].

(ii) The behavior described in (i) applies for polycrystalline lines of a single phase, where the magneto-crystalline anisotropy is virtually averaged out and demagnetizing effects dominate. However, for single crystals, exchange coupled lines or multilayers, anisotropies such as the magneto-crystalline, the unidirectional exchange anisotropy or interlayer coupling are also important [122,133,135,586–588,590,607,624–630,632–636]. Consequently, the magnetic behavior will be affected by several factors, often leading to increasingly complex reversal mechanisms. For example, a change from positive to negative anisotropic MR with temperature in single-crystal Co lines [625]; an increase of exchange bias field (i.e., loop shift in the field axis) with decreasing width in NiFe/NiO (FM/AF) lines [636]; or a linear response in transverse MR in Co/Cu/Co trilayers [133].

(iii) A very active area of research in magnetic lines is the effect of changing the line shape, since in this way domain walls can be controlled (e.g., creation or pinning of domain walls). Some examples of modified shapes are constricted lines (to pin domain walls) [100,101,585,587,614,620, 621,635], zigzag or sharp cornered lines (to create artificial domain walls) [98,589,609, 616–618,622,623,636], or lines connected to large pads of the same material (acting as a sources of domain walls) [100,585,610,619,631]. Some of the research topics include the contribution of the domain walls to the MR [618,624,625], estimation of the speed of a domain wall in a line [632–634], or quantum tunneling of magnetization [615]. Also, the magnetization reversal processes and domain configurations of closed lines (i.e. rings) have been analyzed [99,417].

3.5.2. *Interactions in arrays of lines*

In contrast to arrays of dots, the results of the interactions in arrays of lines for different systems are more consistent [112,135,584,590,591,595,599]. This is because there is essentially only *one* arrangement studied, namely parallel lines separated by an equal distance. Moreover, most of the investigations have been carried out in sufficiently narrow polycrystalline lines that are single domains. In general, the interactions are based on magnetostatic effects, that are relevant when the line separation (s) is less than the line width (w) [584].

The main effect of line interaction is the reduction of the coercive field (or the effective anisotropy) with decreased line separation for fields applied along the line [112,135,584,590, 591,595,599,600] (see Fig. 15). This result is consistent with the intuitive dipole picture discussed earlier. The interaction field due to the neighboring lines will be such that it helps the switching, thus reduced coercivities are expected.

Interestingly, for longitudinal fields, it has been reported that the magnetization of the lines tends to align antiferromagnetically [112], as would be expected for a system of parallel dipoles with 90° bond angle.

For perpendicular fields, the effect of the dipolar coupling is to reduce the saturation field, as compared to isolated lines (see Fig. 15). This is caused by the magnetic charges created along the edges of the lines, which induce a field in the same direction as the applied field. Hence, the effective demagnetizing field is reduced [112,135].

Finally note that dynamic measurements also exhibit some effects from the dipolar interaction. For example, similar to what is found for dots, a

shift of the spin wave frequency is observed [601,602].

3.5.3. Domain wall resistance in lines

One of the novel effects that can be addressed using nanostructured lines is the resistivity of a domain wall. Some current studies on different shaped lines analyze the contribution of the domain wall to the MR, since both negative and positive contributions have been theoretically described and experimentally observed [642–648]. A positive term (i.e., an increment in the resistivity) has been deduced or modeled in base to different mechanisms, such as the backreflection of electrons by the domain wall [649], the Larmor-precession-induced deviation of the conduction electron spin direction during domain wall traversal [644], the mixing of the spin conduction states induced by the non-collinearity of the magnetization within the domain wall [645], the change in the electronic band structure brought about by the magnetization rotation [646], or the supression of weak localization quantum corrections due to the presence of the domain wall [643]. On the other hand, it has been proposed that a quantum correction on the wall contribution to the decoherence of electrons can result in a decrease of resistivity [642]. Also, in a semiclassical approach that considered the spatial dependence of the magnetization, it was found that the domain wall contribution to resistivity could present either negative or positive sign as a function of the differences in the spin-dependent relaxation times of the spin conduction channels [648].

Nanometric zigzag wires have been used to determine the magnetoresistance of the domain walls in polycrystalline Co [98,616,650]. By comparing two different controllable states at the remanence (see Fig. 16(a)), a negative contribution of 1.8 μΩ-cm/wall to MR is found (see Fig. 16(b)) [98]. This negative term is temperature dependent with a maximum decrease in ρ around 100 K [650]. Also, a negative MR due to the domain walls has been reported in Fe(1 1 0) wires [624,651,652], Co wires [614], and NiFe wires [653,654], where it has been related with the anisotropic magnetoresistance of the spins in the wall. On the other hand, positive MR effects associated with domain walls

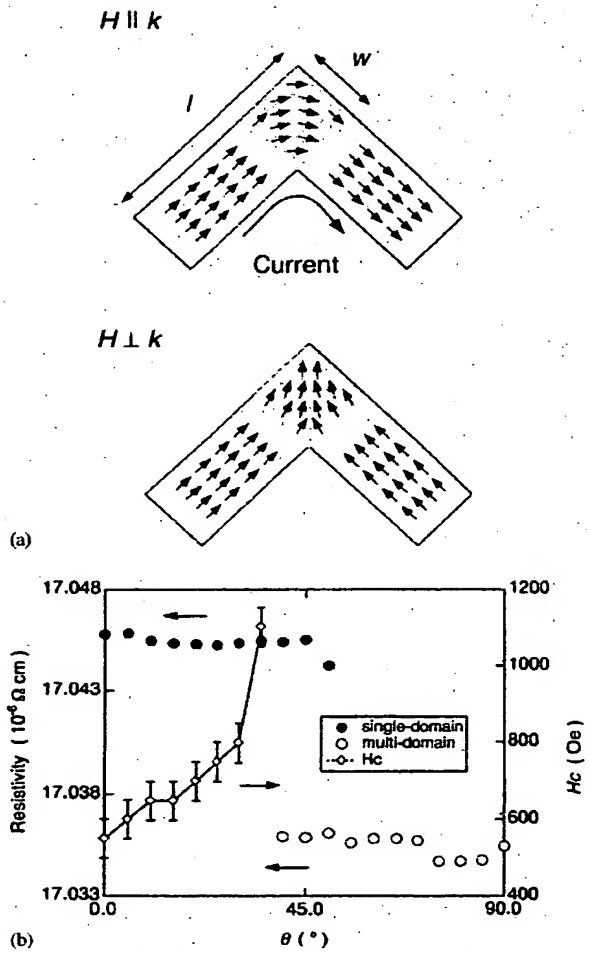

Fig. 16. (a) Schematic illustration of the remanent domain structure near the corner of a zigzag Co wire. (b) Field orientation dependence of the resistivities in remanence and switching fields obtained in a zigzag Co wire (courtesy Taniyama et al. [98]).

have been measured in epitaxial 35 nm wide Co nanowires [655], electrodeposited Co nanowires exchange biased to a $GdCo_{1.6}$ layer [656], etched Co structures [657], and cross-shaped NiFe wires [609]. Also, it has been shown in epitaxial Co wires [625] that the domain wall contribution to the resistivity can be either negative or positive, depending on whether the wire is oriented parallel or perpendicular to the magnetic easy axis.

3.6. Giant magnetoresistance in nanostructured elements

The discovery of giant magnetoresistance (GMR) in Fe/Cr multilayers [3] attracted renewed interests in the research of spin-dependent electron transport in magnetic multilayers [658]. Nanopatterning has been essential to solve one of the great experimental challenges in this field, i.e., the MR measurements in the so-called "current-perpendicular-to-plane" (CPP–GMR) configuration, where the length of the sample is the film thickness. This results in ultra small resistance values, unless the sample cross-section is reduced by microfabrication techniques. Another area of active research in nanostructured GMR elements has been the design of high-density magnetic random access memories (MRAMs). In this section we will start by presenting a brief account of the problem of CPP–GMR, since this topic has already been recently reviewed [345,659–661]. Then, we will discuss size effects on the more standard "current-in-plane" GMR (CIP–GMR) and, finally, the nanometric MRAMs.

(i) *CPP transport in GMR multilayers*: The interest in CPP transport was started by theoretical predictions of a larger GMR effect in this geometry than in the regular CIP–GMR geometry [662]. The CPP–GMR also demonstrates a clear-cut "two current" model of spin transport, and can separate the interface and "bulk" spin-dependent scattering. The first measurements of CPP–GMR were reported by Pratt et al [663] in Ag/Co multilayers with 1 mm^2 cross section, using a SQUID-based sensing system. Another experiment using standard lithographic achieved pillar-like samples with cross sections in the 1 μm^2 range [664,665]. There was, however, the problem of contact resistance and current spreading in the contacts. Larger aspect-ratios have been obtained by the electrodeposition of magnetic multilayers into pores of membranes [73–75,330] (typically Co/Cu and (Fe, Ni)/Cu). Nanowires with diameters in the range of 30–400 nm and length of 20–40 μm ensure uniform current distribution in the cross section. However, until very recently, it has not been possible to perform measurements in a single nanowire [371,666].

A different approach has been the fabrication of magnetic multilayers in V-grooved substrates [227,667,668] as described in Section 2.4.1.2. Depending on the angle of multilayer deposition, two kinds of geometries can be realized. If the magnetic material is evaporated normal to one of the two side planes of the groove, a CPP configuration is obtained due to the self-shadowing effects [227]. On the other hand, if the deposition is performed in the direction normal to the substrate plane, a corrugated multilayer structure is obtained. This is the so-called "current-at-an-angle" (CAP) configuration, since the current flows at an angle of about 50° with respect to the multilayer plane [667,668]. From the measurement of CIP and CAP MR, CPP can be extrapolated.

In the same magnetic multilayer, CPP–GMR is usually found to be larger than CIP–GMR (by a factor of up to 10) and values of up to 115% for Co–Ni–Cu/Cu multilayer [330] and up to 108% in Fe/Cr multilayers [664] have been reported. CPP–GMR is also less sensitive than CIP–GMR to sample inhomogeneities. This makes CPP-based nanodevices attractive and competitive vs. CIP ones for sensor applications in ultrahigh density magnetic storage [371,669].

The connection of GMR with structure of multilayers is crucial for the understanding of this phenomenon. This requires independent measurements of the resistivity, the magnetoresistance and quantitative measurements of the structure (roughness, interdifussion, lattice expansions, etc). Moreover, it must be kept in mind that at short length scales the magnetic structure does not necessarily follow the physical–chemical structure [670,671]. These types of studies have been performed for many years for in-plane resistivity. However, in the CPP geometry there are only a few studies where these have been combined [672,673]. In all cases it is found that structural changes can drastically affect the magnetoresistance. Moreover, this seems to depend strongly on the type of materials that form the superlattice, so probably no universal statements can yet be made.

The characteristic length scale for spin dependent transport in CPP–GMR is not the electronic mean free path, but the spin-flip diffusion length l_{sf}, i.e., the distance over which the conduction

electron spin is relaxed. It is typically in the 5–100 nm range [674], depending on material and sample preparation conditions. Based on a model presented by Valet and Fert [675], the analysis of CPP–GMR data in a variety of multilayer systems [659–661] has allowed for the experimental determination of the bulk and interface scattering spin asymmetry coefficients. They have been found to be comparable to those reported by Campbell and Fert [674] for bulk alloys. Also, in CPP–GMR, the problems of spin accumulation at the interfaces and spin injection appear as fundamental issues. A dramatic effect, recently demonstrated [33–35,452], is the current driven magnetization reversal of a thin magnetic layer, in agreement with theoretical calculations [32,676]. In the perpendicular transport geometry, the spin-polarized currents may transfer angular momentum between the layers and exert a torque on the magnetic moment, resulting in a magnetization switching [32,676,677]. This phenomenon is particularly appealing in MRAM devices since the reading/writing processes may be greatly simplified by using just one current to do both jobs.

(ii) *Size effects in CIP–GMR*: Potential applications of GMR materials in magnetic sensors for high-density magnetic recording require the study of finite size effects down to the nanometer scale. In general, it is found that patterning does not substantially affect the MR amplitude ($\Delta R/R$) [607,678–680], but rather it induces a broadening of the GMR vs. field curve by a magnetostatic effect. Therefore, the sensitivity $[\mathrm{d}(\Delta R/R)/\mathrm{d}H)]_{\max}$ decreases as the size is reduced. Also, an increase in Barkhausen noise for reduced stripe dimensions has been found in NiFe/Ag multilayers [607,681]. On the other hand, geometrically induced GMR has been found in patterned NiFe/Ag [607,682] and Co/Cu multilayers [135] (up to 7.8% for 0.4 μm wide stripes). In this case, spin disorder necessary for the GMR effect is induced by magnetostatic coupling in the patterned elements.

(iii) *Nanometric MRAMs*: Magnetic random access memories are based on the change between low "0" and high "1" resistance states of a thin film device a magnetic field created by an external "word" current. The design of structures with high MR ratios and nanometric dimensions has essentially focused on two different devices: GMR based pseudo-spin valves [683] and magnetic tunnel junctions [14,684].

Pseudo-spin valves consist of a GMR sandwich structure of two FM layers (e.g., NiFeCo) AF-coupled by a spacer (e.g., Cu) [46]. The two magnetic layers have different coercivities so that the top layer is softer than the bottom. Alternatively, the bottom layer is pinned by exchange bias to an AF layer. The "word" current is adjusted so that it is able to switch only the magnetization of the top FM layer from parallel alignment (low-resistance state) to antiparallel alignment (high-resistance state) with respect to the bottom layer (a typical MR curve is shown in Fig. 17(c) [46]). MR ratios as high as 8% have been reported for dimensions down to 0.2 μm at room temperature [685], but they are reduced by edge effects for dimensions down to 0.07 μm [628]. MRAM arrays based on GMR elements have been fabricated by connecting the individual spin valves in series, as shown in the SEM photograph of Fig. 17(a)–(b), for a 5×5 array of 0.25 μm MRAM cells [46]. Practical applications require fast switching times and high-density arrays with negligible magnetic dipolar interactions, which has been demonstrated at least down to 0.25 μm inter-element distance [46]. Dynamic measurements [547–549] in the 0.2–10 ns range have shown that after a switching field pulse, magnetization reverses by rotation in less than 0.5 ns, but damped oscillations persist for several nanoseconds. It is worth noting that nanometric pseudo-spin valve MRAM cells have already been successfully integrated with complementary metal-oxide-semiconductor (CMOS) transistors [686].

A different type of nanometric MRAMs is a magnetic tunnel junction, where the MR effect is provided by spin-dependent tunneling between two FM layers (usually Co and NiFe) across an insulating oxide barrier (usually Al_2O_3). MR ratios as large as 30% have been reported for devices as small as $0.2 \times 0.8\ \mu m^2$ at room temperature [687]. The parallel alignment of the spins in each magnetic layer is favored for reduced sizes, where single domain behavior is more likely [688,689], and the switching characteristics are mainly controlled by shape anisotropy [690,691].

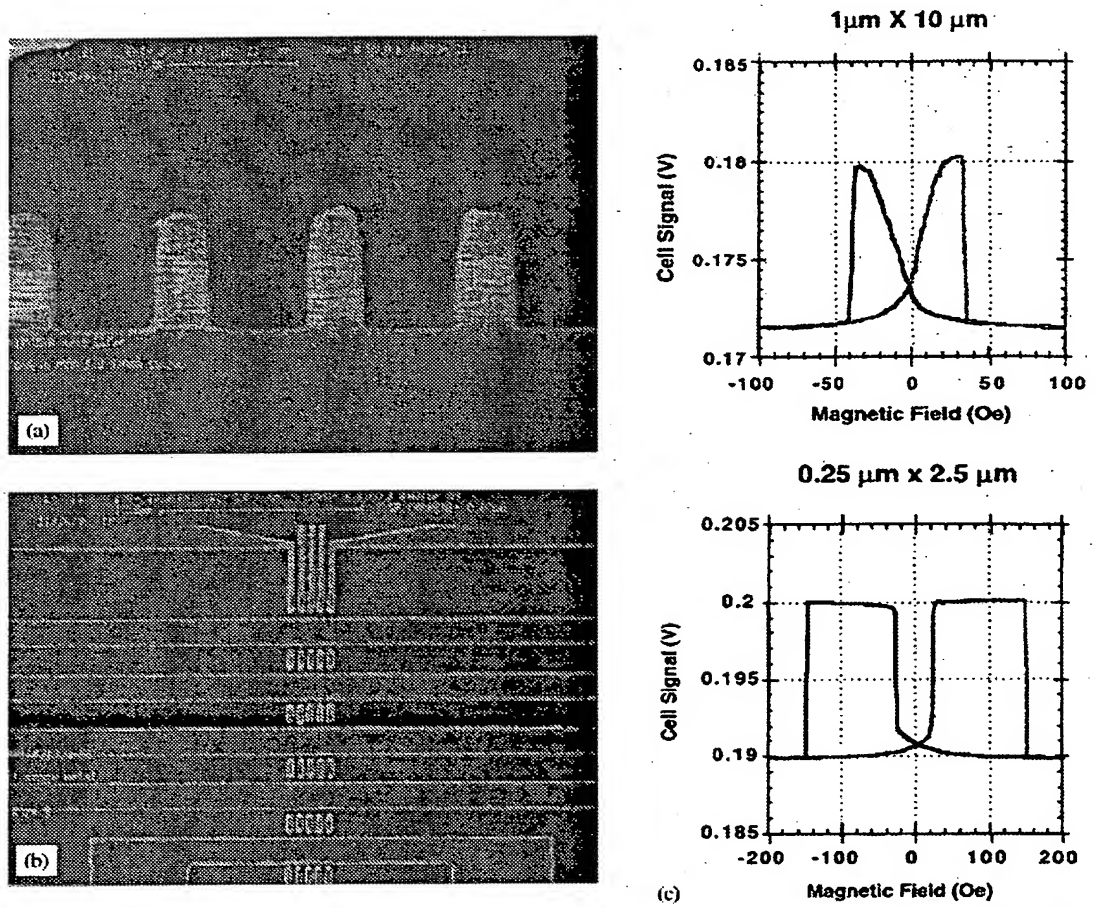

Fig. 17. (a)–(b) SEM photographs of the final metal etch process and a finished 0.25 μm 5 × 5 array for non-volatile magnetoresistive random access memory devices. (c) Switching characteristics for a 1 μm × 10 μm square and a 0.25 μm × 2.5 μm square memory cells. The single domain characteristics of the smaller cell results in cleaner switching performance (courtesy Nordquist et al. [46]).

Dynamic measurements in the nanosecond range [544,692] have shown that magnetization reversal occurs by a combination of rotation processes at the central region of the device and field-dependent viscous domain wall movement near the edges. Low-frequency noise in magnetic tunnel junctions is known to be caused by thermally activated motion of domain walls [693].

3.7. Films with ordered arrays of nanometric antidots

There is also some research in the fabrication and study of magnetic films with patterned arrays of holes, usually called negative dots or "antidots". This kind of systems presents some conceptual advantages for data storage since they may avoid some of the problems of continuous media. Although the extent of these studies is not very large, there are some interesting properties that have been addressed both experimentally and theoretically.

First, it has been observed by scanning Kerr microscopy that an array of square antidots in a permalloy film actually produces a well-defined periodic domain structure at remanence [694,695]. This structure consists of small domains around each antidot, which result from the competition

between the intrinsic anisotropy of the continuous film and the induced spatially variant shape anisotropy. Furthermore, numerical simulations of these permalloy samples have been carried out to explore the signal to noise characteristics and the upper density limit [696,697].

Similarly, the magnetic behavior of Fe films with arrays of holes has been investigated by BLS, Lorentz microscopy and the Kerr effect [698–700]. While the studied circular holes do not significantly modify the anisotropy and coercivity of the continuous films [698], the magnetization reversal process is governed by the antidot array in the case of elliptical holes [699]. Also, studies in this Fe samples with holes of different shape indicate that the anisotropies in the negative arrays are due to the shape of the holes and not to the array itself [700]. In the case of Co films with holes, a stripe domain structure has been observed [109], with the direction of the stripes determined by the previously applied field. The arrays of nanometric antidots are also successful to reduce the demagnetizing field of a MnNiAl layer with the magnetization perpendicular to the sample plane [186].

4. Interactions between magnetic arrays and other systems

Ordered arrays of magnetic dots have not only been studied to understand their intrinsic magnetic properties, but also used to modulate in a controlled fashion the magnetic field applied on the system of interest. In this section, we will describe their use in combination with superconducting films to create artificial arrays of pinning centers, and in hybrid semiconductor/ferromagnet structures to produce a well-defined periodic magnetic field.

4.1. Pinning in a superconductor

Flux pinning in superconductors has been the subject of intense interest because of its intrinsic and technological relevance. In a type II superconductor in the mixed state, the penetration of a magnetic field B forms a triangular lattice of vortices, each carrying a quantum of flux Φ_0, with lattice spacing $a_0 = 1.075(\Phi_0/B)^{1/2}$ [701]. A finite resistivity is found in the superconductor as soon as vortices start to move due to the Lorentz force created by a transport current. Thus, the superconducting critical current is controlled by the pinning force exerted by material imperfections that prevent vortex motion.

In the presence of ordered arrays of artificial pinning centers (thickness modulations [702], holes [703,704], magnetic or metallic particles [705]), a whole range of new phenomena appear associated with the matching of the vortex lattice with the artificial defect structure. The advancement of nanolithography techniques has rendered the ability to reduce the size of these artificial pinning centers to a scale comparable with the coherence length of classical superconductors.

The pinned superconducting films are usually fabricated in a two-step process [706,707]. First, an array of magnetic dots is prepared by e-beam lithography on a Si substrate (shown in Fig. 18(a) is a SEM image of a triangular array of 200 nm diameter Fe dots with lattice constant $d = 600$ nm). Then a superconducting film is deposited on top of the magnetic array, followed by optical lithography to define a bridge for transport measurements (see Fig. 18(b)). A different approach has been used by Fasano et al. [708], in which triangular arrays of magnetic particles are prepared by Bitter decoration of $NbSe_2$ crystals in the presence of a vortex lattice. The resulting periodic pattern is used as a pinning center array in subsequent experiments.

Fig. 18(c) shows the field dependence of the resistivity in the mixed state for a 100 nm thick Nb film grown on an array of Ni dots with lattice constant $d = 410$ nm [706,707]. Clear minima in the resistivity appear at a set of regularly spaced field values B_n. The intervals between consecutive minima (ΔB_0) are constant as shown in the inset of Fig. 18(c), with $\Delta B_0 = 141 \pm 4$ G. This value corresponds to a vortex lattice constant $a_0 = 413 \pm 6$ nm, in good agreement with the spacing of the array $d = 410 \pm 10$ nm. This implies that there is a reduction in the dissipation when there is a matching between the vortex lattice and the magnetic dot array.

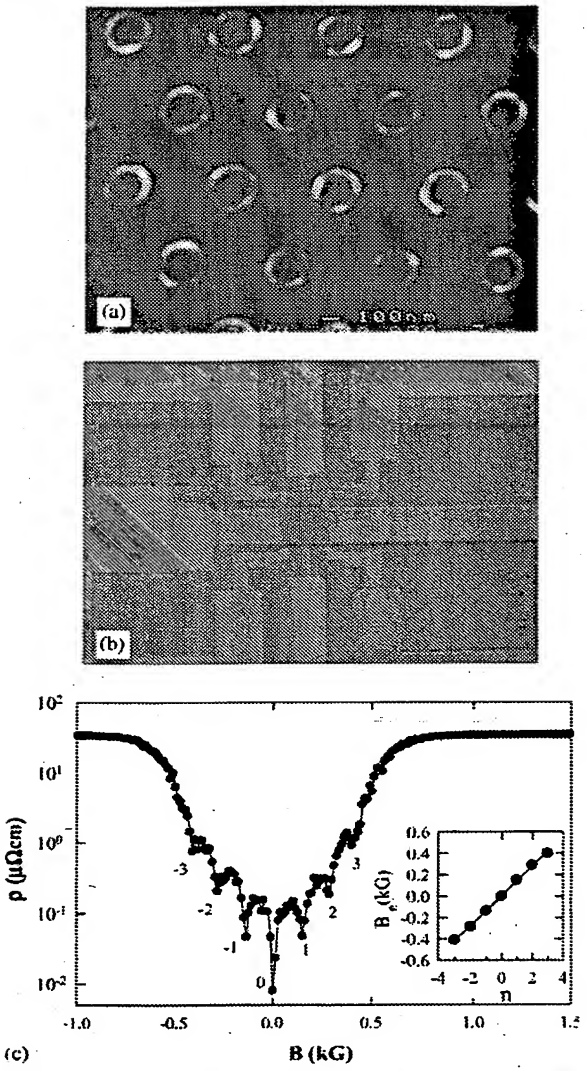

Fig. 18. (a) SEM image of a triangular array of Fe magnetic dots fabricated by e-beam lithography on a Si substrate. (b) Micrograph of a Nb bridge defined by optical lithography in the array region. The width is 40 μm and the distance between the voltage contacts used for transport measurements is 50 μm. (c) Field dependence of the resistivity of a Nb thin film with a triangular array of Ni dots with lattice constant $d = 410$ nm, measured at $T = 8.2$ K and with $J = 2.5 \times 10^4$ A/cm^2. Inset shows the position of the minima B_n versus the index number n. The solid line is a fit to the expression $B_n = n\Delta B_0$ with $\Delta B_0 = 141 \pm 4$ G (after Martín et al. [706]).

Depending on the strength of the pinning sites, synchronized pinning can also be observed as a set of regularly spaced maxima in the critical current vs. field curves close to the superconducting critical temperature ($T > 0.9T_C$), either by transport [709–711] or magnetization [123] measurements. For lower temperatures, this periodic structure is washed out due to the competition of the ordered array with random defects present in the superconducting film. However, at low enough temperatures, the signature of synchronized pinning appears again as the hysteresis loops exhibit quasiperiodic instabilities, with a field-dependent period related to the matching fields [712]. These low-temperature matching anomalies have been related with the existence of matched flux terraces near the edge of the film.

Periodic pinning has been studied as a function of array symmetry and geometrical dimensions. It is found [711] that, as the dot separation becomes smaller than the coherence length, there is a crossover from a weak pinning regime to a superconducting wire network regime for small dot separations. Matching between the vortex lattice and non-triangular arrays of dots (kagome [709], square [710–712] or rectangular [713]) gives rise to the stabilization of new geometrical configurations. This has allowed to probe the elastic properties of the vortex lattice [713] and to study the role of interstitial pinning due to intervortex repulsion [123,709]. Theoretical simulations of interactions between ordered arrays of defects and the vortex lattice [714,715] have predicted a rich variety of dynamical phases induced by these commensurability effects. Also, the effects on vortex pinning of introducing controlled disorder in the magnetic array have been analyzed [716].

The problem of pinning interactions between a magnetic dot and a superconductor requires the numerical solutions of the Ginzburg-Landau equations, with several different kinds of contributing terms [717–719]. Experimentally, in order to clarify the pinning interactions between vortices and magnetic dots, synchronized pinning has been studied as a function of dot material [710,711] and its magnetic state [123,709]. In general, it is found that magnetic (Ni) dots show more pronounced

periodic pinning than non-magnetic (Ag) dots [710,711]. Pinning efficiency is enhanced by saturating the in-plane magnetization of the magnetic dots [123,720], indicating that the stray field created by the dots in the superconductor plays an important role, as can be shown by scanning Hall probe microscopy [721]. Moreover, if the dot magnetic moment has a component perpendicular to the film plane, a large asymmetry is found in the critical current maxima, depending on whether the magnetic dipoles are aligned parallel or antiparallel to the external magnetic field [377,709]. This suggests a pinning mechanism related with the interaction between the vortex field and the dot magnetic moment. Finally, related with this fact, from the analysis of the temperature dependent critical current at the matching field [722], it is found that the mechanism of pinning by magnetic dots can be narrowed to a combination of two: proximity effect around the magnetic dot and magnetic interaction with the dot moment.

4.2. Coupling to a 2D electron gas

Magnetic nanostructures have been used to study the transport properties of two-dimensional electron gases (2DEG) under a periodic magnetic field, following the theoretical predictions [723–725] of commensurability oscillations in the magnetoresistance.

Briefly, a 2DEG is fabricated in a GaAs/AlGaAs heterostructure, where the electrons are trapped in a potential well at the interface between the two materials, so that motion is prohibited along the growth direction. Then, an array of magnetic stripes or dots [726] with periodicity $d \approx 1\,\mu m$ is fabricated on top by electron beam lithography to create a spatially modulated magnetic field on the 2DEG, as shown in Fig. 19(a)–(c) [727]. Typical carrier mobility at 4.2 K is above $10^6\,cm^2/V\,s$, corresponding to a mean free path $\approx 10\,\mu m$, much larger than the magnetic field periodicity.

In this ballistic regime, an oscillatory magnetoresistance ρ_{xx} appears [727–729] (see Fig. 19(d)–(f)) due to the commensurability of the two characteristics length scales of the system: the electron cyclotron radius (R_c) and the spatial periodicity d. The oscillations are periodic in $1/B$, with minima in ρ_{xx} (marked by solid triangles in Fig. 19) given by the condition

$$2R_c = hk_F/\pi eB = (\zeta + 1/4)d, \tag{4}$$

where k_F is the Fermi wave number and $\zeta = 0, 1$, is an integer. This phenomenon is analogous to the Weiss oscillations in the magnetoresistance due to a weak electrostatic modulation in a 2DEG [730]. The presence of a modulated magnetic field modifies the energy spectrum and transforms the degenerated Landau levels into bands of finite width. Eq. (4) corresponds to the flat-band condition (i.e., zero bandwidth) where the additional contribution to the resistivity due to the dispersion associated with the Landau bands vanishes [723,724]. In general, the highly controlled environment of the 2DEG under periodic electric and magnetic field modulations has provided an excellent playground for the theoretical and experimental description of electronic transport in these structures [731–735]. For example, the detailed analysis of the temperature dependence of these oscillations in the magnetoresistance has shown the presence of an electron–electron scattering contribution to the resistivity in these 2DEG [736,737].

The amplitude of the oscillations in the magnetoresistance has been shown to be greatly enhanced as the magnetic field is tilted towards the plane of the 2DEG but normal to the magnetic stripes [738,739] (up to 1500% for Co stripes at 1.3 K [740]). This large magnetoresistance is attributed to the channeling of the 2D electrons in open orbits along lines of zero magnetic field, perpendicular to the transport current [740,741]. The effect is stronger for fields away from the film normal, since in this geometrical configuration the amplitude of the periodic stray field created by the magnetic stripes is greatly enhanced [739]. This magnetoresistance becomes smaller as temperature increases, due to the decrease in electron mean free path. However a 1% magnetoresistance is still observed at room temperature, reflecting the anisotropic character of electron transport in the presence of the modulating magnetic field [740,742].

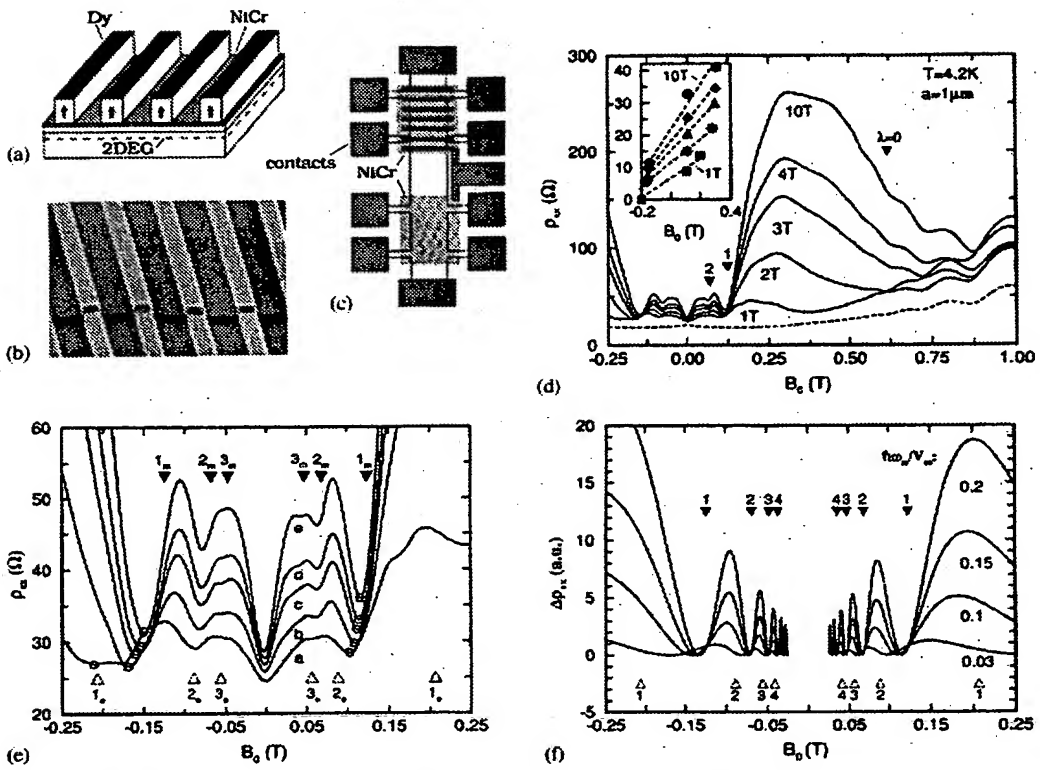

Fig. 19. (a) Sketch of the 1D ferromagnetic Dy grating on top of a GaAs–AlGaAs heterojunction. (b) Electron micrograph of the Dy strips evaporated across a mesa edge: 200 nm height and 1 μm separation. (c) Device geometry containing the ferromagnetic grating and an unpatterned reference Hall bar. (d) Resistivity ρ_{xx} vs. external magnetic field B_0 for different maximum applied field (B^{max}) sweeps (from 1 to 10 T as indicated in the curves). Filled triangles with positions defined by Eq. (4) mark the flat-band condition in a periodic magnetic field. The inset displays the strength of the magnetic modulation B_m (in mT) as a function of B_0, derived from (i) the amplitude of the large resistance maximum at ~0.3 T and (ii) the positions of the ρ_{xx} minima in (e) around −0.16 and 0.12 T. (e) Low-field magnification of (d) showing the shift of the ρ_{xx} minima with increasing B^{max} (from $a = 1$ T to $e = 10$ T). Filled triangles mark the position of the *magnetic* flat-band condition (subscript "m") while the open triangles mark the *electric* ones (subscript "e"). The open circles highlight the positions of the ρ_{xx} minima used to evaluate the B_m's. (f) $\Delta\rho_{xx}$ calculated for different $\hbar\omega_m/2\pi V_m$ ratios, where V_m is the amplitude of the electrical modulation and $\omega_m = eB_m/m^*$ (m^* is the effective electron mass of GaAs). Filled and open triangles again mark magnetic and electric flat-band conditions (courtesy Ye et al. [727]).

Interactions between magnetic particles and 2DEG have also been successfully applied to obtain information on the properties of the magnetic nanostructure through the fabrication of Hall micromagnetometers [196,408,743]. In these devices, a Hall cross is lithographically fabricated from a GaAs/GaAlAs heterostructure, where a 2DEG embedded 60 nm below the surface with typical electron density $n = 3 \times 10^{11}$ cm^{-2} and a high mobility in the range 4×10^5 cm^2/V s. Then, the desired magnetic nanostructure is prepared on top of the active area of the Hall cross by nanolithography. Hall measurements are performed within the ballistic transport regime, where, at low fields, the Hall coefficient R_{xy} is proportional to the average field $\langle B \rangle$ in the cross junction [408], and does not depend on the local magnetic field profile [744]. A second empty Hall cross is fabricated to compensate for the externally applied field [196], so that the measured voltage signal is only determined by the stray field of the magnetic nanostructure, which is directly related to the perpendicular magnetization of the array [199].

Due to the low concentration of 2D electrons ($R_{xy} \propto 1/n$), Hall magnetometers present a high sensitivity which is only limited by Johnson noise. The typical resolution is $\delta B \sim 10^{-4}\,\mathrm{GHz}^{-1/2}$, which corresponds to a flux resolution of $\delta\Phi \approx 10^{-5}\ \Phi_0$ [408]. These numbers can be improved by one order of magnitude if the magnetic array exactly matches the Hall cross size [193]. This high resolution has made ballistic Hall magnetometers a very useful tool in the research of arrays of nanomagnets [194,451] as well as of isolated magnetic particles [409,412,745].

5. Conclusions

The key aspects of the research carried out during recent years on ordered magnetic nanostructures may be summarized in the following areas:

(a) Novel lithography techniques have been developed or improved to allow fabrication of ordered magnetic nanostructures with desirable features, including arrays of elements with reproducible sizes in the range of 10 nm, which can be extended over large areas ($\sim 100 \times 100\,\mathrm{mm}^2$). Often there are many variable parameters that can be used to tune the properties of these nanoelements, such as material, crystallinity (polycrystalline, single-crystal, amorphous), structure (single layer, multilayer, etc), array geometry, etc. Also, magnetic nanostructures can be prepared with very controllable shape: from the simplest dots, bars and lines, to rectangles, triangles or zigzag paths.

(b) The magnetic properties of the nanostructures can be characterized by conventional techniques such as magnetization measurements (VSM, SQUID, AGM, MOKE, ...), when the total area of the patterned array is large enough (that is, when the total magnetic moment of the array is larger than the resolution of the experimental system), or transport measurements, when the nanostructure presents a continuous conduction path. Also, certain local techniques (MFM, electron holography, μ-SQUID, ...) have recently been developed to allow accurate characterization of individual or a small number of nanoelements.

(c) The abundant studies on the behavior of individual dots have revealed that the main magnetic properties of these nanostructures present important differences with respect to continuous films: although the remanent state is essentially metastable, it is often possible to obtain a single-domain state at remanence; shape anisotropy usually plays an important role in magnetization reversal processes; coercive fields of the nanoelements are often larger than the values found in the unpatterned samples; and the spin wave spectrum may be quantized due to the small size of the dots.

(d) When the distance between the nanoelements becomes small enough, important interaction effects due to dipolar fields are observable. Some of these dot interaction effects are: changes in coercivity and switching field width, presence of induced anisotropies, collective behaviors of the elements in magnetization reversal, or dynamic effects such as the shift of the spin wave frequency.

(e) The one-dimension magnetic nanostructures (lines) also present interesting and important differences in their magnetic properties relative to unpatterned films: increase in coercivity, changes in domain structure and reversal mechanisms, quantization of spin wave modes, or dipolar interaction effects. Moreover, fabrication of tailored lines with modified shape has allowed the study of other topics, such as the contribution of the domain wall to the magnetoresistance, the speed of domain wall motion, or different giant magnetoresistance effects.

(f) The arrays of magnetic elements are not only interesting for their intrinsic magnetic properties, but also due to their interaction with other systems. Arrays of magnetic dots can constitute effective ordered pinning centers for the vortex lattice when they interact with type II superconducting films. Also, ordered nanostructures can be used in hybrid semiconductor/ferromagnetic systems to produce a periodic magnetic field that modulates, in a

controlled fashion, the transport properties of two-dimensional electron gases (2DEG).

(g) Technologically, applications of ordered magnetic nanostructures are becoming increasingly important, especially in fields like magnetic recording, sensors, MRAM and magnetoelectronics.

(h) Finally, we should point out that, despite the active research in recent years, there is still a long way to fully understand the properties of magnetic nanostructures. The fabrication of tailored nanostructures, particularly large arrays of ordered, ultrafine ($\sim$10 nm or smaller), uni-disperse nanoelements, remains challenging. More systematic studies of the magnetization reversal processes are necessary, including the associated dynamic effects in the short time scales. It is also crucial to achieve a good understanding of interaction effects in arrays of magnetic nanoelements, or between nanostructures of magnetic materials and other systems.

Acknowledgements

We wish to thank all colleagues who have made their articles available to us. Discussions with M. Vélez, A. Hoffmann, M.I. Montero, O. Stoll, Y. Jaccard, J.M. George, P. Prieto, A.V. Herzog, F. Sharifi, R.C. Dynes, J. Wittborn, K.V. Rao, C. Beeli, W. Kleemann, U. Nowak, K.D. Usadel, M. Grimsditch, J.M. Alameda, F. Briones and Y. Bruynseraede are gratefully acknowledged. Work supported by US-DOE, AFOSR, NSF, Spanish CICYT (grants MAT99-0724 and MAT 2001-2555) and Catalan DGR (1999SGR00340). International collaboration was partially covered by the Del Amo Foundation and NSF. One of us (IKS) thanks the A. von Humboldt Schtiftung and Prof. G. Guentherodt for hospitality in Germany where part of this manuscript was written.

References

[1] G. Prinz, K. Hathaway (Eds.), Magnetoelectronics, Phys. Today 48 (4) (1995) (special issue).
[2] P. Grünberg, R. Schreiber, Y. Pang, M.B. Brodsky, H. Sowers, Phys. Rev. Lett. 57 (1986) 2442.
[3] M.N. Baibich, J.M. Broto, A. Fert, F. Nguyen Van Dau, F. Petroff, P. Etienne, G. Creuzet, A. Friederich, J. Chazelas, Phys. Rev. Lett. 61 (1988) 2472.
[4] P.M. Levy, S. Zhang, A. Fert, Phys. Rev. Lett. 65 (1990) 1643.
[5] S.S.P. Parkin, R. Bhadra, K.P. Roche, Phys. Rev. Lett. 66 (1991) 2152.
[6] B. Dieny, V.S. Speriosu, S.S.P. Parkin, B.A. Gurney, D.R. Wilhoit, D. Mauri, Phys. Rev. B 43 (1991) 1297.
[7] A.E. Berkowitz, J.R. Mitchell, M.J. Carey, A.P. Young, S. Zhang, F.E. Spada, F.T. Parker, A. Hutten, G. Thomas, Phys. Rev. Lett. 68 (1992) 3745.
[8] A. Hernando, J. Phys.: Condens. Matter 11 (1999) 9455.
[9] J.Q. Xiao, J.S. Jiang, C.L. Chien, Phys. Rev. Lett. 68 (1992) 3749.
[10] J.A.C. Bland, B. Heinrich (Eds.), Ultrathin Magnetic Structures, Springer, Berlin, 1994.
[11] R.M. Kusters, J. Singleton, D.A. Keen, R. McGreevy, W. Hayes, Physica B 155 (1989) 362.
[12] R. von Helmolt, J. Wecker, B. Holzapfel, L. Schultz, K. Samwer, Phys. Rev. Lett. 71 (1993) 2331.
[13] S. Jin, T.H. Tiefel, M. McCormack, R.A. Fastnacht, R. Ramesh, L.H. Chen, Science 264 (1994) 413.
[14] J.S. Moodera, L.R. Kinder, T.M. Wong, R. Meservey, Phys. Rev. Lett. 74 (1995) 3273.
[15] J.M. Daughton, J. Appl. Phys. 81 (1997) 3758.
[16] S. Tehrani, J.M. Slaughter, E. Chen, M. Durlam, J. Shi, M. DeHerrera, IEEE Trans. Magn. 35 (1999) 2814.
[17] W.H. Meiklejohn, C.P. Bean, Phys. Rev. 102 (1956) 1413; W.H. Meiklejohn, C.P. Bean, Phys. Rev. 105 (1957) 904.
[18] J. Nogués, I.K. Schuller, J. Magn. Magn. Mater. 192 (1999) 203.
[19] A.E. Berkowitz, K. Takano, J. Magn. Magn. Mater. 200 (1999) 552.
[20] R.L. Stamps, J. Phys. D 33 (2000) R247.
[21] M. Kiwi, J. Magn. Magn. Mater. 234 (2001) 584.
[22] R.A. de Groot, F.M. Mueller, P.G. Van Engen, K.H.J. Buschow, Phys. Rev. Lett. 50 (1983) 2024.
[23] S.P. Lewis, P.B. Allen, T. Sasaki, Phys. Rev. B 55 (1997) 10253.
[24] H.Y. Hwang, S.-W. Cheong, Science 278 (1997) 1607.
[25] J.M.D. Coey, A.E. Berkowitz, Ll. Balcells, F.F. Putris, A. Barry, Phys. Rev. Lett. 80 (1998) 3815.
[26] W.E. Pickett, J.S. Moodera, Phys. Today 54(5) (2001) 39, and references therein.
[27] M. Johnson, R.H. Silsbee, Phys. Rev. Lett. 55 (1985) 1790.
[28] J.M. Kikkawa, D.D. Awschalom, Phys. Rev. Lett. 80 (1998) 4313; J.M. Kikkawa, D.D. Awschalom, Nature 397 (1999) 139.
[29] Y. Ohno, D.K. Young, B. Beschoten, F. Matsukura, H. Ohno, D.D. Awschalom, Nature 402 (1999) 790.
[30] H. Ohno, J. Magn. Magn. Mater. 200 (1999) 110.
[31] D.D. Awschalom, N. Samarth, J. Magn. Magn. Mater. 200 (1999) 130.

[32] J. Slonczewski, J. Magn. Magn. Mater. 159 (1996) L1.
[33] J.A. Katine, F.J. Albert, R.A. Buhrman, E.B. Myers, D.C. Ralph, Phys. Rev. Lett. 84 (2000) 3149.
[34] W.H. Rippard, A.C. Perrella, P. Chalsani, F.J. Albert, J.A. Katine, R.A. Buhrman, Appl. Phys. Lett. 77 (2000) 1357.
[35] F.J. Albert, J.A. Katine, R.A. Buhrman, D.C. Ralph, Appl. Phys. Lett. 77 (2000) 3809.
[36] R. Jansen, P.S. Anil Kumar, O.M.J. Van't Erve, R. Vlutters, P. de Haan, J.C. Lodder, Phys. Rev. Lett. 85 (2000) 3277.
[37] G.A. Prinz, Phys. Today 48 (4) (1995) 58; G.A. Prinz, Science 282 (1998) 1660.
[38] J. de Boeck, G. Borghs, Phys. World 12 (4) (1999) 27.
[39] S.A. Wolf, T. Treger, IEEE Trans. Magn. 36 (2000) 2748; S.A. Wolf, D.D. Awschalom, R.A. Burham, J.M. Daughton, S. von Molnár, M.L. Roukes, A.Y. Chtchelkanova, D.M. Treger, Science 294 (2001) 1488.
[40] E. Grochowski, D. Thompson, IEEE Trans. Magn. 30 (1994) 3797.
[41] E. Grochowski, R.F. Hoyt, IEEE Trans. Magn. 32 (1996) 1850.
[42] K. O'Grady, H. Laidler, J. Magn. Magn. Mater. 200 (1999) 616.
[43] L.F. Thompson, C.G. Wilson, M. Bowden (Eds.), Introduction to Microlithography, 2nd Edition, American Chemical Society, Washington DC, 1994, and references therein.
[44] J. Canning, J. Vac. Sci. Technol. B 15 (1997) 2109.
[45] E.J. Lerner, The Ind. Phys. 5 (3) (1999) 18.
[46] K. Nordquist, S. Pandharkar, M. Durlam, D. Resnick, S. Teherani, D. Mancini, T. Zhu, J. Shi, J. Vac. Sci. Technol. B 15 (1997) 2274.
[47] S.Y. Chou, J. Magn. Soc. Japan 21 (1997) 1023.
[48] R.L. White, R.M.H. New, R.F.W. Pease, IEEE Trans. Magn. 33 (1997) 990.
[49] R.P. Cowburn, Science 287 (2000) 1466.
[50] B. Barbara, J. Magn. Magn. Mater. 156 (1996) 123.
[51] K.M. Krishnan (Ed.), Magnetism on a Microscopic Scale, MRS Bull. 20 (10) (1995).
[52] D.D. Awschalom, S. Von Molnár, Physical Properties of Nanometer-Scale Magnets, in: G. Timp (Ed.), Nanotechnology, Springer, New York, 1998 (Chapter 12).
[53] K. Ounadjela, R.L. Stamps, Mesoscopic Magnetism in Metals, in: H.S. Nalwa (Ed.), Handbook of Nanostructured Materials and Nanotechnology, Vol. 2, Academic Press, San Diego, 2000 (Chapter 9).
[54] R.P. Cowburn, Philos. Trans. R. Soc. Lond. A 358 (2000) 281.
[55] R.P. Cowburn, J. Phys. D 33 (2000) R1.
[56] S.Y. Chou, Proc. IEEE 85 (1997) 652.
[57] K.J. Kirk, Contemp. Phys. 41 (2000) 63.
[58] S.O. Demokritov, B. Hillebrands, J. Magn. Magn. Mater. 200 (1999) 706.
[59] V.V. Moshchalkov, V. Bruyndoncx, L. Van Look, M.J. Van Bael, Y. Bruynseraede, A. Tonomura, Quantization and Confinement Phenomena in Nanostructured Superconductors, in: H.S. Nalwa (Ed.), Handbook of Nanostructured Materials and Nanotechnology, Vol. 3, Academic Press, San Diego, 2000 (Chapter).
[60] F.M. Peeters, J. De Boeck, Hybrid Magnetic-Semiconductor Nanostructures, in: H.S. Nalwa (Ed.), Handbook of Nanostructured Materials and Nanotechnology, Vol. 3, Academic Press, San Diego, 2000 (Chapter 7).
[61] C.A. Ross, Ann. Rev. Mater. Sci. 31 (2001) 203.
[62] D. Elliott, Microlithography: Process Technology for IC Fabrication, McGraw-Hill, New York, 1986, and references therein.
[63] J.R. Sheats, B.W. Smith (Eds.), Microlithography Science and Technology, Marcel Dekker, New York, 1998, and references therein.
[64] J.L. Vossen, W. Kern (Eds.), Thin Film Processes, Academic Press, New York, 1978, and references therein.
[65] Y.D. Park, J.A. Caballero, A. Cabbibo, J.R. Childress, H.D. Hudspeth, T.J. Schultz, F. Sharifi, J. Appl. Phys. 81 (1997) 4717.
[66] F. Sharifi, A.V. Herzog, R.C. Dynes, Phys. Rev. Lett. 71 (1993) 428.
[67] A.V. Herzog, P. Xiong, F. Sharifi, R.C. Dynes, Phys. Rev. Lett. 76 (1996) 668.
[68] P.C. Searson, T.P. Moffat, Crit. Rev. Surf. Chem. 3 (1994) 171, and references therein.
[69] C.A. Ross, Ann. Rev. Mater. Sci. 24 (1994) 159, and references therein.
[70] W.D. Williams, N. Giordano, Phys. Rev. B 33 (1986) 8146.
[71] W. Schwarzacher, K. Attenborough, A. Michel, G. Nabiyouni, J.P. Meier, J. Magn. Magn. Mater. 165 (1997) 23.
[72] G.P. Heydon, S.R. Hoon, A.N. Farley, S.L. Tomlinson, M.S. Valera, K. Attenborough, W. Schwarzacher, J. Phys. D 30 (1997) 1083.
[73] L. Piraux, J.M. George, J.F. Despres, C. Leroy, E. Ferain, R. Legras, K. Ounadjela, A. Fert, Appl. Phys. Lett. 65 (1994) 2484.
[74] A. Blondel, J.P. Meier, B. Doudin, J.-Ph. Ansermet, Appl. Phys. Lett. 65 (1994) 3019.
[75] K. Liu, K. Nagodawithana, P.C. Searson, C.L. Chien, Phys. Rev. B 51 (1995) 7381.
[76] B. Doudin, G. Redmond, S.E. Gilbert, J.-Ph. Ansermet, Phys. Rev. Lett. 79 (1997) 933.
[77] J.A. Rogers, K.E. Paul, R.J. Jackman, G.M. Whitesides, Appl. Phys. Lett. 70 (1997) 2658.
[78] J. Aizenberg, J.A. Roger, K.E. Paul, G.M. Whitesides, Appl. Phys. Lett. 71 (1997) 3773.
[79] J. Tominaga, T. Nakano, N. Atoda, Appl. Phys. Lett. 73 (1998) 2078.
[80] M.M. Alkaisi, R.J. Blaikie, S.J. McNab, Microelectron. Eng. 53 (2000) 237.
[81] M. Kuwahara, T. Nakano, J. Tominaga, M.B. Lee, N. Atoda, Microelectron. Eng. 53 (2000) 535.
[82] T. Pokhil, D. Song, J. Nowak, J. Appl. Phys. 87 (2000) 6319.
[83] J.F. Smyth, S. Schultz, D. Kern, H. Schmid, D. Yee, J. Appl. Phys. 63 (1988) 4237.

[84] P.B. Fischer, S.Y. Chou, Appl. Phys. Lett. 62 (1993) 2989.
[85] R.M.H. New, R.F.W. Pease, R.L. White, J. Vac. Sci. Technol. B 12 (1994) 3196.
[86] W. Xu, J. Wong, C.C. Cheng, R. Johnson, A. Scherer, J. Vac. Sci. Technol. B 13 (1995) 2372.
[87] D. Streblechenko, M.R. Scheinfein, J. Vac. Sci. Technol. A 16 (1998) 1374.
[88] S.Y. Chou, P.R. Krauss, L. Kong, J. Appl. Phys. 79 (1996) 6101.
[89] S.M. Chérif, J.F. Hennequin, J. Magn. Magn. Mater. 165 (1997) 504.
[90] J.I. Martín, Y. Jaccard, A. Hoffmann, J. Nogués, J.M. George, J.L. Vicent, I.K. Schuller, J. Appl. Phys. 84 (1998) 411.
[91] T. Devolder, C. Chappert, Y. Chen, E. Cambril, H. Bernas, J.P. Jamet, J. Ferre, Appl. Phys. Lett. 74 (1999) 3383.
[92] J.I. Martín, J.L. Vicent, J.V. Anguita, F. Briones, J. Magn. Magn. Mater. 203 (1999) 156.
[93] T. Ono, H. Miyajima, K. Shigeto, T. Shinjo, J. Magn. Magn. Mater 198–199 (1999) 225.
[94] J. Wong, A. Scherer, M. Todorovic, S. Schultz, J. Appl. Phys. 85 (1999) 5489.
[95] Y.D. Park, K.B. Jung, M. Overberg, D. Temple, S.J. Pearton, P.H. Holloway, J. Vac. Sci. Technol. B 18 (2000) 16.
[96] B. Khamsehpour, C.D.W. Wilkinson, J.N. Chapman, A.B. Johnston, J. Vac. Sci. Technol. B 14 (1996) 3361.
[97] D.J. Smith, R.E. Dunin-Borkowski, M.R. McCartney, B. Kardynal, M.R. Scheinfein, J. Appl. Phys. 87 (2000) 7400.
[98] T. Taniyama, I. Nakatani, T. Namikawa, Y. Yamazaki, Phys. Rev. Lett. 82 (1999) 2780.
[99] J. Rothman, M. Kläui, L. Lopez-Diaz, C.A.F. Vaz, A. Bleloch, J.A.C. Bland, Z. Cui, R. Speaks, Phys. Rev. Lett. 86 (2001) 1098.
[100] C.C. Yao, D.G. Hasko, Y.B. Xu, W.Y. Lee, J.A.C. Bland, J. Appl. Phys. 85 (1999) 1689.
[101] Y. Yokoyama, Y. Suzuki, S. Yuasa, K. Ando, K. Shigeto, T. Shinjo, P. Gogol, J. Millat, A. Thiaville, T. Ono, T. Kawagoe, J. Appl. Phys. 87 (2000) 5618.
[102] P. Vavassori, V. Metlushko, M. Grimsditch, B. Ilic, P. Neuzil, R. Kumar, Phys. Rev. B 61 (2000) 5895.
[103] K.J. Kirk, J.N. Chapman, C.D. Wilkinson, Appl. Phys. Lett. 71 (1997) 539.
[104] J. Yu, U. Rüdiger, L. Thomas, S.S.P. Parkin, A.D. Kent, J. Appl. Phys. 85 (1999) 5501.
[105] M. Herrmann, S. McVitie, J.N. Chapman, J. Appl. Phys. 87 (2000) 2994.
[106] S.Y. Chou, P.R. Krauss, J. Magn. Magn. Mater. 155 (1996) 151.
[107] C. Haginoya, K. Koike, Y. Hirayama, J. Yamamoto, M. Ishibashi, O. Kitakami, Y. Shimada, Appl. Phys. Lett. 75 (1999) 3159.
[108] T. Schrefl, J. Fidler, K.J. Kirk, J.N. Chapman, J. Magn. Magn. Mater. 175 (1997) 193.
[109] Y. Otani, S.G. Kim, T. Kohda, K. Fukamichi, IEEE Trans. Magn. 34 (1998) 1090.
[110] J. Raabe, R. Pulwey, R. Sattler, T. Schweinböck, J. Zweck, D. Weiss, J. Appl. Phys. 88 (2000) 4437.
[111] K.J. Kirk, J.N. Chapman, S. McVitie, P.R. Aitchison, C.D.W. Wilkinson, J. Appl. Phys. 87 (2000) 5105.
[112] A.O. Adeyeye, R.P. Cowburn, M.E. Welland, J. Magn. Magn. Mater. 213 (2000) L1.
[113] M. Schneider, H. Hoffmann, J. Zweck, Appl. Phys. Lett. 77 (2000) 2909.
[114] R.P. Cowburn, D.K. Koltsov, A.O. Adeyeye, M.E. Welland, Appl. Phys. Lett. 73 (1998) 3947.
[115] R.P. Cowburn, D.K. Koltsov, A.O. Adeyeye, M.E. Welland, Phys. Rev. Lett. 83 (1999) 1042.
[116] C.E. Moreau, J.A. Caballero, R. Loloee, W.P. Pratt Jr., N.O. Birge, J. Appl. Phys. 87 (2000) 6316.
[117] K.J. Kirk, J.N. Chapman, J. Magn. Soc. Japan 21 (1997) 1005.
[118] J.G. King, W. Williams, C.D. Wilkinson, S. McVitie, J.N. Chapman, Geophys. Res. Lett. 23 (1996) 2847.
[119] H. Kubota, T. Ikari, Y. Ando, H. Kato, T. Miyazaki, J. Appl. Phys. 87 (2000) 6325.
[120] M. Vélez, R. Morales, J.M. Alameda, J.I. Martín, J.L. Vicent, F. Briones, J. Appl. Phys. 87 (2000) 5654.
[121] M.S. Wei, S.Y. Chou, J. Appl. Phys. 76 (1994) 6679.
[122] A. Maeda, M. Kume, T. Ogura, K. Kuroki, T. Yamada, M. Nishikawa, Y. Harada, J. Appl. Phys. 76 (1994) 6667.
[123] M.J. Van Bael, K. Temst, V.V. Moshchalkov, Y. Bruynseraede, Phys. Rev. B 59 (1999) 14674.
[124] R.M.H. New, R.F.W. Pease, R.L. White, J. Magn. Magn. Mater. 155 (1996) 140.
[125] I. Nakatani, IEEE Trans. Magn. 32 (1996) 4448.
[126] A.O. Adeyeye, J.A.C. Bland, C. Daboo, J. Lee, U. Ebels, H. Ahmed, J. Appl. Phys. 79 (1996) 6120.
[127] C. Haginoya, S. Heike, M. Ishibashi, K. Nakamura, K. Koike, T. Yoshimura, J. Yamamoto, Y. Hirayama, J. Appl. Phys. 85 (1999) 8327.
[128] J. Yu, A.D. Kent, S.S.P. Parkin, J. Appl. Phys. 87 (2000) 5049.
[129] M. Fraune, U. Rüdiger, G. Güntherodt, S. Cardoso, P. Freitas, Appl. Phys. Lett. 77 (2000) 3815.
[130] T. Devolder, C. Chappert, Y. Chen, E. Cambril, H. Launois, H. Bernas, J. Ferré, J.P. Jamet, J. Vac. Sci. Technol. B 17 (1999) 3177.
[131] T. Devolder, C. Chappert, V. Mathet, H. Bernas, Y. Chen, J.P. Jamet, J. Ferré, J. Appl. Phys. 87 (2000) 8671.
[132] S.E. Russek, W.E. Bailey, IEEE Trans. Magn. 36 (2000) 2990.
[133] K. Matsuyama, K. Matsuo, Y. Nozaki, J. Appl. Phys. 85 (1999) 5474.
[134] J.A. Katine, F.J. Albert, R.A. Buhrman, Appl. Phys. Lett. 76 (2000) 354.
[135] C. Shearwood, S.J. Blundell, M.J. Baird, J.A.C. Bland, M. Gester, H. Ahmed, H.P. Hughes, J. Appl. Phys. 75 (1994) 5249.
[136] M. Hanson, C. Johansson, B. Nilsson, P. Isberg, R. Wäppling, J. Appl. Phys. 85 (1999) 2793.

[137] Y.B. Xu, A. Hirohata, L. Lopez-Diaz, H.T. Leung, M. Tselepi, S.M. Gardiner, W.Y. Lee, J.A.C. Bland, F. Rousseaux, E. Cambril, H. Launois, J. Appl. Phys. 87 (2000) 7019.
[138] J.I. Martín, J.L. Vicent, J.L. Costa-Krämer, J.L. Menéndez, A. Cebollada, J.V. Anguita, F. Briones, IEEE Trans. Magn. 36 (2000) 3002.
[139] H. Demand, M. Hehn, K. Ounadjela, R.L. Stamps, E. Cambril, A. Cornette, F. Rousseaux, J. Appl. Phys. 87 (2000) 5111.
[140] S. Ganesan, C.M. Park, K. Hattori, H.C. Park, R.L. White, H. Koo, R.D. Gomez, IEEE Trans. Magn. 36 (2000) 2987.
[141] M. Farhoud, H.I. Smith, M. Hwang, C.A. Ross, J. Appl. Phys. 87 (2000) 5120.
[142] K.B. Jung, H. Cho, K.P. Lee, J. Marburger, F. Sharifi, R.K. Singh, D. Kumar, K.H. Dahmen, S.J. Pearton, J. Vac. Sci. Technol. B 17 (1999) 3186.
[143] K.B. Jung, J. Hong, J.R. Childress, S.J. Pearton, F. Sharifi, M. Jenson, A.T. Hurst, J. Magn. Magn. Mater. 198–199 (1999) 204.
[144] P.R. Krauss, P.B. Fischer, S.Y. Chou, J. Vac. Sci. Technol. B 12 (1994) 3639.
[145] S.Y. Chou, M.S. Wei, P.R. Krauss, P.B. Fischer, J. Appl. Phys. 76 (1994) 6673.
[146] R. O'Barr, S.Y. Yamamoto, S. Schultz, W. Xu, A. Scherer, J. Appl. Phys. 81 (1997) 4730.
[147] J. Bae, S. Kim, M. Mondol, M. Farhoud, M. Hwang, K. Youcef-Toumi, J. Appl. Phys. 87 (2000) 5123.
[148] D. Welipitiya, C.N. Borca, P.A. Dowben, I. Gobulukoglu, H. Jiang, B.W. Robertson, J. Zhang, Mat. Res. Soc. Symp. Proc. 475 (1997) 257.
[149] M.A. McCord, J. Vac. Sci. Technol. B 15 (1997) 2125.
[150] J.P. Silverman, J. Vac. Sci. Technol. B 15 (1997) 2117.
[151] Y. Chen, R.K. Kupka, F. Rousseaux, F. Carcenac, D. Decanini, M.F. Ravet, H. Launois, J. Vac. Sci. Technol. B 12 (1994) 3959.
[152] F. Rousseaux, D. Decanini, F. Carcenac, E. Cambril, M.F. Ravet, C. Chappert, N. Bardou, B. Bartenlian, P. Veillet, J. Vac. Sci. Technol. B 13 (1995) 2787.
[153] M. Hehn, K. Ounadjela, J.-P. Bucher, F. Rousseaux, D. Decanini, B. Bartenlian, C. Chappert, Science 272 (1996) 1782.
[154] N. Bardou, B. Bartenlian, F. Rousseaux, D. Decanini, F. Carcenac, E. Cambril, M.F. Ravet, C. Chappert, P. Veillet, P. Beauvillain, R. Mégy, W. Geerts, J. Ferré, J. Magn. Magn. Mater. 156 (1996) 139.
[155] C. Miramond, C. Fermon, F. Rousseaux, D. Decanini, F. Carcenac, J. Magn. Magn. Mater. 165 (1997) 500.
[156] B. Hillebrands, C. Mathieu, C. Hartmann, M. Bauer, O. Büttner, S. Riedling, B. Roos, S.O. Demokritov, B. Bartenlian, C. Chappert, D. Decanini, F. Rousseaux, E. Cambril, A. Müller, B. Hoffmann, U. Hartmann, J. Magn. Magn. Mater. 175 (1997) 10.
[157] W. Schwarzacher, O.I. Kasyutich, P.R. Evans, M.G. Darbyshire, G. Yi, V.M. Fedosyuk, F. Rousseaux, E. Cambril, D. Decanini, J. Magn. Magn. Mater. 198–199 (1999) 185.
[158] J. Jorzick, S.O. Demokritov, B. Hillebrands, B. Bartenlian, C. Chappert, D. Decanini, F. Rousseaux, E. Cambril, Appl. Phys. Lett. 75 (1999) 3859.
[159] M. Hehn, R. Ferré, K. Ounadjela, J.-P. Bucher, F. Rousseaux, J. Magn. Magn. Mater. 165 (1997) 5.
[160] O. Fruchart, J.-P. Nozières, W. Wernsdorfer, D. Givord, F. Rousseaux, D. Decanini, Phys. Rev. Lett. 82 (1999) 1305.
[161] O. Fruchart, W. Wernsdorfer, J.-P. Nozières, D. Givord, F. Rousseaux, D. Mailly, D. Decanini, F. Carcenac, J. Magn. Magn. Mater. 198–199 (1999) 228.
[162] J.-E. Wegrowe, O. Fruchart, J.-P. Nozières, D. Givord, F. Rousseaux, D. Decanini, J.Ph. Ansermet, J. Appl. Phys. 86 (1999) 1028.
[163] J.-P. Jamet, S. Lemerle, P. Meyer, J. Ferré, B. Bartenlian, N. Bardou, C. Chappert, P. Veillet, F. Rousseaux, D. Decanini, H. Launois, Phys. Rev. B 57 (1998) 14320.
[164] M. Farhoud, M. Hwang, H.I. Smith, M.L. Schattenburg, J.M. Bae, K. Youcef-Toumi, C.A. Ross, IEEE Trans. Magn. 34 (1998) 1087.
[165] M. Farhoud, J. Ferrera, A.J. Lochtefeld, T.E. Murphy, M. Schattenburg, J. Carter, C.A. Ross, H.I. Smith, J. Vac. Sci. Technol. B 17 (1999) 3182.
[166] S. Kreuzer, K. Prügl, G. Bayreuther, D. Weiss, Thin Solid Films 318 (1998) 219.
[167] T.A. Savas, M. Farhoud, H.I. Smith, M. Hwang, C.A. Ross, J. Appl. Phys. 85 (1999) 6160.
[168] C.A. Ross, R. Chantrell, M. Hwang, M. Farhoud, T. Savas, Y. Hao, H.J. Smith, F.M. Ross, M. Redjdal, F.B. Humphrey, Phys. Rev. B 62 (2000) 14252.
[169] M.A.M. Haast, I.R. Heskamp, L. Abelmann, J.C. Lodder, T.J.A. Popma, J. Magn. Magn. Mater. 193 (1999) 511.
[170] M.A.M. Haast, J.R. Schuurhuis, L. Abelmann, J.C. Lodder, T.J. Popma, IEEE Trans. Magn. 34 (1998) 1006.
[171] M. Hwang, M.C. Abraham, T.A. Savas, H.I. Smith, R.J. Ram, C.A. Ross, J. Appl. Phys. 87 (2000) 5108.
[172] Y. Hao, M. Walsh, M. Farhoud, C.A. Ross, H.I. Smith, J.Q. Wang, L. Malkinski, IEEE Trans. Magn. 36 (2000) 2996.
[173] C. Pike, A. Fernandez, J. Appl. Phys. 85 (1999) 6668.
[174] M. Schneider, H. Hoffmann, J. Appl. Phys. 86 (1999) 4539.
[175] M. Zölfl, S. Kreuzer, D. Weiss, G. Bayreuther, J. Appl. Phys. 87 (2000) 7016.
[176] A. Fernandez, M.R. Gibbons, M.A. Wall, C.J. Cerjan, J. Magn. Magn. Mater. 190 (1998) 71.
[177] A. Fernandez, C.J. Cerjan, J. Appl. Phys. 87 (2000) 1395.
[178] C.A. Ross, T.A. Savas, H.I. Smith, M. Hwang, R. Chantrell, IEEE Trans. Magn. 35 (1999) 3781.
[179] C.A. Ross, H.I. Smith, T. Savas, M. Schattenburg, M. Farhoud, M. Hwang, M. Walsh, M.C. Abraham, R.J. Ram, J. Vac. Sci. Technol. B 17 (1999) 3168.
[180] J. Lohau, S. Kirsch, A. Carl, E.F. Wassermann, Appl. Phys. Lett. 76 (2000) 3094.

[181] M. Thielen, S. Kirsch, H. Weinforth, A. Carl, E.F. Wassermann, IEEE Trans. Magn. 34 (1998) 1099.
[182] A. Carl, S. Kirsch, J. Lohau, H. Weinforth, E.F. Wassermann, IEEE Trans. Magn. 35 (1999) 3106.
[183] A. Fernandez, P.J. Bedrossian, S.L. Baker, S.P. Vernon, D.R. Kania, IEEE Trans. Magn. 32 (1996) 4472.
[184] G. Meier, M. Kleber, D. Grundler, D. Heitmann, R. Wiesendanger, Appl. Phys. Lett. 72 (1998) 2168.
[185] E.F. Wassermann, M. Thielen, S. Kirsch, A. Pollmann, H. Weinforth, A. Carl, J. Appl. Phys. 83 (1998) 1753.
[186] W. Van Roy, E.L. Carpi, M. Van Hove, A. Van Esch, R. Bogaerts, J. de Boeck, G. Borghs, J. Magn. Magn. Mater. 121 (1993) 197.
[187] C. Ross, H. Smith, Data Storage 5 (10) (1998) 41.
[188] K. Bessho, Y. Iwasaki, S. Hashimoto, J. Appl. Phys. 79 (1996) 5057.
[189] K. Bessho, Y. Iwasaki, S. Hashimoto, IEEE Trans. Magn. 32 (1996) 4443.
[190] T. Schaub, R. Wiesendanger, H.J. Güntherodt, Nanotechnology 3 (1992) 77.
[191] C.X. Guo, D.J. Thomson, Ultramicroscopy 42–44 (1992) 1452.
[192] S. Wirth, J.J. Heremans, S. von Molnár, M. Field, K.L. Campman, A.C. Gossard, D.D. Awschalom, IEEE Trans. Magn. 34 (1998) 1105.
[193] S. Wirth, S. von Molnár, Appl. Phys. Lett. 76 (2000) 3283.
[194] S. Wirth, S. von Molnár, M. Field, D.D. Awschalom, J. Appl. Phys. 85 (1999) 5249.
[195] S. Wirth, S. von Molnár, J. Appl. Phys. 87 (2000) 7010.
[196] A.D. Kent, S. von Molnár, S. Gider, D.D. Awschalom, J. Appl. Phys. 76 (1994) 6656.
[197] S. Gider, J. Shi, D.D. Awschalom, P.F. Hopkins, K.L. Campman, A.C. Gossard, A.D. Kent, S. von Molnár, Appl. Phys. Lett. 69 (1996) 3269.
[198] D.D. Awschalom, D.P. di Vincenzo, Phys. Today 48 (4) (1995) 43.
[199] S. Wirth, M. Field, D.D. Awschalom, S. von Molnár, Phys. Rev. B 57 (1998) R14028.
[200] M.A. McCord, D.D. Awschalom, Appl. Phys. Lett. 57 (1990) 2153.
[201] A.D. Kent, T.M. Shaw, S. von Molnár, D.D. Awschalom, Science 262 (1993) 1249.
[202] D.D. Awschalom, M.A. McCord, G. Grinstein, Phys. Rev. Lett. 65 (1990) 783.
[203] W. Schindler, D. Hofmann, J. Kirshner, J. Appl. Phys. 87 (2000) 7007.
[204] D. Hofmann, W. Schindler, J. Kirshner, Appl. Phys. Lett. 73 (1998) 3279.
[205] S. Gadetsky, T. Suzuki, J.K. Erwin, M. Mansuripur, IEEE Trans. Magn. 30 (1994) 4404.
[206] S. Gadetsky, T. Suzuki, J.K. Erwin, M. Mansuripur, IEEE Trans. Magn. 31 (1995) 3253.
[207] S. Gadetsky, J.K. Erwin, M. Mansuripur, T. Suzuki, J. Appl. Phys. 79 (1996) 5687.
[208] T. Iwanaga, M. Nakada, R. Katayama, IEEE Trans. Magn. 31 (1995) 3221.
[209] T.H. Wu, J.C. Wu, B.M. Chen, H.P. Shieh, IEEE Trans. Magn. 34 (1998) 1994.
[210] T.H. Wu, J.C. Wu, B.M. Chen, H.P. Shieh, J. Magn. Magn. Mater. 202 (1999) 62.
[211] T.H. Wu, J.C. Wu, Y.W. Huang, B.M. Chen, H.P. Shieh, J. Appl. Phys. 85 (1999) 5980.
[212] A. Ishikawa, T. Ohno, S. Sakano, Y. Shiroishi, J. Magn. Magn. Mater. 120 (1993) 357.
[213] T. Iwanaga, H. Honma, K. Kayanuma, S. Segawa, M. Nakada, R. Katayama, H. Inada, Jpn. J. Appl. Phys. 32 (1993) 5449.
[214] K. Katayama, T. Iwanaga, H. Inada, K. Okanoue, R. Katayama, K. Yoshihara, Y. Yamanaka, M. Tsunekane, O. Okada, Proc. SPIE 1316 (1990) 35.
[215] D.J. Twisselmann, B.T. Adekor, M. Farhoud, H.I. Smith, P.C. Dorsey, C.A. Ross, Mater. Res. Soc. Symp. Proc. 517 (1998) 193.
[216] D.J. Twisselmann, M. Farhoud, H.I. Smith, C.A. Ross, J. Appl. Phys. 85 (1999) 4292.
[217] S. Landis, B. Rodmacq, B. Dieny, B. Dal'Zotto, S. Tedesco, M. Heitsmann, Appl. Phys. Lett. 75 (1999) 2473.
[218] S. Landis, B. Rodmacq, B. Dieny, Phys. Rev. B 62 (2000) 12271.
[219] A. Jander, R.S. Indeck, M.W. Muller, IEEE Trans. Magn. 35 (1999) 3995.
[220] K. Matsuyama, S. Komatsu, Y. Nozaki, J. Appl. Phys. 87 (2000) 4724.
[221] J.C.A. Huang, L.C. Wu, M.M. Chen, T.H. Wu, J.C. Wu, Y.W. Huang, C.H. Lee, C.M. Fu, J. Magn. Magn. Mater. 209 (2000) 90.
[222] J.J. McClelland, W.R. Anderson, R.J. Celotta, Proc. SPIE 2995 (1997) 90.
[223] D.A. Tulshinsky, M.H. Kelley, J.J. McClelland, R. Gupta, R.J. Celotta, J. Vac. Sci. Technol. A 16 (1998) 1817.
[224] T. Shinjo, T. Ono, J. Magn. Magn. Mater. 177-181 (1998) 31.
[225] T. Ono, Y. Sugita, T. Shinjo, J. Phys. Soc. Japan 65 (1996) 3021.
[226] T. Shinjo, T. Ono, K. Shigeto, Y. Suguita, Acta Phys. Polonica A 91 (1997) 27.
[227] M.A.M. Gijs, M.T. Johnson, A. Reinders, P.E. Huisman, P.J.M. Van de Veerdonk, S.K.J. Lenczowski, R.M.J. Van Gansewinkel, Appl. Phys. Lett. 66 (1995) 1839.
[228] J. Jorritsma, M.A.M. Gijs, J.M. Kerkhof, J.G.H. Stienen, Nanotechnol. 7 (1996) 263.
[229] M.A.M. Gijs, S.K.J. Lenczowski, J.B. Giesbers, R.J.M. Van der Veerdonk, M.T. Johnson, R.M. Jungblut, A. Reinders, R.M.J. Van Gansewinkel, J. Magn. Magn. Mater. 151 (1995) 333.
[230] W. Oepts, M.A.M. Gijs, A. Reinders, R.M. Jungblut, R.M.J. Van Gansewinkel, W.J.M. de Jonge, Phys. Rev. B 53 (1996) 14024.
[231] M.A.M. Gijs, A. Reinders, R.M. Jungblut, W. Oepts, W.J.M. de Jonge, J. Magn. Magn. Mater. 165 (1997) 17.
[232] J. Jorritsma, J.A. Mydosh, J. Appl. Phys. 84 (1998) 901.

[233] R. Krams, F. Lauks, R.L. Stamps, B. Hillebrands, G. Güntherodt, H.P. Oepen, J. Magn. Magn. Mater. 121 (1993) 483.
[234] J. Hauschild, U. Gradmann, H.J. Elmers, Appl. Phys. Lett. 72 (1998) 3211.
[235] J. Shen, R. Skomski, M. Klaua, H. Jenniches, S. Sundar Manoharan, J. Krischner, J. Appl. Phys. 81 (1997) 3901.
[236] A. Dellmeyer, C. Carbone, W. Eberhardt, C. Pampuch, O. Rader, W. Gudat, P. Gambardella, K. Kern, Phys. Rev. B 61 (2000) R5133.
[237] J. Chen, J.L. Erskine, Phys. Rev. Lett. 68 (1992) 1212.
[238] M. Sussiau, F. Nguyen Van Dau, P. Galtier, A. Schuhl, Appl. Phys. Lett. 69 (1996) 857.
[239] F. Nguyen Van Dau, M. Sussiau, A. Schuhl, P. Galtier, J. Appl. Phys. 81 (1997) 4482.
[240] M. Sussiau, A. Encinas, F. Nguyen Van Dau, A. Vaurès, A. Schuhl, P. Galtier, Mat. Res. Soc. Symp. Proc. 475 (1997) 195.
[241] C. Teichert, J. Barthel, H.P. Oepen, J. Krischner, Appl. Phys. Lett. 74 (1999) 588.
[242] A. Sugawara, T. Coyle, G.G. Hembree, M.R. Scheinfein, Appl. Phys. Lett. 70 (1997) 1043.
[243] A. Sugawara, G.G. Hembree, M.R. Scheinfein, J. Appl. Phys. 82 (1997) 5662.
[244] A. Sugawara, M.R. Scheinfein, Phys. Rev. B 56 (1997) R8499.
[245] A. Sugawara, D. Streblechenko, M. McCartney, M.R. Scheinfein, IEEE Trans. Magn. 34 (1998) 1081.
[246] L. Ressier, A. Schuhl, F. Nguyen Van Dau, K. Postava, M. Goiranm, J.P. Peyerade, A.R. Fert, J. Appl. Phys. 81 (1997) 5464.
[247] H. Jaffrès, L. Ressier, J.P. Peyrade, A.R. Fert, P. Gogol, A. Thiaville, A. Schuhl, F. Nguyen Van Dau, J. Appl. Phys. 84 (1998) 4375.
[248] H. Jaffrès, L. Ressier, K. Postava, A. Schuhl, F. Nguyen Van Dau, M. Goiran, J.P. Redoulès, J.P. Peyrade, A.R. Fert, J. Magn. Magn. Mater. 184 (1998) 19.
[249] L. Ressier, H. Jaffrès, E. Snoeck, D. Bertrand, A.R. Fert, J.P. Peyrade, A. Schuhl, F. Nguyen Van Dau, Mat. Sci. Forum 269–272 (1998) 955.
[250] L. Ressier, H. Jaffrès, A. Schuhl, F. Nguyen Van Dau, M. Goiran, J.P. Redoulès, J.P. Peyrade, A.R. Fert, Mat. Res. Soc. Symp. Proc. 475 (1997) 239.
[251] P.R. Krauss, S.Y. Chou, J. Vac. Sci. Technol. B 13 (1995) 2850.
[252] L. Kong, L. Zhuang, S.Y. Chou, IEEE Trans. Magn. 33 (1997) 3019.
[253] W. Wu, B. Cui, X.Y. Sun, W. Zhang, L. Zhuang, L. Kong, S.Y. Chou, J. Vac. Sci. Technol. B 16 (1998) 3825.
[254] B. Cui, L. Kong, X. Sun, S.Y. Chou, J. Appl. Phys. 85 (1999) 5534.
[255] L. Kong, L. Zhuang, M. Li, B. Cui, S.Y. Chou, Jpn. J. Appl. Phys. 37 (1998) 5973.
[256] S.Y. Chou, P.R. Kraus, W. Zhang, L. Guo, L. Zhuang, J. Vac. Sci. Technol. B 15 (1997) 2897.
[257] S.P. Li, A. Lebib, D. Peyrade, M. Natali, Y. Chen, Appl. Phys. Lett. 77 (2000) 2743.
[258] S. Palacin, P.C. Hidber, J.P. Bourgoin, C. Miramond, C. Ferman, G.M. Whitesides, Chem. Mater. 8 (1996) 1316.
[259] Z. Zhong, B. Gates, Y. Xia, B. Qin, Langmuir 16 (2000) 10369.
[260] C. Stamm, F. Marty, A. Vaterlaus, V. Weich, S. Egger, U. Maier, U. Ramsperger, H. Fuhrmann, D. Pescia, Science 282 (1998) 449.
[261] F. Marty, A. Vaterlaus, V. Weich, C. Stamm, U. Maier, D. Pescia, J. Appl. Phys. 85 (1999) 6166.
[262] G. Carter, J. Phys. D 34 (2001) R1.
[263] K. Koike, H. Matsuyama, Y. Hirayama, K. Tanahashi, T. Kanemura, O. Kitakami, Y. Shimada, Appl. Phys. Lett. 78 (2001) 784.
[264] J. Lohau, A. Moser, C.T. Rettner, M.E. Best, B.D. Terris, Appl. Phys. Lett. 78 (2001) 990.
[265] Y. Yakushiji, S. Mitani, N. Takahashi, H. Fujimori, J. Magn. Soc. Japan 24 (2000) 567.
[266] A.Y. Toporov, R.M. Langford, A.K. Petford-Long, Appl. Phys. Lett. 77 (2000) 3063.
[267] X. Lin, J.G. Zhu, W. Messner, IEEE Trans. Magn. 36 (2000) 2999.
[268] N.I. Polushkin, S.A. Gusev, M.N. Drozdov, Y.K. Verevkin, V.N. Petryakov, J. Appl. Phys. 81 (1997) 5478.
[269] J. Wittborn, C. Canalias, K.V. Rao, N.I. Polushkin, in: M.R.J. Gibbs (Ed.), Modern Trends in Magnetostriction Study and Application, Kluwer Academic Press, Amsterdam, 2000, p. 263.
[270] C. Chappert, H. Bernas, J. Ferré, V. Kottler, J.P. Jamet, Y. Chen, E. Cambril, T. Devolder, F. Rousseaux, V. Mathet, H. Launois, Science 280 (1998) 1919.
[271] T. Aign, P. Meyer, S. Lemerle, J.P. Jamet, J. Ferré, V. Mathet, C. Chappert, J. Gierak, C. Vieu, F. Rousseaux, H. Launois, H. Bernas, Phys. Rev. Lett. 81 (1998) 5656.
[272] T. Devolder, C. Vieu, H. Bernas, J. Ferré, C. Chappert, J. Gierak, J.P. Jamet, T. Aign, P. Meyer, Y. Chen, F. Rousseaux, V. Mathet, H. Launois, O. Kaitasov, C.R. Acad. Sci. Paris 327 Série II (1999) 915.
[273] H. Bernas, T. Devolder, C. Chappert, J. Ferré, V. Kottler, Y. Chen, C. Vieu, J.P. Jamet, V. Mathet, E. Cambril, O. Kaitasov, S. Lemerle, F. Rousseaux, H. Launois, Nucl. Instrum. Methods B 148 (1999) 872.
[274] C. Vieu, J. Gierak, H. Launois, T. Aign, P. Meyer, J.P. Jamet, J. Ferré, C. Chappert, V. Mathet, H. Bernas, Microelectron. Eng. 53 (2000) 191.
[275] B.D. Terris, L. Folks, D. Weller, J.E.E. Baglin, J. Kellock, H. Rothuizen, P. Vettiger, Appl. Phys. Lett. 75 (1999) 403.
[276] B.D. Terris, D. Weller, L. Folks, J.E.E. Baglin, A.J. Kellock, H. Rothuizen, P. Vetrtiger, J. Appl. Phys. 87 (2000) 7004.
[277] W.H. Bruenger, M. Torkler, C. Dzionk, B.D. Terris, L. Folks, D. Weller, H. Rothuizen, P. Vettiger, G. Stangl, W. Fallmann, Microelectron. Eng. 53 (2000) 605.
[278] H. Takeshita, Y. Suzuki, H. Akinaga, W. Mizutani, K. Tanaka, T. Katayama, A. Itoh, Appl. Phys. Lett. 68 (1996) 3040.

[279] H. Takeshita, Y. Suzuki, H. Akinaga, W. Mizutani, T. Katayama, A. Itoh, K. Tanaka, J. Magn. Magn. Mater. 165 (1997) 38.
[280] O. Fruchart, M. Klaua, J. Barthel, J. Krischner, Appl. Surf. Sci. 162-163 (2000) 529.
[281] S. Padovani, P. Molinàs-Mata, F. Scheurer, J.P. Bucher, Appl. Phys. A 66 (1998) S1199.
[282] O. Fruchart, M. Klaua, J. Barthel, J. Kirschner, Phys. Rev. Lett. 83 (1999) 2769.
[283] D.D. Chambliss, R.J. Wilson, S. Chiang, Phys. Rev. Lett. 66 (1991) 1721.
[284] J. Shen, R. Skomski, M. Klaua, H. Jenniches, S. Sundar Manoharan, J. Kirschner, Phys. Rev. B 56 (1997) 2340.
[285] H. Burne, M. Giovannini, K. Bromann, K. Kern, Nature 394 (1998) 451.
[286] P. Ohresser, G. Ghiringhelli, O. Tjernberg, N.B. Brookes, M. Finazzi, Phys. Rev. B 62 (2000) 5803.
[287] J. de la Figuera, M.A. Huerta-Garnica, J.E. Prieto, C. Ocal, R. Miranda, Appl. Phys. Lett. 66 (1995) 1006.
[288] S.L. Silva, C.R. Jenkins, S.M. York, F.M. Leibsle, Appl. Phys. Lett. 76 (2000) 1128.
[289] T.M. Parker, L.K. Wilson, N.G. Condon, F.M. Leibsle, Phys. Rev. B 56 (1997) 6458.
[290] J.-L. Lin, D.Y. Petrovykh, A. Kirakosian, H. Rauscher, F.J. Himpsel, P.A. Dowben, Appl. Phys. Lett. 78 (2001) 829.
[291] A. Dallmeyer, C. Carbone, W. Eberhardt, C. Pampuch, O. Rader, W. Gudat, P. Gambarella, K. Kern, Phys. Rev. B 61 (2000) R5133.
[292] Tober, R.F.Marks, D.D. Chambliss, K.P. Roche, M.F. Toney, A.J. Kellock, R.F.C. Farrow, Appl. Phys. Lett. 77 (2000) 2728.
[293] K.L. Lee, R.R. Thomas, A. Viehbeck, E.J.M. O'Sullivan, J. Vac. Sci. Technol. B 11 (1993) 2204.
[294] M. Malac, R.F. Egerton, M.J. Brett, B. Dick, J. Vac. Sci. Technol. B 17 (1999) 2671.
[295] B. Dick, M.J. Brett, T.J. Smy, M.R. Freeman, M. Malac, R.F. Egerton, J. Vac. Sci. Technol. A 18 (2000) 1838.
[296] C.T. Seip, C.J. O'Connor, Nanostruct. Mater. 12 (1999) 183.
[297] C. Petit, A. Taleb, M.P. Pileni, J. Phys. Chem. B 103 (1999) 1805.
[298] S. Sun, C.B. Murray, D. Wller, L. Folks, A. Moser, Science 287 (2000) 1989.
[299] C.T. Black, C.B. Murray, R.L. Sandstrom, S. Sun, Science 290 (2000) 1131.
[300] S. Sun, C.B. Murray, J. Appl. Phys. 85 (1999) 4325.
[301] S. Sun, C.B. Murray, H. Doyle, Mat. Res. Soc. Symp. Proc. 577 (1999) 385.
[302] A.L. Oppegard, F.J. Darnell, H.C. Miller, J. Appl. Phys. 32 (Suppl.) (1961) 184S.
[303] L. Zhang, A. Manthiram, Phys. Rev. B 54 (1996) 3462.
[304] M. Giersig, M. Hilgendorff, J. Phys. D 32 (1999) L111.
[305] M. Park, C. Harrison, P. Chaikin, R.A. Register, D.H. Adamson, Science 276 (1997) 1401.
[306] P. Mansky, Y. Liu, E. Huang, T.P. Russell, C. Hawker, Science 275 (1997) 1458.
[307] E. Huang, L. Rockford, T.P. Russell, C.J. Hawker, Nature 395 (1998) 757.
[308] E. Huang, S. Pruzinsky, T.P. Russell, J. Mays, C.J. Hawker, Macromolecules 32 (1999) 5299.
[309] K. Liu, S.M. Baker, M. Tuominen, T.P. Russell, I.K. Schuller, Phys. Rev. B 63 (2001) 060403.
[310] T. Thurn-Albercht, J. Schotter, G.A. Kästle, N. Emley, T. Shibauchi, L. Krusin-Elbaum, K. Guarini, C.T. Black, M.T. Tuominen, T.P. Russell, Science 290 (2000) 2126.
[311] J.C. Hulteen, P. Van Duyne, J. Vac. Sci. Technol. A 13 (1995) 1553.
[312] M. Winzer, M. Kleiber, N. Dix, R. Wiesendanger, Appl. Phys. A 63 (1996) 617.
[313] R. Wiesendanger, M. Bode, M. Kleiber, M. Löhndorf, R. Pascal, A. Wadas, D. Weiss, J. Vac. Sci. Technol. B 15 (1997) 1330.
[314] S.P. Li, W.S. Lew, Y.B. Xu, A. Hirohata, A. Samad, F. Baker, J.A.C. Bland, Appl. Phys. Lett. 76 (2000) 748.
[315] C. Haginoya, M. Ishibashi, K. Koike, Appl. Phys. Lett. 71 (1997) 2934.
[316] O.D. Velev, P.M. Tessier, A.M. Lenhoff, E.W. Kaler, Nature 401 (1999) 548.
[317] F. Keller, M.S. Hunter, D.L. Robinson, J. Electrochem. Soc. 100 (1953) 411.
[318] G.E. Thompson, R.C. Furneaux, G.C. Wood, J.A. Richardson, J.S. Gode, Nature 272 (1978) 433.
[319] R.C. Furneaux, W.R. Rigby, A.P. Davidson, United States Patent 4,687,551, 1987.
[320] M. Moskovits, J.M. Xu, United States Patent 5,581,091, 1996.
[321] S. Kawai, R. Ueda, J. Electrochem. Soc. 122 (1975) 32.
[322] M. Saito, M. Kirihara, T. Taniguchi, M. Miyagi, Appl. Phys. Lett. 55 (1989) 607.
[323] M. Shiraki, Y. Wakui, T. Tokushima, N. Tsuya, IEEE Trans. Magn. Mag-21 (1985) 1465.
[324] M. Zheng, L. Menon, H. Zeng, Y. Liu, S. Bandyopadhyay, R.D. Kirby, D.J. Sellmyer, Phys. Rev. B 62 (2000) 12282.
[325] S. Yang, H. Zhu, D. Yu, Z. Jin, S. Tang, Y. Du, J. Magn. Magn. Mater. 222 (2000) 97.
[326] Y. Peng, H.-L. Zhang, S.-L. Pan, H.-L. Li, J. Appl. Phys. 87 (2000) 7405.
[327] H. Zeng, M. Zheng, R. Skomski, D.J. Sellmyer, Y. Liu, L. Menon, S. Bandyopadhyay, J. Appl. Phys. 87 (2000) 4718.
[328] M. Sun, G. Zangari, R.M. Metzger, IEEE Trans. Magn. 36 (2000) 3005.
[329] H.R. Khan, K. Petrikowski, J. Magn. Magn. Mater. 215–216 (2000) 526.
[330] P.R. Evans, G. Yi, W. Schwarzacher, Appl. Phys. Lett. 76 (2000) 481.
[331] K. Liu, J. Nogués, C. Leighton, H. Masuda, K. Nishio, I.V. Roshchin, I.K. Schuller, Appl. Phys. Lett., in press.
[332] H. Masuda, K. Nishio, N. Baba, Thin Solid Films 223 (1993) 1.
[333] H. Masuda, K. Fukuda, Science 268 (1995) 1466.

[334] J.A. Barnard, H. Fujiwara, V.R. Inturi, J.D. Jarratt, T.W. Scharf, J.L. Weston, Appl. Phys. Lett. 69 (1996) 2758.
[335] K. Liu, C.L. Chien, IEEE Trans. Magn. 34 (1998) 1021.
[336] A. Butera, J.L. Weston, J.A. Barnard, IEEE Trans. Magn. 34 (1998) 1024.
[337] H. Cao, C. Tie, Z. Xu, J. Hong, H. Sang, Appl. Phys. Lett. 78 (2001) 1592.
[338] R.J. Tonucci, B.L. Justus, A.J. Campillo, C.E. Ford, Science 258 (1992) 783.
[339] D.H. Pearson, R.J. Tonucci, Adv. Mater. 8 (1996) 1031.
[340] P.P. Nguyen, D.H. Pearson, R.J. Tonucci, K. Babcock, J. Electrochem. Soc. 145 (1998) 247.
[341] R.J. Tonucci, D.H. Pearson, D.S. Katzer, A. Rosenberg, H.B. Dietrich, Superlattice Microstruct. 20 (1996) 627.
[342] G.E. Possin, Rev. Sci. Instrum. 41 (1970) 772.
[343] L. Sun, P.C. Searson, C.L. Chien, Appl. Phys. Lett. 74 (1999) 2803.
[344] T.M. Whitney, J.S. Jiang, P.C. Searson, C.L. Chien, Science 261 (1993) 1319.
[345] J.-Ph. Ansermet, J. Phys.: Condens. Matter 10 (1998) 6027.
[346] K. Liu, C.L. Chien, P.C. Searson, K. Yu-Zhang, IEEE Trans. Magn. 34 (1998) 1093.
[347] K. Liu, C.L. Chien, P.C. Searson, K. Yu-Zhang, Appl. Phys. Lett. 73 (1998) 1436.
[348] S. Dubois, C. Marchal, J.M. Beuken, L. Piraux, J.L. Duvail, A. Fert, J.M. George, J.L. Maurice, Appl. Phys. Lett. 70 (1997) 396.
[349] W. Wernsdorfer, B. Doudin, D. Mailly, K. Hasselbach, A. Benoit, J. Meier, J.-Ph. Ansermet, B. Barbara, Phys. Rev. Lett. 77 (1996) 1873.
[350] Y. Jaccard, Ph. Guittienne, D. Kelly, J.-E. Wegrowe, J.-Ph. Ansermet, Phys. Rev. B 62 (2000) 1141.
[351] K. Liu, C.L. Chien, P.C. Searson, Phys. Rev. B 58 (1998) R14681.
[352] L. Sun, P.C. Searson, C.L. Chien, Phys. Rev. B 61 (2000) R6463.
[353] A. Encinas-Oropesa, M. Demand, L. Piraux, I. Huynen, U. Ebels, Phys. Rev. B 63 (2001) 104415.
[354] O. Fruchart, J.P. Nozières, B. Kevorkian, J.C. Toussaint, D. Givord, F. Rousseaux, D. Decanini, F. Carcenac, Phys. Rev. B 57 (1998) 2596.
[355] M. Hanson, B. Nilsson, in: G.C. Hadjipanayis, R.W. Siegel (Eds.), Nanophase Materials, Kluwer Academic Press, Amsterdam, 1994, p. 569.
[356] J.F. Smyth, S. Schultz, D.R. Fredkin, D.P. Kern, S.A. Rishton, H. Schmid, M. Cali, T.R. Koehler, J. Appl. Phys. 69 (1991) 5262.
[357] E. Girgis, J. Schelten, J. Shi, J. Janersky, S. Tehrani, H. Goronkin, Appl. Phys. Lett. 76 (2000) 3780.
[358] T. Kohda, Y. Otani, V. Novosad, K. Fukamichi, S. Yuasa, M. Nyvlt, T. Katayama, IEEE Trans. Magn. 35 (1999) 3472.
[359] R.D. Gomez, M.C. Shih, R.M.H. New, R.F.W. Pease, R.L. White, J. Appl. Phys. 80 (1996) 342.
[360] G.A. Gibson, S. Schultz, J. Appl. Phys. 73 (1993) 4516.
[361] G.A. Gibson, J.F. Smyth, S. Schultz, D.P. Kern, IEEE Trans. Magn. 27 (1991) 5187.
[362] R.M.H. New, R.F.W. Pease, R.L. White, J. Vac. Sci. Technol. B 13 (1995) 1089.
[363] J. Shi, T. Zhu, S. Tehrani, Y.F. Zheng, J.G. Zhu, J. Magn. Magn. Mater. 198–199 (1999) 251.
[364] J. Shi, S. Tehrani, M.R. Scheinfein, Appl. Phys. Lett. 76 (2000) 2588.
[365] J. Shi, S. Tehrani, Appl. Phys. Lett. 77 (2000) 1692.
[366] M. Hehn, K. Ounadjela, S. Padovani, J.P. Bucher, J. Arabski, N. Bardou, B. Bartenlian, C. Chappert, F. Rousseaux, D. Decanini, F. Carcenac, E. Cambril, M.F. Ravet, J. Appl. Phys. 79 (1996) 5068.
[367] K. Ounadjela, M. Hehn, R. Ferré, in: G.C. Hadjipanayis (Ed.), Magnetic Hysteresis in Novel Magnetic Materials, Kluwer Academic Publishers, Amsterdam, 1997, p. 485.
[368] W. Wernsdorfer, K. Hasselbach, A. Sulpice, A. Benoit, J.E. Wergowe, L. Thomas, B. Barbara, D. Mailly, Phys. Rev. B 53 (1996) 3341.
[369] J.-E. Wegrowe, W. Wernsdorfer, L. Thomas, B. Barbara, A. Sulpice, K. Hasselbach, A. Benoit, D. Mailly, Phys. Rev. B 53 (1996) 6536.
[370] T.H.P. Chang, D.P. Kern, E. Kratschmer, K.Y. Lee, H.E, M.A.McCord Luhn, S.A. Rishton, Y. Valdimirsky, IBM J. Res. Dev. 32 (1988) 462.
[371] J.L. Duvail, S. Dubois, L. Piraux, A. Vaurès, A. Fert, D. Adam, M. Champagne, F. Rousseaux, D. Decanini, J. Appl. Phys. 84 (1998) 6359.
[372] Y. Otani, T. Kohda, V. Novosad, K. Fukamichi, S. Yuasa, T. Katayama, J. Appl. Phys. 87 (2000) 5621.
[373] J. Shi, T. Zhu, M. Durlam, E. Chen, S. Tehrani, Y.F. Zheng, J.G. Zhu, IEEE Trans. Magn. 34 (1998) 997.
[374] J. Shi, S. Tehrani, T. Zhu, Y.F. Zheng, J.G. Zhu, Appl. Phys. Lett. 74 (1999) 2525.
[375] Y. Otani, T. Kohda, S.G. Kim, K. Fukamichi, O. Kitakami, Y. Shimada, J. Magn. Magn. Mater. 198–199 (1999) 483.
[376] S. Evoy, D.W. Carr, L. Sekaric, Y. Suzuki, J.M. Parpia, H.G. Craighead, J. Appl. Phys. 87 (2000) 404.
[377] M.J. Van Bael, L. Van Look, K. Temst, M. Lange, J. Bekaert, U. May, G. Güntherodt, V.V. Moshchalkov, Y. Bruynseraede, Physica C 332 (2000) 12.
[378] R.P. Cowburn, A.O. Adeyeye, M.E. Welland, Phys. Rev. Lett. 81 (1998) 5414.
[379] R. Mattheis, D. Berkov, N. Gorn, J. Magn. Magn. Mater. 198–199 (1999) 216.
[380] R.P. Cowburn, D.K. Koltsov, A.O. Adeyeye, M.E. Welland, Europhys. Lett. 48 (1999) 221.
[381] R.P. Cowburn, A.O. Adeyeye, M.E. Welland, New J. Phys. 1 (1999) 16.1.
[382] R.P. Cowburn, D.K. Koltsov, A.O. Adeyeye, M.E. Welland, J. Appl. Phys. 87 (2000) 7082.
[383] R.P. Cowburn, D.K. Koltsov, A.O. Adeyeye, M.E. Welland, J. Appl. Phys. 87 (2000) 7067.
[384] J.L. Costa-Krämer, J.I. Martín, J.L. Menéndez, A. Cebollada, J.V. Anguita, F. Briones, J.L. Vicent, Appl. Phys. Lett. 76 (2000) 3091.

[385] M. Grimsditch, Y. Jaccard, I.K. Schuller, Phys. Rev. B 58 (1998) 11539.
[386] G. Gubboitti, L. Albini, G. Carlotti, M. de Crescenzi, E. di Fabrizo, A. Gerardino, O. Donzelli, F. Nizzoli, H. Koo, R.D. Gomez, J. Appl. Phys. 87 (2000) 5633.
[387] P. Vavassori, O. Donzelli, V. Metlushko, M. Grimsditch, B. Ilic, P. Neuzil, R. Kumar, J. Appl. Phys. 88 (2000) 999.
[388] J.A. Johnson, M. Grimsditch, V. Metlushko, P. Vavassori, B. Ilic, P. Neuzil, R. Kumar, Appl. Phys. Lett. 77 (2000) 4410.
[389] L. Thomas, S.S.P. Parkin, J. Yu, U. Rüdiger, A.D. Kent, Appl. Phys. Lett. 76 (2000) 766.
[390] P. Vavassori, O. Donzelli, L. Callegaro, M. Grimsditch, V. Metlushko, IEEE Trans. Magn. 36 (2000) 2993.
[391] N. Bardou, B. Bartenlian, C. Chappert, R. Mégy, P. Veillet, J.P. Renard, F. Rousseaux, M.F. Ravet, J.P. Jamet, P. Meyer, J. Appl. Phys. 79 (1996) 5848.
[392] N. Bardou, B. Bartenlian, F. Rousseaux, D. Decanini, F. Carcenac, C. Chappert, P. Veillet, P. Beauvillain, R. Mégy, Y. Suzuki, J. Ferré, J. Magn. Magn. Mater. 148 (1995) 293.
[393] B. Hillebrands, C. Mathieu, M. Bauer, S.O. Demokritov, B. Bartenlian, C. Chappert, D. Decanini, F. Rousseaux, F. Carcenac, J. Appl. Phys. 81 (1997) 4993.
[394] C. Mathieu, C. Hartman, M. Bauer, O. Buettner, S. Riedling, B. Ross, S.O. Demokritov, B. Hillebrands, B. Bartenlian, C. Chappert, D. Decanini, F. Rousseaux, E. Cambril, A. Müller, B. Hoffmann, U. Hartmann, Appl. Phys. Lett. 70 (1997) 2912.
[395] J. Jorzick, S.O. Demokritov, B. Hillebrands, B. Bartenlian, C. Chappert, D. Decanini, F. Rousseuax, E. Cambril, J. Appl. Phys. 87 (2000) 5082.
[396] P.H. Bryant, J.F. Smyth, S. Schultz, D.R. Fredkin, Phys. Rev. B 47 (1993) 11255.
[397] A. Maeda, M. Kume, Mater. Sci. Eng. A 217–218 (1996) 207.
[398] B.P. Toperverg, G.P. Felcher, V.V. Metlushko, V. Leiner, R. Siebrecht, O. Nikonov, Physica B 283 (2000) 149.
[399] S.J. Bending, G.D. Howells, A.N. Grigorenko, M.J. Van Bael, J. Bekaert, K. Temst, L.Van. Look, V.V. Moshchalkov, Y. Bruynseraede, G. Borghs, R.G. Humphreys, Physica C 332 (2000) 20.
[400] M. Todorovic, S. Schultz, J. Wong, A. Scherer, Appl. Phys. Lett. 74 (1999) 2516.
[401] S.Y. Yamamoto, R. O'Barr, S. Schultz, A. Scherer, IEEE Trans. Magn. 33 (1997) 3016.
[402] S.Y. Yamamoto, S. Schultz, J. Appl. Phys. 81 (1997) 4696.
[403] M. Hehn, K. Ounadjela, R. Ferré, W. Grange, F. Rousseaux, Appl. Phys. Lett. 71 (1997) 2833.
[404] R.D. Gomez, T.V. Luu, A.O. Park, K.J. Kirk, J.N. Chapman, J. Appl. Phys. 85 (1999) 6163.
[405] H. Koo, T.V. Luu, R.D. Gomez, V.V. Metlushko, J. Appl. Phys. 87 (2000) 5114.
[406] W. Wernsdorfer, K. Hasselbach, D. Mailly, B. Barbara, A. Benoit, L. Thomas, G. Suran, J. Magn. Magn. Mater. 145 (1995) 33.
[407] W. Wernsdorfer, D. Mailly, A. Benoit, J. Appl. Phys. 87 (2000) 5094.
[408] A.K. Geim, S.V. Dubonos, J.G.S. Lok, I.V. Grigorieva, J.C. Maan, L. Theil Hansen, P.E. Lindelof, Appl. Phys. Lett. 71 (1997) 2379.
[409] J.G.S. Lok, A.K. Geim, J.C. Maan, S.V. Dubonos, L. Theil Hansen, P.E. Lindelof, Phys. Rev. B 58 (1998) 12201.
[410] J. de Boeck, T. Sands, J.P. Harbison, A. Scherer, H. Gilcheist, T. Cheeks, M. Tanaka, V.G. Keramidasm, Electron. Lett. 29 (1993) 421.
[411] V. Kubrak, F. Rahman, B.L. Gallagher, P.C. Main, M. Henini, C.H. Marrows, M.A. Howson, Appl. Phys. Lett. 74 (1999) 2507.
[412] F.G. Monzon, D.S. Patterson, M.L. Roukes, J. Magn. Magn. Mater. 195 (1999) 19.
[413] V. Kubrak, A.W. Rushforth, A.C. Neumann, F. Rahman, B.L. Gallagher, P.C. Main, M. Henini, C.H. Marrows, B.J. Hickey, Physica E 7 (2000) 997.
[414] S.V. Dubonos, A.K. Geim, K.S. Novoselov, J.G.S. Lok, J.C. Maan, M. Henini, Physica E 6 (2000) 746.
[415] S. McVitie, J.N. Chapman, MRS Bull. 20 (10) (1995) 55.
[416] S. Hefferman, J.N. Chapman, S. McVitie, J. Magn. Magn. Mater. 95 (1991) 76.
[417] A. Tonomura, T. Matsuda, R. Suzuki, A. Fukuhara, N. Osakabe, H. Umezaki, J. Endo, K. Shinagawa, Y. Sugita, H. Fujiwara, Phys. Rev. Lett. 48 (1982) 1443.
[418] C. Beeli, B. Doudin, P. Stadelmann, Phys. Rev. Lett. 75 (1995) 4630.
[419] R.E. Dunin-Borkowski, M.R. McCartney, B. Kardynal, D.J. Smith, J. Appl. Phys. 84 (1998) 374.
[420] O. Pietzsch, A. Kubetzka, M. Bode, R. Wiesendanger, Phys. Rev. Lett. 84 (2000) 5212.
[421] J. Wittborn, K.V. Rao, J. Nogués, I.K. Schuller, Appl. Phys. Lett. 76 (2000) 2931.
[422] T. Eimüller, P. Fischer, G. Schütz, M. Scholz, G. Bayreuther, P. Guttmann, G. Schmahl, M. Köhler, J. Appl. Phys. 89 (2001) 7162.
[423] V. Cross, S.F. Lee, G. Faini, A. Cornette, A. Hamzic, A. Fert, J. Magn. Magn. Mater. 165 (1997) 512.
[424] S. de Haan, J.C. Lodder, J. Magn. Magn. Mater. 168 (1997) 321.
[425] J. Aumentado, V. Chandrasekhar, Appl. Phys. Lett. 74 (1999) 1898.
[426] J. Aumentado, V. Chandrasekhar, Physica B 284-288 (2000) 1742.
[427] S.A. Rishton, Y. Lu, R.A. Altman, A.C. Marley, X.P. Bian, C. Jahnes, R. Viswanathan, G. Xiao, W.J. Gallagher, S.S.P. Parkin, Microelectron. Eng. 35 (1997) 249.
[428] K. Bussman, G.A. Prinz, S.F. Cheng, D. Wang, Appl. Phys. Lett. 75 (1999) 2476.
[429] M. Löhndorf, A. Wadas, G. Lütjering, D. Weiss, R. Wiessendanger, Z. Phys. B 101 (1996) 1.
[430] S.Y. Chou, M. Wei, P.R. Krauss, P.B. Fischer, J. Vac. Sci. Technol. B 12 (1994) 3695.

[431] R.M.H. New, R.F.W. Pease, R.L. White, R.M. Osgood, K. Babcock, J. Appl. Phys. 79 (1996) 5851.
[432] R.M.H. New, R.F.W. Pease, R.L. White, IEEE Trans. Magn. 31 (1995) 3805.
[433] M. Lederman, G.A. Gibson, S. Schultz, J. Appl. Phys. 73 (1993) 6961.
[434] S.Y. Chou, P.R. Krauss, M.S. Wei, P.B. Fischer, Scripta Metall. Mater. 33 (1995) 1537.
[435] T. Chang, M. Lagerquist, J.G. Zhu, J.H. Judy, P.B. Fischer, S.Y. Chou, IEEE Trans. Magn. 28 (1992) 3138.
[436] A. Born, C. Hahn, M. Löhndorf, A. Wadas, C. Witt, R. Wiesendanger, J. Vac. Sci. Technol. B 14 (1996) 3625.
[437] M. Lederman, D.R. Fredkin, R. O'Barr, S. Schultz, M. Ozaki, J. Appl. Phys. 75 (1994) 6217.
[438] M. Kleiber, F. Kümmerlen, M. Löhndorf, A. Wadas, D. Weiss, R. Wiedendanger, Phys. Rev. B 58 (1998) 5563.
[439] K. Babcock, M. Dugas, S. Manalis, V. Elings, Mat. Res. Soc. Symp. Proc. 355 (1995) 311.
[440] S.Y. Chou, Data Storage 2 (5) (1995) 35.
[441] J.C. Wu, H.W. Huang, Y.W. Huang, T.H. Wu, IEEE Trans. Magn. 35 (1999) 3481.
[442] J.C. Wu, Y.W. Hwang, H.W. Hwang, T.H. Wu, Jpn. J. Appl. Phys. 38 (1999) 6711.
[443] J. Wong, A. Scherer, M. Barbic, S. Schultz, J. Vac. Sci. Technol. B 17 (1999) 3190.
[444] T. Shinjo, T. Okuno, R. Hassdorf, K. Shigeto, T. Ono, Science 289 (2000) 930.
[445] J.C. Wu, H.W. Hwang, T.H. Wu, IEEE Trans. Magn. 36 (2000) 2978.
[446] R.E. Dunin-Borowski, M.R. McCartney, B. Kardynal, D.J. Smith, M.R. Scheinfein, Appl. Phys. Lett. 75 (1999) 2641.
[447] C. Beeli, J. Nogués, J.M. George, I.K. Schuller, to be published.
[448] K.J. Kirk, J.N. Chapman, C.D.W. Wilkinson, J. Appl. Phys. 85 (1999) 5237.
[449] K.J. Kirk, J.N. Chapman, P.R. Aitchison, S. McVitie, B. Khamsehpour, M. Ruhrig, C.D.W. Wilkinson, in: G.C. Hadjipanayis (Ed.), Magnetic Hysteresis in Novel Magnetic Materials, Kluwer Academic Publishers, Amsterdam, 1997, p. 309.
[450] K.J. Kirk, J.N. Chapman, S. McVitie, P.R. Aitchison, C.D.W. Wilkinson, Appl. Phys. Lett. 75 (1999) 3683.
[451] D. Grundler, G. Meier, K.B. Broocks, C. Heyn, D. Heitmann, J. Appl. Phys. 85 (1999) 6175.
[452] E.B. Myers, D.C. Ralph, J.A. Katine, R.N. Louie, R.A. Buhrman, Science 285 (2000) 867.
[453] H.Y. Wong, J.N. Chapman, S. McVitie, S.J. Hefferman, J. Magn. Magn. Mater. 104–107 (1992) 329.
[454] G.J. Parker, C. Cerjan, J. Appl. Phys. 87 (2000) 5514.
[455] M. Hwang, M. Farhoud, Y. Hao, M. Walsh, T.A. Savas, H.I. Smith, C.A. Ross, IEEE Trans. Magn. 36 (2000) 3173.
[456] T. Schrefl, J. Fidler, K.J. Kirk, J.N. Chapman, J. Appl. Phys. 85 (1999) 6169.
[457] J.G. Deak, R.H. Koch, J. Magn. Magn. Mater. 213 (2000) 25.
[458] B.D. Cullity, Introduction to Magnetic Materials, Addison-Wesley Publishing Company, Reading, MA, 1972.
[459] W. Wernsdorfer, K. Hasselbach, D. Mailly, B. Barbara, A. Benoit, L. Thomas, G. Suran, J. Magn. Magn. Mater. 140-144 (1995) 389.
[460] L. Kong, S.Y. Chou, J. Appl. Phys. 80 (1996) 5205.
[461] S. McVitie, J.N. Chapman, Microsc. Microanal. 3 (1997) 146.
[462] M. Pardavi-Horvath, J. Magn. Magn. Mater. 198–199 (1999) 219.
[463] M.E. Schabes, H.N. Bertram, J. Appl. Phys. 64 (1988) 1347.
[464] D.R. Fredkin, T.R. Koehler, J. Appl. Phys. 67 (1990) 5544.
[465] D.R. Fredkin, T.R. Koehler, IEEE Trans. Magn. 25 (1989) 3473.
[466] Y.D. Yan, E. della Torre, J. Appl. Phys. 66 (1989) 320.
[467] W. Williams, D.J. Dunlop, Nature 337 (1989) 634.
[468] Y. Uesaka, Y. Nakatani, N. Hayashi, J. Appl. Phys. 67 (1990) 5146.
[469] N.A. Usov, S.E. Peschany, J. Magn. Magn. Mater. 110 (1992) L1.
[470] J. Gadbois, J.G. Zhu, IEEE Trans. Magn. 31 (1995) 3802.
[471] R.P. Cowburn, M.E. Welland, Appl. Phys. Lett. 72 (1998) 2041.
[472] R.P. Cowburn, M.E. Welland, Phys. Rev. B 58 (1998) 9217.
[473] R.P. Cowburn, M.E. Welland, J. Appl. Phys. 86 (1999) 1035.
[474] W. Rave, K. Ramstöck, A. Hubert, J. Magn. Magn. Mater. 183 (1998) 329.
[475] A. Thiaville, D. Tomás, J. Miltat, Phys. Stat. Sol. (a) 170 (1998) 125.
[476] X.H. Huang, M. Pardavi-Horvath, IEEE Trans. Magn. 32 (1996) 4180.
[477] A. Aharoni, Introduction to the Theory of Magnetism, Oxford Science Publications, Oxford, 1996.
[478] A. Lebib, S.P. Li, M. Natali, Y. Chen, J. Appl. Phys. 89 (2001) 3892.
[479] O. Kazakova, M. Hanson, P. Blomquist, R. Wäppling, J. Appl. Phys. 90 (2001) 2440.
[480] S.J. Hefferman, J.N. Chapman, S. McVitie, J. Magn. Magn. Mater. 83 (1990) 223.
[481] J.N. Chapman, S. McVitie, S.J. Hefferman, J. Appl. Phys. 69 (1991) 6078.
[482] R.H. Kodama, J. Magn. Magn. Mater. 200 (1999) 359.
[483] R.H. Kodama, A.E. Berkowitz, E.J. McNiff Jr., S. Foner, Phys. Rev. Lett. 77 (1996) 394.
[484] R.H. Kodama, S.A. Makhlouf, A.E. Berkowitz, Phys. Rev. Lett. 79 (1997) 1393.
[485] J.T. Richardson, W.O. Milligan, Phys. Rev. 102 (1956) 1289.
[486] S.A. Makhlouf, F.T. Parker, F.E. Spada, A.E. Berkowitz, J. Appl. Phys. 81 (1997) 5561.
[487] D. Hinzke, U. Nowak, Phys. Rev. B 61 (2000) 6734.
[488] U. Nowak, Ann. Rev. Comput. Phys. IX (2001) 105.

[489] M. Masuda, S. Shiomi, M. Shiraki, Jpn. J. Appl. Phys. 26 (1987) 1680.
[490] G.W. Spratt, Y. Uesaka, Y. Nakatani, N. Hayashi, IEEE Trans. Magn. 27 (1991) 4790.
[491] Y. Uesaka, Y. Nakatani, N. Hayashi, J. Magn. Magn. Mater. 123 (1993) 209.
[492] P.V. Hendriksen, S. Mørup, G. Christiansen, K.W. Jacobsen, in: G.C. Hadjipanayis, G.A. Prinz (Eds.), Science and Technology of Nanostructured Magnetic Materials, Plenum Press, New York, 1991, p. 573.
[493] H.N. Bertram, J.C. Mallinson, J. Appl Phys. 40 (1969) 1301.
[494] L. Thurlings, W. Kitzen, IEEE Trans. Magn. 16 (1980) 53.
[495] J.J. Lu, M.T. Lin, C.C. Kuo, H.L. Huang, J. Appl. Phys. 85 (1999) 5558.
[496] W. Chen, S. Zhang, H.N. Bertram, J. Appl. Phys. 71 (1992) 5579.
[497] I. Klik, J.S. Yang, C.R. Chang, J. Appl. Phys. 76 (1994) 6493.
[498] W. Chen, D.R. Fredkin, T.R. Koehler, IEEE Trans. Magn. 28 (1992) 3168.
[499] H.N. Bertram, C. Seberino, J. Magn. Magn. Mater. 193 (1999) 388.
[500] P.I. Belov, R.S. Gekht, V.A. Ignatchenko, Sov. Phys. JETP 57 (1983) 636.
[501] K. De'Bell, A.B. MacIsaac, I.N. Booth, J.P. Whitehead, Phys. Rev. B 55 (1997) 15108.
[502] D.R. Fredkin, T.R. Koehler, IEEE Trans. Magn. 23 (1987) 3385.
[503] P.H.W. Ridley, G.W. Roberts, M.A. Womgsom, R.W. Chantrell, J. Gore, M. Maylin, IEEE Trans. Magn. 35 (1999) 3874.
[504] D. Süß, T. Schrefl, J. Fidler, J.N. Chapman, J. Magn. Magn. Mater. 196-197 (1999) 617.
[505] P.H.W. Ridley, G.W. Roberts, R.W. Chantrell, J. Appl. Phys. 87 (2000) 5523.
[506] K.Y. Guslienko, S.B. Choe, S.C. Shin, Appl. Phys. Lett. 76 (2000) 3609.
[507] K.Y. Guslienko, Appl. Phys. Lett. 75 (1999) 394.
[508] E. Olive, P. Molho, Phys. Rev. B 58 (1998) 9238.
[509] K.Y. Guslienko, Phys. Lett. A 278 (2001) 293.
[510] V.E. Klymenko, V.M. Rozenbaum, V.V. Kukhtin, O.V. Shramko, Solid State Commun. 88 (1993) 373.
[511] V.N. Kondratyev, H.O. Lutz, Phys. Rev. Lett. 81 (1998) 4508.
[512] R. Kretschmer, K. Binder, Z. Phys. B 34 (1979) 375.
[513] M.R. Scheinfein, K.E. Schmidt, K.R. Heim, G.G. Hembree, Phys. Rev. Lett. 76 (1996) 1541.
[514] R.E. Dunin-Borkowski, M.R. McCartney, D.J. Smith, S.S.P. Parkin, Ultramicroscopy 74 (1998) 61.
[515] M. Pardavi-Horvath, G. Zheng, G. Vertesy, A. Magni, IEEE Trans. Magn. 32 (1996) 4469.
[516] W. Andrä, H. Danan, U. Röpke, IEEE Trans. Magn. 20 (1984) 102.
[517] E.R. Wuori, J.H. Judy, IEEE Trans. Magn. 20 (1984) 1867.
[518] J.G. Brankov, D.M. Danchev, Physica A 144 (1987) 128.
[519] M. Redi, P.W. Anderson, Proc. Nat. Acad. Sci. 78 (1981) 27.
[520] S.K. Misra, Phys. Rev. B 26 (1982) 2633.
[521] T. Niemeyer, Physica 57 (1972) 281.
[522] J.M. Luttinger, L. Tisza, Phys. Rev. 70 (1946) 954.
[523] P.H.W. Ridley, G.W. Roberts, R.W. Chantrell, K.J. Kirk, J.N. Chapman, IEEE Trans. Magn. 36 (2000) 3161.
[524] R.L. Stamps, R.E. Camley, Phys. Rev. B 60 (1999) 11694.
[525] S. Prakash, C.L. Henley, Phys. Rev. B 42 (1990) 6574.
[526] V. Russier, C. Petit, J. Legrand, M.P. Pileni, Appl. Surf. Sci. 164 (2000) 193.
[527] V. Russier, J. Appl. Phys. 89 (2001) 1287.
[528] W. Kleemann, O. Petracic, C. Binek, G.N. Kakazu, Y.G. Pogorelov, J.B. Sousa, S. Cardoso, P.P. Freitas, Phys. Rev. B 63 (2001) 134423.
[529] A. Hernando, D.X. Chen, M. Pardavi-Horvath, J.M. González, Phys. Rev. B 63 (2001) 052404.
[530] X. Batlle, A. Labarta, J. Phys. D 35 (2002) R15, and references therein.
[531] C.H. Back, H.C. Siegmann, J. Magn. Magn. Mater. 200 (1999) 774.
[532] P. Bryant, S. Schultz, D.R. Fredkin, J. Appl. Phys. 69 (1991) 5877.
[533] M. Lederman, S. Schultz, M. Ozaki, Phys. Rev. Lett. 73 (1994) 1986.
[534] C. Salling, R. O'Barr, S. Schultz, I. McFadyen, M. Ozaki, J. Appl. Phys 75 (1994) 7989.
[535] T. Chang, J.G. Zhu, J. Appl. Phys. 75 (1994) 5553.
[536] W. Wernsdorfer, E. Bonet Orozco, K. Hasselbach, A. Benoit, B. Barbara, N. Demoncy, A. Loiseau, H. Pascard, D. Mailly, Phys. Rev. Lett. 78 (1997) 1791.
[537] L. Néel, Ann. Geophys. 5 (1949) 99.
[538] W.F. Brown, Phys. Rev. 130 (1963) 1677.
[539] W.D. Doyle, S. Stinnet, C. Dawson, L. He, J. Magn. Soc. Japan 22 (1998) 91.
[540] W.K. Hiebert, A. Stankiewicz, M.R. Freeman, Phys. Rev. Lett. 79 (1997) 1134.
[541] C.H. Back, D. Weller, J. Heidmann, D. Mauri, D. Guarisco, E.L. Garwin, H.C. Siegmann, Phys. Rev. Lett. 81 (1998) 3251.
[542] Y. Acremann, C.H. Back, M. Buess, O. Portmann, A. Vaterlaus, D. Pescia, H. Melchior, Science 290 (2000) 492.
[543] B.C. Choi, M. Belov, W.K. Hiebert, G.E. Ballentine, M.R. Freeman, Phys. Rev. Lett. 86 (2001) 728.
[544] R.H. Koch, J.G. Deak, D.W. Abraham, P.L. Trouilloud, R.A. Altman, Y. Lu, W.J. Gallagher, R.E. Scheuerlein, K.P. Roche, S.S.P. Parkin, Phys. Rev. Lett. 81 (1998) 4512.
[545] C.H. Back, R. Allenspach, W. Weber, S.S.P. Parkin, D. Weller, E.L. Garwin, H.C. Siegmann, Science 285 (1999) 864.
[546] T.J. Silva, C.S. Lee, T.M. Crawford, C.T. Rogers, J. Appl. Phys. 85 (1999) 7849.
[547] B.A. Everitt, A.V. Pohm, R.S. Beech, A. Fink, J.M. Daughton, IEEE Trans. Magn. 34 (1998) 1060.

[548] S.E. Russek, J.O. Oti, S. Kaka, Y. Chen, J. Appl. Phys. 85 (1999) 4773.
[549] S.E. Russek, S. Kaka, M.J. Donahue, J. Appl. Phys. 87 (2000) 7070.
[550] M. Bonfim, G. Ghiringhelli, F. Montaigne, S. Pizzini, N.B. Brookes, F. Petroff, J. Vogel, J. Camarero, A. Fontaine, Phys. Rev. Lett. 86 (2001) 3646.
[551] R.L. Stamps, R.E. Camley, Phys. Rev. B 60 (1999) 12264.
[552] R.L. Stamps, Aust. J. Phys. 53 (2000) 567.
[553] E.Y. Tsymbal, Appl. Phys. Lett. 77 (2000) 2740.
[554] G. Mukhopadhyay, P. Apell, M. Hanson, J. Magn. Magn. Mater. 203 (1999) 286.
[555] J. Kaczér, L. Murtinová, Phys. Stat. Sol. (a) 23 (1974) 79.
[556] K.L. Metlov, J. Magn. Magn. Mater. 215–216 (2000) 37.
[557] L. Landau, E. Lifshitz, Phys. Z. Sowjetunion 8 (1935) 153.
[558] W.F. Brown Jr., J. Phys. Radium 20 (1959) 101.
[559] A. Aharoni, Phys. Rev. 123 (1961) 732.
[560] W.F. Brown Jr., Micromagnetics, Interscience, New York, 1963.
[561] E.H. Frei, W.F. Brown Jr., J. Appl. Phys. 39 (1968) 993.
[562] W.F. Brown Jr., J. Appl. Phys. 49 (1978) 1937.
[563] A.S. Arrot, J. Appl. Phys. 69 (1991) 5212.
[564] A. Aharoni, IEEE Trans. Magn. 29 (1993) 2596.
[565] M. Redjdal, F.B. Humphrey, J. Appl. Phys. 79 (1996) 6464.
[566] D.R. Fredkin, T.R. Koehler, IEEE Trans. Magn. 26 (1990) 1518.
[567] D.R. Fredkin, T.R. Koehler, J.F. Smyth, S. Schultz, J. Appl. Phys. 69 (1991) 5276.
[568] T.R. Koehler, B. Yang, W. Chen, D.R. Fredkin, J. Appl. Phys. 73 (1993) 6504.
[569] R. Hertel, H. Kronmüller, J. Appl. Phys. 85 (1999) 6190.
[570] S. Haratani, T. Aoyama, I. Sato, IEEE Trans. Magn. 36 (2000) 3164.
[571] Y. Zheng, J.-G. Zhu, J. Appl. Phys. 81 (1997) 5471.
[572] C. Kõnig, M. Sperlich, R. Heinesch, R. Calarco, J.O. Hauch, U. Rüdiger, G. Güntherodt, S. Kirsch, B. Özyilmaz, A.D. Kent, Appl. Phys. Lett. 79 (2001) 3648.
[573] M. Redjdal, P.W. Gross, A. Kazmi, F.B. Humphrey, J. Appl. Phys. 85 (1999) 6193.
[574] T.-N. Fang, J.-G. Zhu, J. Appl. Phys. 87 (2000) 7061.
[575] C. Seberino, H.N. Bertram, J. Appl. Phys. 85 (1999) 5543.
[576] R.D. McMichael, J. Eicke, M.J. Donahue, D.G. Porter, J. Appl. Phys. 87 (2000) 7058.
[577] N.A. Usov, J. Magn. Magn. Mater. 203 (1999) 277.
[578] K. Matsuyama, F. Nakamura, Y. Nozaki, J. Magn. Magn. Mater. 198-199 (1999) 248.
[579] R. Hertel, J. Appl. Phys. 90 (2001) 5752.
[580] L. Néel, Science 174 (1971) 985.
[581] H. Rubio, S. Suárez, S. Brown, J.W. Harrell, Phys. Rev. B 64 (2001) 094430.
[582] U. Nowak, D. Hinzke, J. Appl. Phys. 85 (1999) 4337.
[583] K.Y. Guslienko, A.N. Slavin, J. Appl. Phys. 87 (2000) 6337.
[584] A.O. Adeyeye, J.A.C. Bland, C. Daboo, D.G. Hasko, Phys. Rev. B 56 (1997) 3265.
[585] J.I. Martín, J. Nogués, I.K. Schuller, M.J. Van Bael, K. Temst, C. Van Haesendonck, V.V. Moshchalkov, Y. Bruynseraede, Appl. Phys. Lett. 72 (1998) 255.
[586] M. Kume, A. Maeda, T. Tanuma, K. Kuroki, J. Appl. Phys. 79 (1996) 6402.
[587] A. Maeda, T. Tanuma, M. Kume, Mater. Sci. Eng. A 217–218 (1996) 203.
[588] A. Maeda, M. Kume, S. Oikawa, K. Kuroki, J. Magn. Soc. Japan 19 (1995) 397.
[589] T. Taniyama, I. Nakatani, T. Sato, T. Namikawa, Y. Yamazaki, IEEE Trans. Magn. 35 (1999) 3478.
[590] S.J. Blundell, C. Shearwood, M. Gester, M.J. Baird, J.A.C. Bland, H. Ahmed, J. Magn. Magn. Mater. 135 (1994) L17.
[591] A.O. Adeyeye, J.A.C. Bland, C. Daboo, J. Magn. Magn. Mater. 188 (1998) L1.
[592] A.O. Adeyeye, G. Lauhoff, J.A.C. Bland, C. Daboo, D.G. Hasko, H. Ahmed, Appl. Phys. Lett. 70 (1997) 1046.
[593] A.O. Adeyeye, J.A.C. Bland, C. Daboo, D.G. Hasko, H. Ahmed, J. Appl. Phys. 82 (1997) 469.
[594] W.Y. Lee, C.C. Yao, A. Hirohata, Y.B. Xu, H.T. Leung, S.M. Gardiner, S. McPhail, B.C. Choi, D.G. Hasko, J.A.C. Bland, J. Appl. Phys. 87 (2000) 3032.
[595] A. Maeda, M. Kume, S. Oikawa, K. Kuroki, J. Magn. Soc. Japan 19 (1995) 309.
[596] C. Shearwood, H. Ahmed, L.M. Nicholson, J.A.C. Bland, M.J. Baird, M. Patel, H.P. Hughes, Microelectron. Eng. 21 (1993) 431.
[597] J.I. Martín, J.L. Costa-Krämer, F. Briones, J.L. Vicent, J. Magn. Magn. Mater. 221 (2000) 215.
[598] Y. Souche, V. Novosad, B. Pannetier, O. Geoffroy, J. Magn. Magn. Mater. 177–181 (1998) 1277;
Y. Souche, O. Geoffroy, V. Novosad, V. Pishko, B. Pannetier, J. Magn. Soc. Japan 20 (Suppl. S1) (1996) 393.
[599] Y. Nozaki, T. Ono, K. Motohashi, H. Miyajima, T. Kinoshita, J. Magn. Magn. Mater. 177–181 (1998) 1271.
[600] G. Armelles, J.L. Costa-Krämer, J.I. Martín, J.V. Anguita, J.L. Vicent, Appl. Phys. Lett. 77 (2000) 2039.
[601] J. Jorzick, S.O. Demokritov, C. Mathieu, B. Hillebrands, B. Bartenlian, C. Chappert, F. Rousseaux, A.N. Slavin, Phys. Rev. B 60 (1999) 15194.
[602] S.M. Chérif, Y. Roussigné, P. Moch, J.F. Hennequin, M. Laburne, J. Appl. Phys. 85 (1999) 5477.
[603] S.M. Chérif, Y. Roussigné, C.D. Dugautier, P. Moch, J. Magn. Magn. Mater. 222 (2000) 337.
[604] S.M. Chérif, Y. Roussigné, P. Moch, Phys. Rev. B 59 (1999) 9482.
[605] A. Ercole, A.O. Adeyeye, C. Daboo, J.A.C. Bland, D.G. Hasko, J. Appl. Phys. 81 (1997) 5452.
[606] A. Ercole, A.O. Adeyeye, J.A.C. Bland, D.G. Hasko, Phys. Rev. B 58 (1998) 345.
[607] S.C. Sanders, R.W. Cross, S.E. Russek, A. Roshko, J.O. Oti, J. Appl. Phys. 79 (1996) 6240.
[608] Y. Nozaki, K. Matsuyama, T. Ono, H. Miyajima, Jpn. J. Appl. Phys. 38 (1999) 6282.

[609] Y.B. Xu, C.A.F. Vaz, A. Hirohata, H.T. Leung, C.C. Yao, J.A.C. Bland, E. Cambril, F. Rousseaux, H. Launois, Phys. Rev. B 61 (2000) 14901.
[610] A. Hirohata, Y.B. Xu, C.C. Yao, H.T. Leung, W.Y. Lee, S.M. Gardiner, D.G. Hasko, J.A.C. Bland, S.N. Holmes, J. Appl. Phys. 87 (2000) 4727.
[611] A. Hirohata, C.C. Yao, H.T. Leung, Y.B. Xu, C.M. Guertler, J.A.C. Bland, IEEE Trans. Magn. 36 (2000) 3068.
[612] W.Y. Lee, A. Hirohata, H.T. Leung, Y.B. Xu, S.M. Gardiner, C.C. Yao, J.A.C. Bland, IEEE Trans. Magn. 36 (2000) 3018.
[613] V. Kubrak, F. Rahman, N. Overend, B.L. Gallagher, P.C. Main, J. de Boeck, M. Behest, C.H. Marrows, M.A. Howson, Physica B 256–258 (1998) 380.
[614] Y. Otani, S.G. Kim, K. Fukamichi, IEEE Trans. Magn. 34 (1998) 1096.
[615] K. Hong, N. Giordano, J. Phys.: Condens. Matter 8 (1996) L301.
[616] T. Taniyama, I. Nakatani, H. Yanagihara, E. Kita, J. Magn. Magn. Mater. 196–197 (1999) 77.
[617] W.Y. Lee, Y.B. Xu, C.A.F. Vaz, A. Hirohata, H.T. Leung, C.C. Yao, B.C. Choi, J.A.C. Bland, F. Rousseaux, E. Cambril, H. Launois, IEEE Trans. Magn. 35 (1999) 3883.
[618] Y.B. Xu, C.A.F. Vaz, A. Hirohata, C.C. Yao, W.Y. Lee, J.A.C. Bland, F. Rousseaux, E. Cambril, H. Launois, J. Appl. Phys. 85 (1999) 6178.
[619] K. Shigeto, T. Shinjo, T. Ono, Appl. Phys. Lett. 75 (1999) 2815.
[620] A.O. Adeyeye, R.P. Cowburn, M.E. Welland, J. Appl. Phys. 87 (2000) 299.
[621] Y. Yokoyama, K. Shigeto, P. Gogol, J. Miltat, A. Thiaville, T. Kawagoe, Y. Suzuki, S. Yuasa, K. Ando, J. Magn. Soc. Japan 24 (2000) 555.
[622] T. Kimura, F. Wakaya, J. Yanagisawa, Y. Yuba, K. Gamo, J. Magn. Magn. Mater. 222 (2000) 79.
[623] T. Kimura, K. Ikushima, F. Wakaya, K. Gamo, J. Magn. Soc. Japan 24 (2000) 471.
[624] A.D. Kent, U. Rüdiger, J. Yu, S. Zhang, P.M. Levy, S.S.P. Parkin, IEEE Trans. Magn. 34 (1998) 1096.
[625] S.G. Kim, Y. Otani, K. Fukamichi, S. Yuasa, M. Nyvlt, T. Katayama, IEEE Trans. Magn. 35 (1999) 2862.
[626] T. Ono, H. Miyajima, K. Shigeto, T. Shinjo, Appl. Phys. Lett. 72 (1998) 1116.
[627] Y.D. Park, H.D. Hudspeth, T.J. Schultz, A. Cabbibo, J.A. Caballero, F. Sharifi, J.R. Childress, Mater. Res. Soc. Symp. Proc. 475 (1997) 303.
[628] L. Kong, Q. Pan, B. Cui, M. Li, S.Y. Chou, J. Appl. Phys. 85 (1999) 5492.
[629] T. Ono, H. Miyajima, K. Shigeto, K. Mibu, N. Hosoito, T. Shinjo, J. Appl. Phys. 85 (1999) 6181.
[630] K. Shigeto, T. Ono, H. Miyajima, T. Sinjo, J. Magn. Magn. Mater. 198-199 (1999) 58.
[631] K. Shigeto, T. Okuno, T. Shinjo, Y. Suzuki, T. Ono, J. Appl. Phys. 88 (2000) 6636.
[632] T. Ono, H. Miyajima, K. Shigeto, K. Mibu, N. Hosoito, T. Shinjo, Science 284 (1999) 468.
[633] T. Ono, H. Miyajima, K. Shigeto, T. Shinjo, J. Magn. Soc. Japan 24 (2000) 1136.
[634] T. Shinjo, Philos. Mag. B 80 (2000) 207.
[635] A. Nemoto, Y. Otani, S.G. Kim, K. Fukamichi, O. Kitakami, Y. Shimada, Appl. Phys. Lett. 74 (1999) 4026.
[636] Y. Otani, A. Nemoto, S.G. Kim, K. Fukamichi, O. Kitakami, Y. Shimada, J. Magn. Magn. Mater. 198–199 (1999) 434.
[637] M.H. Kryder, K.Y. Ahn, N.J. Mazzeo, S. Schwarlz, S.M. Kane, IEEE Trans. Magn. 16 (1980) 99.
[638] C.H. Bajorek, C. Coker, L.T. Romankiw, D.A. Thompson, IBM J. Res. Dev. 18 (1974) 542.
[639] N. Ali, J.T. Masden, P. Hill, A. Chin, Int. J. Mod. Phys. B 7 (1993) 4196.
[640] A. Chin, J.T. Masden, N. Ali, J. Appl. Phys. 67 (1990) 5664.
[641] S. Dubois, J. Colin, J.L. Duvail, L. Piraux, Phys. Rev. B 61 (2000) 14315.
[642] G. Tatara, H. Fukuyama, Phys. Rev. Lett. 78 (1997) 3773.
[643] Y. Lyanda-Geller, I.L. Aleiner, P.M. Goldbart, Phys. Rev. Lett. 81 (1998) 3215.
[644] M. Viret, D. Vignoles, D. Cole, J.M.D. Coey, W. Allen, D.S. Daniel, J.F. Gregg, Phys. Rev. B 53 (1996) 8464.
[645] P.M. Levy, S. Zhang, Phys. Rev. Lett. 79 (1997) 5110.
[646] J.B.A.N. Van Hoof, K.M. Schep, P.J. Kelley, G.E.W. Bauer, J. Magn. Magn. Mater. 177 (1998) 188.
[647] M. Viret, Y. Samson, P. Warin, A. Marty, F. Ott, E. Søndergård, O. Klein, C. Fermon, Phys. Rev. Lett. 85 (2000) 3962.
[648] R.P. van Gorkom, A. Brataas, G.E.W. Bauer, Phys. Rev. Lett. 83 (1999) 4401.
[649] G.G. Cabrera, L.M. Falicov, Phys. Stat. Sol. (b) 61 (1974) 539.
[650] T. Taniyama, I. Nakatani, T. Yakabe, Y. Yamakazi, Appl. Phys. Lett. 76 (2000) 613.
[651] U. Rüdiger, J. Yu, S. Zhang, A.D. Kent, S.S.P. Parkin, Phys. Rev. Lett. 80 (1998) 5639.
[652] U. Rüdiger, J. Yu, A.D. Kent, S.S.P. Parkin, Appl. Phys. Lett. 73 (1998) 1298.
[653] T. Nagahama, K. Mibu, T. Shinjo, J. Appl. Phys. 87 (2000) 5648.
[654] H. Sato, R. Hanada, H. Sugawara, Y. Aoki, T. Ono, H. Miyajima, T. Shinjo, Phys. Rev. B 61 (2000) 3227.
[655] U. Ebels, A. Radulescu, Y. Henry, L. Piraux, K. Ounadjela, Phys. Rev. Lett. 84 (2000) 983.
[656] J.-E. Wegrowe, A. Comment, Y. Jaccard, J.-Ph. Ansermet, N.M. Dempsey, J.-P Nozières, Phys. Rev. B 61 (2000) 12216.
[657] M. Viret, L. Delfosse, P. Warin, F. Ott, C. Fermon, C. R. Acad. Sci. Paris 327 (1999) 907.
[658] I.K. Schuller, S. Kim, C. Leighton, J. Magn. Magn. Mater. 200 (1999) 571.
[659] M.A.M. Gijs, G. Bauer, Adv. Phys. 46 (1997) 285.

[660] J. Brass, W.P. Pratt, J. Magn. Magn. Mater. 200 (1999) 274.
[661] A. Fert, L. Piraux, J. Magn. Magn. Mater. 200 (1999) 338.
[662] S. Zhang, P.M. Levy, J. Appl. Phys. 69 (1991) 4786.
[663] W.P. Pratt, S.F. Lee, J.M. Slaughter, R. Loloee, P.A. Schroeder, J. Bass, Phys. Rev. Lett. 66 (1991) 3060.
[664] M.A.M. Gijs, S.K.J. Lenczowski, J.B. Giesbers, Phys. Rev. Lett. 70 (1993) 3343.
[665] W. Vavra, S.F. Cheng, A. Fink, J.J. Krebs, G.A. Prinz, Appl. Phys. Lett. 66 (1995) 2579.
[666] J.-E. Wegrowe, S.E. Gilbert, D. Kelly, B. Doudin, J.P. Ansermet, IEEE Trans. Magn. 34 (1998) 968.
[667] P.M. Levy, S. Zhang, T. Ono, T. Shinjo, Phys. Rev. B 52 (1995) 16049.
[668] T. Ono, Y. Sujita, K. Shigeto, K. Mibu, N. Hosoito, T. Shinjo, Phys. Rev. B 55 (1997) 14457.
[669] J.P. Spallas, Y. Huai, S. Vernon, B. Fuchs, B. Law, D.R. Kania, D. Kroes, M. Thomas, D. O'Kane, Z.C.H. Tan, IEEE Trans. Magn. 32 (1996) 4710.
[670] J.W. Cable, M.R. Khan, G.P. Felcher, I.K. Schuller, Phys. Rev. B 34 (1986) 1643.
[671] M.J. Pechan, J.F. Ankner, D.M. Kelly, C.F. Majkrzak, I.K. Schuller, J. Appl. Phys. 75 (1994) 6178.
[672] M.C. Cyrille, S. Kim, M.E. Gómez, J. Santamaría, K.M. Krishnan, I.K. Schuller, Phys. Rev. B 62 (2000) 3361.
[673] M.C. Cyrille, S. Kim, M.E. Gómez, J. Santamaría, C. Leighton, I.K. Schuller, Phys. Rev. B 62 (2000) 15079.
[674] I.A. Campbell, A. Fert, in: E. P. Wolfarth (Ed.), Ferromagnetic Materials, Vol. 3, North Holland, Amsterdam, 1982, p. 751 (Chapter 9).
[675] T. Valet, A. Fert, Phys. Rev. B 48 (1993) 7099.
[676] J. Slonczewski, J. Magn. Magn. Mater. 195 (1999) L261.
[677] L. Berger, Phys. Rev. B 54 (1996) 9353.
[678] M. Kame, A. Maeda, T. Tanuma, K. Kuroki, J. Appl. Phys. 79 (1996) 6402.
[679] J.A. Katine, A. Palanisami, R.A. Buhrman, Appl. Phsy. Lett. 74 (1999) 1883.
[680] Y.D. Park, D. Temple, K.B. Jung, D. Kumar, P.H. Holloway, S.J. Pearton, J. Vac. Sci. Technol. B 17 (1999) 2471.
[681] S.E. Russek, R.W. Cross, S.C. Sanders, J.O. Oti, IEEE Trans. Magn. 31 (1995) 3939.
[682] T.L. Hylton, M.A. Parker, K.R. Coffey, J.K. Howard, R. Fontana, C. Tsang, Appl. Phys. Lett. 67 (1995) 1154.
[683] D.D. Tang, P.K. Wang, V.S. Speriosu, S. Le, K.K. Kung, IEEE Trans. Magn. 6 (1995) 3206.
[684] A.G. Wang, Y. Nakamura, IEEE Trans. Magn. 32 (1996) 4022.
[685] A.V. Pohm, R.S. Beech, J.M. Daughton, B.A. Everitt, E.Y. Chen, M. Durlam, K. Nordquist, T. Zhu, S. Tehrani, IEEE Trans. Magn. 32 (1996) 4645.
[686] S. Tehrani, E. Chen, M. Durlam, M. DeHerrera, J.M. Slaughter, J. Shi, G. Kerszykowski, J. Appl. Phys. 85 (1999) 5822.
[687] S.S.P. Parkin, K.P. Roche, M.G. Samant, P.M. Rice, R.B. Beyers, R.E. Scheruerlein, W.J. O'Sullivan, S.L. Brown, J. Bucchigano, D.W. Abraham, Y. Lu, M. Rooks, P.L. Trouilloud, R.A. Wagner, W.J. Gallagher, J. Appl. Phys. 85 (1999) 5828.
[688] Y. Lu, P.L. Trouilloud, D.W. Abraham, R. Koch, J. Slonczewski, S. Brown, J. Bucchignano, E. O'Sullivan, R.A. Wagner, W.J. Gallagher, S.S.P. Parkin, J. Appl. Phys. 85 (1999) 5267.
[689] A. Anguelouch, B.D. Schrag, G. Xiao, Y. Lu, P.L. Trouilloud, W.J. Gallagher, S.S.P. Parkin, Appl. Phys. Lett. 76 (2000) 622.
[690] Y. Lu, R.A. Altman, A. Marley, S.A. Rishton, P.L. Trouilloud, G. Xiao, W.J. Gallagher, S.S.P. Parkin, Appl. Phys. Lett. 70 (1997) 2610.
[691] W.J. Gallagher, S.S.P. Parkin, Y. Lu, X.P. Bian, A. Marley, K.P. Roche, R.A. Altman, S.A. Richton, C.A. Jahnes, T.M. Shaw, G. Xiao, J. Appl. Phys. 81 (1997) 3741.
[692] R.H. Koch, G. Grinstein, G.A. Keefe, Y. Lu, P.L. Trouilloud, W.J. Gallagher, S.S.P. Parkin, Phys. Rev. Lett. 84 (2000) 5419.
[693] S. Ingvarsson, G. Xiao, S.S.P. Parkin, W.J. Gallagher, G. Grinstein, R. Koch, Phys. Rev. Lett. 85 (2000) 3289.
[694] R.P. Cowburn, A.O. Adeyeye, J.A.C. Bland, Appl. Phys. Lett. 70 (1997) 2309.
[695] R.P. Cowburn, A.O. Adeyeye, J.A.C. Bland, J. Magn. Magn. Mater. 173 (1997) 193.
[696] L. Torres, L. López-Diaz, J. Iñiguez, Appl. Phys. Lett. 73 (1998) 3766.
[697] L. Torres, L. Lopez-Diaz, O. Alejos, J. Iñiguez, J. Appl. Phys. 85 (1999) 6208.
[698] P. Vavassori, V. Metlushko, R.M. Osgood III, M. Grimsditch, U. Welp, G. Crabtree, W. Fan, S.R.J. Brueck, B. Ilic, P.J. Hesketh, Phys. Rev. B 59 (1999) 6337.
[699] I. Guedes, N.J. Zaluzec, M. Grimsditch, V. Metlushko, P. Vavassori, B. Ilic, P. Neuzil, R. Kumar, Phys. Rev. B 62 (2000) 11719.
[700] M. Grimsditch, I. Guedes, P. Vavassori, V. Metlushko, B. Ilic, P. Neuzil, R. Kumar, J. Appl. Phys. 89 (2001) 7096.
[701] M. Tinkham, Introduction to Superconductivity, McGraw-Hill, New York, 1975.
[702] O. Daldini, P. Martinoli, J.L. Olsen, G. Berner, Phys. Rev. Lett. 32 (1974) 218.
[703] A.T. Fiory, A.F. Hebard, S. Somekh, Appl. Phys. Lett. 32 (1978) 73.
[704] M. Baert, V.V. Metlushko, R. Jonckheere, V.V. Moshchalkov, Y. Bruynseraede, Phys. Rev. Lett. 74 (1995) 3269.
[705] Y. Otani, B. Pannetier, J.P. Nozières, D. Givord, J. Magn. Magn. Mater. 126 (1993) 622.
[706] J.I. Martín, M. Vélez, J. Nogués, I.K. Schuller, Phys. Rev. Lett. 79 (1997) 1929.
[707] J.I. Martín, M. Vélez, J. Nogués, A. Hoffmann, Y. Jaccard, I.K. Schuller, J. Magn. Magn. Mater. 177-181 (1998) 915.
[708] Y. Fasano, J.A. Herbsommer, F. de la Cruz, F. Pardo, P.L. Gammel, E. Bucher, D.J. Bishop, Phys. Rev. B 60 (1999) R15047.

[709] D.J. Morgan, J.B. Ketterson, Phys. Rev. Lett. 80 (1998) 3614.
[710] Y. Jaccard, J.I. Martín, M.C. Cyrille, M. Vélez, J.L. Vicent, I.K. Schuller, Phys. Rev. B 58 (1998) 8232.
[711] A. Hoffmann, P. Prieto, I.K. Schuller, Phys. Rev. B 61 (2000) 6958.
[712] A. Terentiev, D.B. Watkins, L.E. De Long, L.D. Cooley, D.J. Morgan, J.B. Ketterson, Phys. Rev. B 61 (2000) R9249.
[713] J.I. Martín, M. Vélez, A. Hoffmann, I.K. Schuller, J.L. Vicent, Phys. Rev. Lett. 83 (1999) 1022.
[714] C. Reichardt, C.J. Olson, F. Nori, Phys. Rev. Lett. 78 (1997) 2648.
[715] C. Reichardt, F. Nori, Phys. Rev. Lett. 82 (1999) 414.
[716] D.M. Silevitch, D.H. Reich, C.L. Chien, S.B. Field, H. Shtrikman, J. Appl. Phys. 89 (2001) 7478.
[717] I.K. Marmorkos, A. Matulis, F.M. Peeters, Phys. Rev. B 53 (1996) 2677.
[718] I.F. Lyuksyutov, V. Pokrovsky, Phys. Rev. Lett. 81 (1998) 2344.
[719] S.L. Cheng, H.A. Fertig, Phys. Rev. B 60 (1999) 13107.
[720] L. Van Look, M.J. Van Bael, K. Temst, J.G. Rodrigo, M. Morelle, V.V. Moshchalkov, Y. Bruynseraede, Physica C 332 (2000) 356.
[721] M.J. Van Bael, J. Bekaert, K. Temst, L. Van Look, V.V. Moshchalkov, Y. Bruynseraede, Phys. Rev. Lett. 86 (2001) 155.
[722] J.I. Martín, M. Vélez, A. Hoffmann, I.K. Schuller, J.L. Vicent, Phys. Rev. B 62 (2000) 9110.
[723] F.M. Peeters, P. Vasilopoulos, Phys. Rev. B 47 (1993) 1466.
[724] D.P. Xue, G. Xiao, Phys. Rev. B 45 (1992) 5986.
[725] R. Yagi, Y. Iye, J. Phys. Soc. Japan 62 (1993) 1279.
[726] P.D. Ye, D. Weiss, K. von Klitzing, K. Eberl, H. Nickel, Appl. Phys. Lett. 67 (1995) 1441.
[727] P.D. Ye, D. Weiss, R.R. Gerhardts, M. Seeger, K. von Klitzing, K. Eberl, H. Nickel, Phys. Rev. Lett. 74 (1995) 3013.
[728] S. Izawa, S. Katsumoto, A. Endo, Y. Iye, J. Phys. Soc. Japan 64 (1995) 706.
[729] E. Skuras, A.R. Long, S. Chowdhury, M. Rahman, K.J. Kirk, J.H. Davies, J. Appl. Phys. 90 (2001) 2623.
[730] R.R. Gerhardts, D. Weiss, K. von Klitzing, Phys. Rev. Lett. 62 (1989) 1173.
[731] I.S. Ibrahim, F.M. Peeters, Phys. Rev. B 52 (1995) 17321.
[732] Z.L. Ji, D.W.L. Sprung, Phys. Rev. B 56 (1997) 1045.
[733] U.J. Gossmann, S. Manolescu, R.R. Gerhardts, Phys. Rev. B 57 (1998) 1680.
[734] E. Badran, S.E. Ulloa, Physica B 249–251 (1998) 339.
[735] K.W. Edmonds, B.L. Gallagher, P.C. Main, N. Overend, R. Wirtz, A. Nogaret, M. Henini, C.H. Marrows, B.J. Hickey, S. Thoms, Phys. Rev. B 64 (2001) 041303.
[736] M. Kato, A. Endo, S. Katsumoto, Y. Iye, Phys. Rev. B 58 (1998) 4876.
[737] N. Overend, A. Nogaret, B.L. Gallagher, P.C. Main, R. Wirtz, R. Newbury, M.A. Howson, S.P. Beaumont, Physica B 249-251 (1998) 326.
[738] A. Nogaret, S. Carlton, B.L. Gallagher, P.C. Main, M. Henini, R. Wirtz, R. Newbury, M.A. Howson, S.P. Beaumont, Phys. Rev. B 55 (1997) R16037.
[739] P.D. Ye, D. Weiss, R.R. Gerhardts, K. von Klitzing, S. Tarucha, Physica B 249–251 (1998) 330.
[740] N. Overend, A. Nogaret, B.L. Gallagher, P.C. Main, M. Henini, C.H. Marrows, M.A. Howson, S.P. Beaumont, Appl. Phys. Lett. 72 (1998) 1724.
[741] J.E. Muller, Phys. Rev. Lett. 68 (1992) 385.
[742] N. Overend, A. Nogaret, B.L. Gallagher, P.C. Main, M. Henini, R. Wirtz, R. Newbury, C.H. Marrows, M.A. Howson, S.P. Beaumont, J. Magn. Magn. Mater. 177–181 (1998) 898.
[743] F.G. Monzon, M. Johnson, M.L. Roukes, Appl. Phys. Lett. 71 (1997) 3087.
[744] F.M. Peeters, X.Q. Li, Appl. Phys. Lett. 72 (1998) 572.
[745] V. Kubrak, A. Neumann, B.L. Gallagher, P.C. Main, M. Henini, C.H. Marrows, B.J. Hickey, J. Appl. Phys. 87 (2000) 5986.